



SAPIENZA
UNIVERSITÀ DI ROMA

Facoltà di Scienze Matematiche Fisiche e Naturali

PhD in Chemical Sciences

XXX Cycle

**Oxidative Functionalization of Organic
Compounds Promoted by Nonheme
Fe and Mn Complexes**

Supervisor

Prof. Osvaldo Lanzalunga

Candidate

Alessia Barbieri

Academic year 2016/2017

Dean of the Doctoral School Prof. Osvaldo Lanzalunga

Index

Chapter 1: Oxidation reactions catalyzed by nonheme iron and manganese complexes	1
Introduction	2
Aim of the work	15
References	16
Chapter 2: Analysis of the ms timescale evolution of nonheme iron complexes oxidation by simultaneous X-Ray and UV/Vis spectroscopies	20
Introduction	21
Results and Discussion	22
Conclusion	28
Experimental Section	28
References	29
Chapter 3: Electron transfer mechanism in the oxidation of aryl sulfides promoted by nonheme iron complexes	32
Introduction	33
Results and Discussion	37
Oxidation of aryl diphenylmethyl sulfides promoted by $[(N4Py)Fe^{IV}(O)]^{2+}$	37
<i>Photochemical Oxidation</i>	37
<i>Biomimetic Oxidation by $[(N4Py)Fe^{IV}(O)]^{2+}$</i>	41
Oxidation of aryl 1-methyl-1-phenylethyl sulfides promoted by $[(N4Py)Fe^{IV}(O)]^{2+}$ and $[(Bn-TPEN)Fe^{IV}(O)]^{2+}$: the rate of the oxygen rebound process	46
<i>Laser Flash Photolysis Studies</i>	47
<i>Biomimetic Oxidation by $[(N4Py)Fe^{IV}(O)]^{2+}$ and $[(Bn-TPEN)Fe^{IV}(O)]^{2+}$</i>	48
<i>Determination of oxygen rebound rate constants (k_{OT})</i>	51
Oxidation of aryl 1-methyl-1-phenylethyl sulfides promoted by $[(PDP)Fe^{II}(SbF_6)_2]$ and $[(BPMCN)Fe^{II}(OTf)_2]$: the rate of the oxygen rebound process	52
Conclusion	55
Experimental Section	56
References	59

Chapter 4: Oxidation of alcohols and aromatics with H₂O₂ catalyzed by a nonheme imine based iron complex	63
Introduction	64
Results and Discussion	68
Oxidation of alcohols with H ₂ O ₂ catalyzed by [(L ₁) ₂ Fe(OTf) ₂]	68
Oxidation of aromatic compounds with H ₂ O ₂ catalyzed by [(L ₁) ₂ Fe(OTf) ₂]	74
<i>Mechanistic outlook</i>	77
Conclusion	81
Experimental Section	81
References	82
Chapter 5: Inhibition process of the Mn^{II}/PCA/butanedione catalytic system by catechol and guaiacol substrates	87
Introduction	88
Results and Discussion	92
Conclusion	99
Experimental Section	99
References	100
Chapter 6: Selective methylene oxidation of linear alkyl amines with H₂O₂ catalyzed by a Mn-nonheme complex guided by supramolecular recognition	103
Introduction	104
Results and Discussion	107
Synthesis, characterization and features of 1 -Fe and 1 -Mn complexes	107
Site-selectivity of 1 -Mn guided by Supramolecular recognition	110
Conclusion	114
Experimental Section	115
References	119
Chapter 7: General Conclusion	122
Appendix	124
Instrument	124
References	126
List of publication	126

Chapter 1

Oxidation reactions catalyzed by nonheme iron and manganese complexes

The development of simple and efficient catalysts for regio- and stereoselective oxidations of organic compounds based on atom economic and environmentally friendly approaches, is still a changelling task for modern chemistry.

This chapter provides a general up-to-date overview of the efforts made in the last two decades in the research of synthetic and biomimetic iron and manganese nonheme complexes able to mimic natural oxygenases.

The synthetic potential of the processes promoted by iron and manganese aminopyridine or imine based complexes, is described, with a major focus on the detailed knowledge of the intimate reactions mechanism and of the nature of the active species involved in their catalytic cycle.

1.1 Introduction

The selective oxidation of organic compounds is an essential step in many biological and industrial processes. Nature employs a number of heme¹ and nonheme² iron and manganese enzymes to carry out such transformations with an exceptional regio- and stereoselectivity under mild and environmentally friendly conditions. In the last decades, considerable efforts have been done in the synthesis of biomimetic iron and manganese heme porphyrin catalysts³ and more recently nonheme catalysts⁴ that are able to mimic the activity of the metalloenzymes in the oxidations of a variety of organic substrates.^{4b,5,6} Many of these catalysts have demonstrated interesting catalytic properties in important oxidative processes such as the oxidation of aliphatic C-H bonds and the epoxidation of olefins.^{5,6}

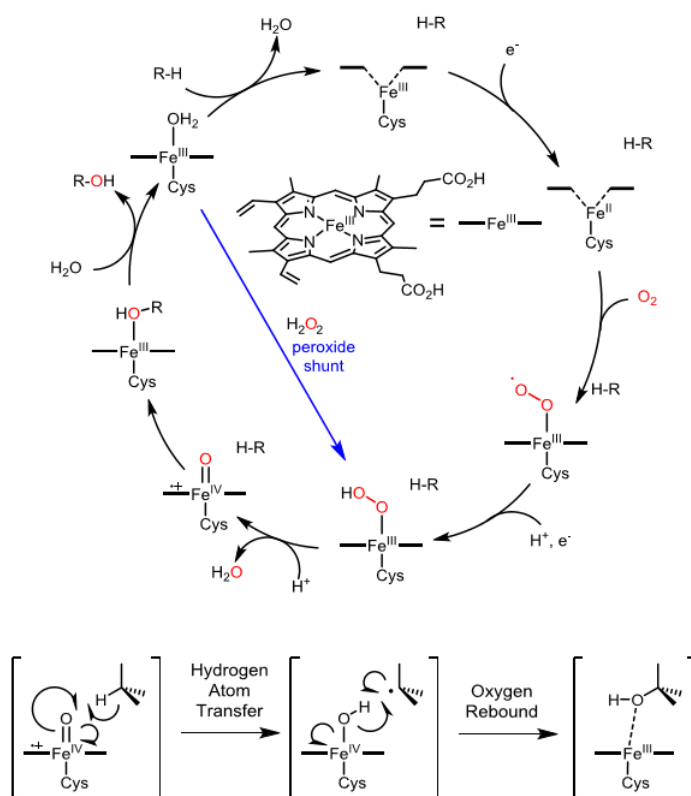
These catalysts contain abundant and non-toxic iron or manganese as metal center. In the presence of inexpensive and environmentally friendly terminal oxidants, such as H₂O₂, high valent metal-oxo active species are produced with structures that closely resemble the oxidizing intermediates of natural enzymes.^{4b,c} Both heme and nonheme iron complexes have been more extensively studied than their manganese counterparts. Relatively few information is presently available in the characterization of the active oxidizing species and in the reaction mechanism for the reactions promoted by manganese complexes. In this introduction the iron based catalytic systems will be first described, followed by the manganese ones.

Despite iron porphyrin model complexes in combination with several oxidants were demonstrated to reproduce the heme enzyme oxidative activity with promising results, several difficulties mainly associated to the complex synthetic procedures, have limited their application. The flatness of the porphyrin ligands facilitates the formation of stable and catalytically inactive μ -oxo Fe^{III} dimers. In the enzyme, this problem is solved by physical separation of the iron centers, but in the case of artificial models, this requirement would demand elaborated structures and so the consequent synthetic efforts make such kind of complexes less attractive. On the contrary, nonheme iron enzymes have simpler active sites generally consisting of facial triad (His)₂-(Asp/Glu) motifs around the iron with the three amino acids that occupy one face of an octahedron leaving the three other sites on the opposite face for the substrate coordination.^{2c,4a} For this reason a number of research groups have turned their

attention toward the processes catalyzed by nonheme complexes. Some mechanistic studies and catalytic analysis on iron and manganese nonheme model systems, will be described in this thesis.

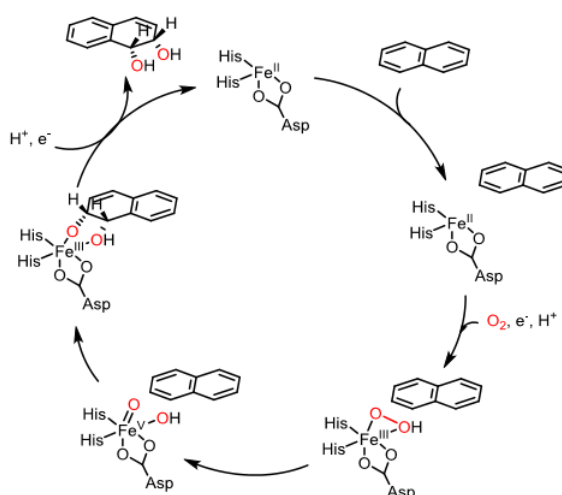
In nature the enzymes containing iron complexes in their active sites are classified into three main families: heme proteins (such as Cyt P450),¹ mononuclear and dinuclear nonheme enzymes (such as Rieske dioxygenase⁷ and soluble methane monooxygenase⁸ respectively). These enzymes are primarily involved in the detoxification and excretion processes of xenobiotics and in the metabolism of exogenous and endogenous substances by oxidative processes.¹

In Cyt P450, the iron(III) porphyrin cofactor is attached to the protein backbone through coordination of a cysteine at one of the axial positions on the metal, leaving the other prone for the O₂ binding and activation.¹ After the substrate binding, the resting state P-Fe^{III} (P= porphyrin), is converted to its high spin isomer through the loss of a coordinated water molecule and reduced to P-Fe^{II}. The P-Fe^{II} species traps oxygen forming a ferric hydroperoxo complex P-Fe^{III}(OOH), called 'compound 0' (Cpd 0) (see Scheme 1). Thanks to the assistance of a proton, the O-O bond is cleaved heterolitically with the formation of H₂O and P⁺•-Fe^{IV}=O, (Cpd 1), responsible for the oxidation step and characterized spectroscopically in various natural and synthetic systems.¹ The actual C-H oxidation process proceeds in two steps (Scheme 1, bottom):⁹ an initial hydrogen atom abstraction followed by rapid oxygen rebound. Afterwards the oxygenated product is replaced by a water molecule in the iron coordination sphere, allowing the system to cycle again. The use of peroxides or oxygen atom donors as oxidants, allows the direct formation of Cpd 0 or Cpd 1 respectively in a process called "peroxide shunt". In Scheme 1, in blue, is represented as example the "peroxide shunt" process upon interaction of P-Fe^{III} with H₂O₂.



Scheme 1. Consensus reaction cycle for the Cyt P450.

The only class of nonheme iron enzymes characterized by an oxygen activation mechanism closely related to that of heme enzymes, are the Rieske dioxygenases such as naphthalene 1,2-dioxygenase (NDO) that catalyses the *cis*-dihydroxylation of naphthalene.⁷ Also in this case, the O-O heterolysis of Fe^{III}-OOH intermediates, leads to the formation of a high valent oxidizing species (Fe^V=O) that inserts two oxygen atoms in the aromatic moiety generating the *cis*-diol (Scheme 2).⁷



Scheme 2. Proposed catalytic cycle of NDO.

The largest subfamily of nonheme iron enzymes is represented by $\text{Fe}^{\text{II}}\text{-}\alpha\text{-ketoglutarate}$ ($\alpha\text{-KG}$)-dependent enzymes that couples the oxidative transformation of substrates with the oxidative decarboxylation of the cofactor $\alpha\text{-KG}$ to CO_2 and succinate.^{2a,b} Differently from Rieske dioxygenases, the active species of nonheme iron enzymes as $\alpha\text{-KG}$ -dependent dioxygenases, is an high-spin ($S=2$) ($\text{Fe}^{\text{IV}}=\text{O}$). In 2004 has been characterized the first $\text{Fe}(\text{IV})\text{-oxo}$ nonheme complex in the catalytic cycle of taurine/2-oxoglutarate dioxygenase (TauD) in which the iron is coordinated by a combination of two histidine and two carboxylated ligands (Figure 1). Subsequently, similar structures have been found also in the catalytic cycle of prolyl 4-hydroxylase and halogenase CytC3.^{2b}

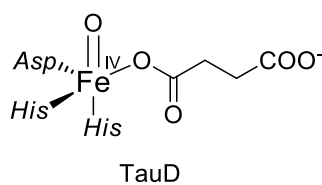


Figure 1. Structure proposed for high-valent intermediates of TauD.

Significant efforts have been devoted to the design and the studies of synthetic catalyst systems able to mimic the efficiency of the natural metalloenzymes.⁴ Unlike the enzyme intermediates

just mentioned, the synthetic complexes can have a low-spin iron (IV) center ($S=1$) as active species, presumably due to the stronger ligand field environment consisting of tetradentate and pentadentate amino and amidic ligands.¹⁰ In 1997 Que reported the first example of a nonheme iron(II) catalyst, [(TPA)Fe] (TPA= tris(2-pyridylmethyl)amine), capable to promote the stereoselective oxidation of unactivated C-H bonds.¹¹ Four years later, Nam and Que reported the first complete characterization (UV-Vis, Mössbauer and ESI-MS) of its active species, [(TPA)Fe^{IV}=O], prepared with stoichiometric peracetic acid (AcO₂H) in CH₃CN at -40 °C (Figure 2, left side).^{10a} However only in 2003 the unexpected quite stability ($t_{1/2} \sim 10$ h at 25 °C) of a mononuclear nonheme iron(IV)-oxo complex bearing a macrocyclic TMC ligand,^{10b} (TMC= 1,4,8,11-tetramethyl-1,4,8,11-tetraazacyclotradecene) has allowed to obtain the first X-ray crystal structure of an iron(IV)-oxo complex, prepared using iodosylbenzene (PhIO) as oxidant in CH₃CN at -40 °C^{10b} (Figure 2, right side).

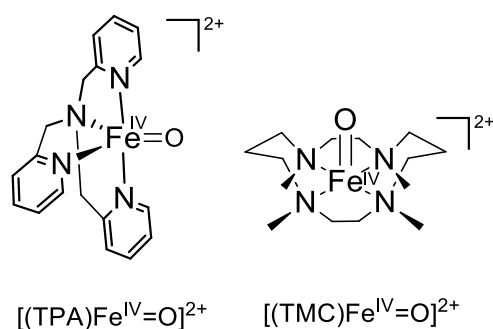


Figure 2. Iron(IV)-oxo complexes $[(\text{TPA})\text{Fe}^{\text{IV}}(\text{O})]^{2+}$ and $[(\text{TMC})\text{Fe}^{\text{IV}}(\text{O})]^{2+}$.

Since then, a large number of mononuclear nonheme iron(IV)-oxo complexes, sufficiently stable, have been synthesized, spectroscopically characterized and employed in reactivity studies of oxidation reactions at low or ambient temperature.^{3c,10c-f} X-ray analysis and EXAFS revealed short Fe-O bond distance of ~ 1.64 Å, indicating double-bond character between the iron ion and the oxygen atom, supported also by $\nu(\text{Fe}-\text{O})$ frequencies around 830 cm^{-1} .^{3c,4a} Furthermore, Mössbauer analysis indicated a low spin Fe(IV) oxidation state for all the synthetic nonheme iron(IV)-oxo complexes except for $[(\text{H}_2\text{O})_5\text{Fe}^{\text{IV}}=\text{O}]^{2+}$,¹² and spectroscopic characterizations exhibited near-IR absorption bands between 650 and 1050 nm with low extinction coefficients (ϵ_{max} of $250\text{-}400\text{ M}^{-1}\text{ cm}^{-1}$).^{3c,4a} Figure 3 shows some example of

tetradentate and pentadentate amino based iron complexes that have been demonstrated to be among the best models of natural nonheme oxygenases.^{4a-c}

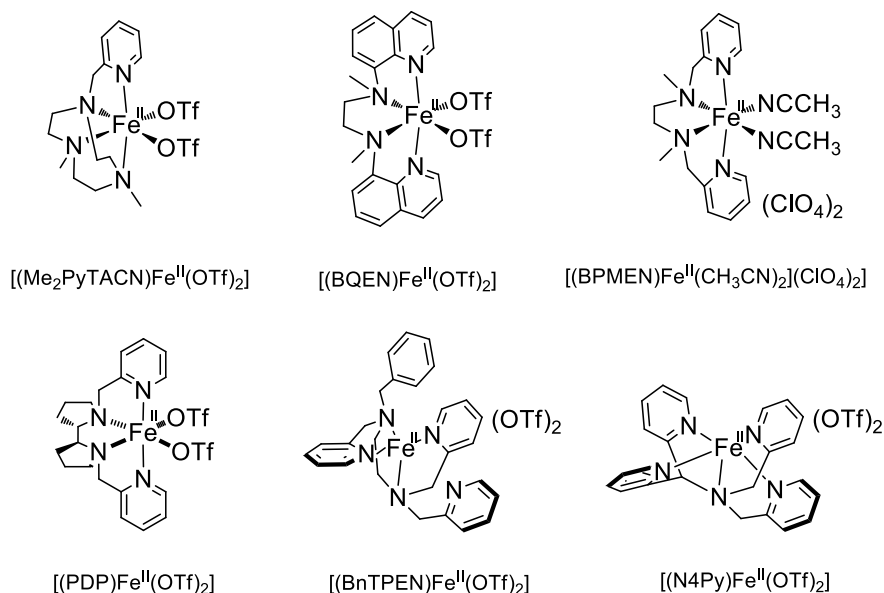
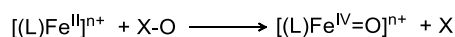


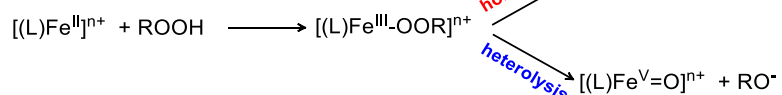
Figure 3. Examples of tetradentate and pentadentate nonheme iron complexes.

Various oxygen atom donors can be used to generate the active species ($\text{Fe}^{\text{IV}}=\text{O}$ or $\text{Fe}^{\text{V}}=\text{O}$) such as $\text{PhIO}^{10\text{b},13}$, peracids (e.g., *m*-CPBA and peracetic acid),^{10a,b,e,13b} O_3 ,¹⁴ and NaOX ($\text{X} = \text{Cl}$ or Br)^{10c} as single-oxygen atom donors, hydroperoxides (e.g., H_2O_2 and *t*BuOOH),^{10a,b,12,13b} and O_2 ¹⁵ (Scheme 3).

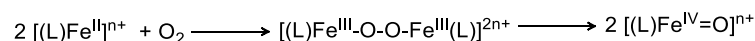
(a) Single oxygen atom donors



(b) Hydroperoxides



(c) Molecular oxygen



Scheme 3. Generation of iron-oxo complexes using different oxidants.

While two-electron oxidation of Fe(II) to the Fe(IV)-oxo species was proposed in presence of single-oxygen atom donors (Scheme 3, reaction a),^{10a,b} Fe(III)-OOR intermediate could homolytically cleave to form Fe(IV)=O species and RO• or heterolytically cleave to form a Fe(V)=O species (Scheme 3, reaction b).^{12,16} The formation of Fe(IV)=O or Fe(V)=O active species depend on different factors including the nature of the oxidant but also the nature of the ligand and the geometry around the metal center. Change in the terminal oxidant or in the nature of the ligands, allow simple modification in the catalytic system and in the resulting complex structures that translate into important variation in the oxidation selectivity exhibited by the catalysts.^{4b,c,17}

Finally, in presence of O₂, an activation mechanism in which two molecules of iron(II) complex react with O₂ to give two molecules of iron(IV)-oxo complex passing through a di-(μ-oxo)diiron(III) intermediate, was proposed.¹⁵

The nonheme iron(IV) or iron(V)-oxo active species have been demonstrated to mimic the enzymatic activity being able to promote a wide range of oxidative processes such as aliphatic and aromatic hydroxylation, *N*-, *O*-, *S*-oxidation, dealkylation and olefin epoxidation with high regio- and stereoselectivity (Figure 4).^{4b}

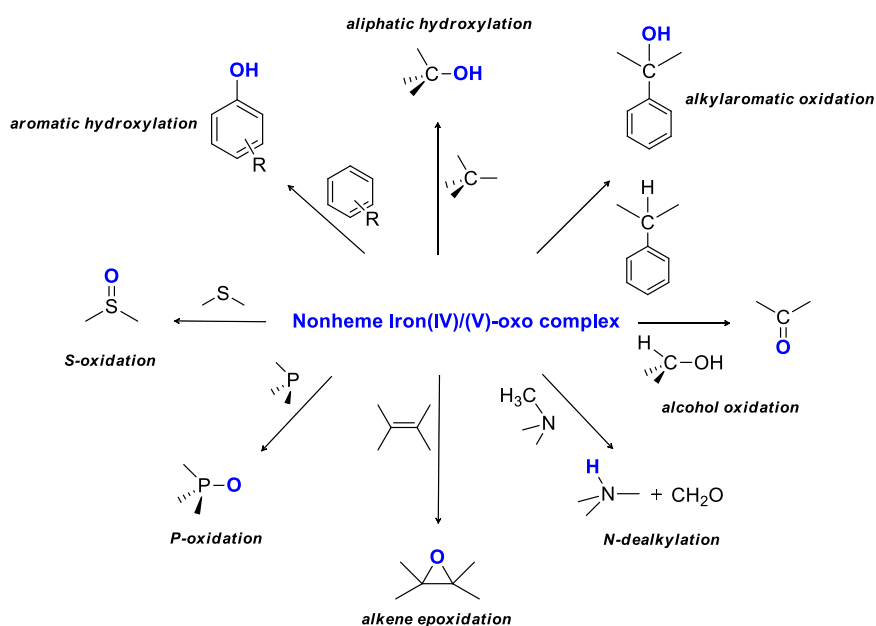


Figure 4. Oxidation reactions mediated by mononuclear nonheme iron(IV) and iron(V)-oxo complexes.

One of the main challenge in developing catalysts with H₂O₂ as terminal oxidant, is to identify reaction conditions that minimize the production of free radicals and generate a more selective metal-based mechanism. Several mechanistic criteria have been carried out to discern between free radicals and metal based oxidation processes. Intermolecular kinetic isotope effect determined by competitive oxidation of a hydrocarbon and its deuterated counterparts, can be used to identify the active species responsible for the oxidation process. Indeed, hydroxyl radicals do not discriminate between C-H and C-D bond strengths, yielding KIE values between 1 and 2.22 so higher values (from about 3 up to 48) are typical for metal-based oxidants.^{5a,18} Alcohol/ketone ratio (A/K) in the oxidation of cyclohexane or cyclooctane is close to 1 in presence of a radical chain mechanism due to Russel-type terminations while is higher (> 5) in a metal-based process.^{13a,18,19} A high degree of regio- and stereoselectivity is characteristic for a metal-based oxidation. Thus, high ratio of tertiary over secondary C-H bond oxidation products (3°/2° ratio) is expected in the oxidation of adamantane moreover a high retention of configuration (>90%) should be expected in the hydroxylation of *cis*-1,2-dimethylcyclohexane.¹⁸ Labelling experiments provide information about the origin of the O atom present in the products: if the ¹⁸O-atom comes from the oxidant or from adventitious water, a metal-oxo species should be involved.^{19a,20}

Many efforts have been devoted to the comprehension of the catalytic mechanism and to the identification of the intermediates competent for the oxidative transformations. Besides the importance in the rational design of new catalysts with superior activity and predictability, the knowledge of the catalytic mechanism and of the active species involved, are important to understand the oxidation pathways for iron oxygenases.^{3c,4,21} The selectivity exhibited in these reactions supports a metal-based mechanism rather than a radical one assisted by a OH•.¹⁸

Que and co-workers fully characterized the (TPA)Fe^{III}-OOH intermediate (sluggish oxidant)²¹ generated upon reaction of (TPA)Fe^{II} with an excess of H₂O₂ at -40 °C in CH₃CN, as well as the incorporation of ¹⁸O into the oxidation products from H₂¹⁸O.^{19a,21a,22} These results suggested the incorporation of H₂¹⁸O into a metal-based intermediate that later underwent a heterolytic cleavage of the O-O assisted by bound water to form an elusive Fe^V(O)(OH) oxidant (Figure 5). Further direct spectroscopic evidence for the putative Fe^V(O)(OH) oxidant was obtained by

Costas and Cronin from variable temperature electrospray mass spectrometric experiments with their catalyst $[(\text{Me}_2\text{PyTACN})\text{Fe}^{\text{II}}(\text{OTf})_2]$ (see Figure 3).²³

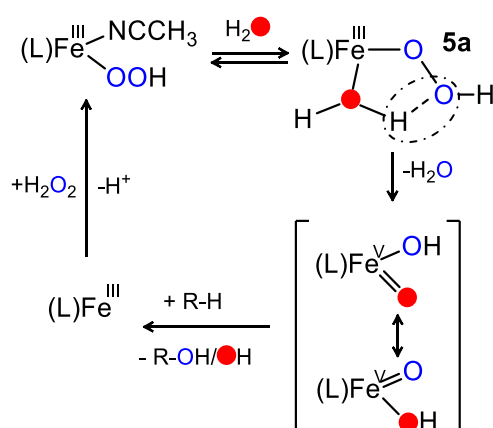


Figure 5. Proposed mechanism for the water-assisted activation of H_2O_2 by nonheme iron oxidation catalysts.

Similar activation mechanism has been proposed also for other tetradentate ligand based complexes with two *cis* labile sites, while pentadentate ligand based complexes in presence of hydroperoxides such as H_2O_2 , undergo a homolytic cleavage of O-O bond in $\text{Fe}(\text{III})\text{-OOR}$ (see Scheme 3).^{19a,24-26} By contrast, in most cases, pentadentate complexes in the presence of single-oxygen atom donors as PhIO , show metal-based mechanism promoted by $\text{Fe}(\text{IV})=\text{O}$.

As first noted by White and Jacobsen in 2001,²⁷ the introduction of AcOH in the catalytic system, can increase both the yields, the selectivity and eventually the enantioselectivities^{6e,g,28,29} (for asymmetric reactions) in olefin or C-H oxidations.^{5f} These results demonstrate that the carboxylate moiety can significantly affect the selectivity-determining step and therefore must be bound to the metal-based oxidant. Parallel investigation, performed to understand the role of water, have been carried out to explain the remarkable role of the AcOH in the iron-catalyzed oxidations. Accordingly, a similar mechanism assisted by carboxylic acid, where the metal-bound AcOH replaces the metal-bound water, has been proposed (Figure 6).

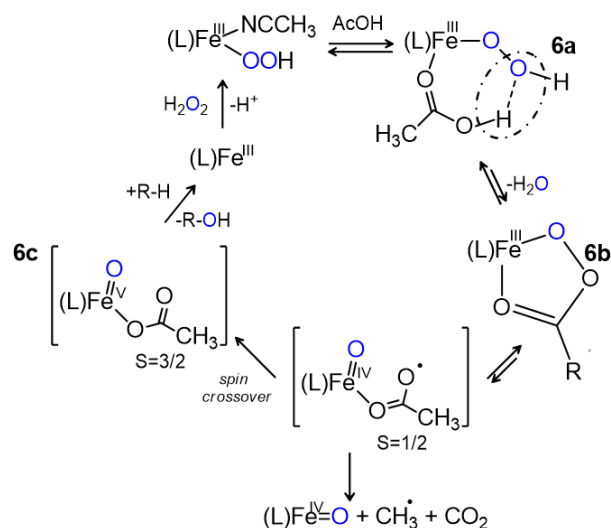


Figure 6. Proposed mechanism for the AcOH-assisted activation of H₂O₂ by nonheme iron oxidation catalysts.

The AcOH adduct **6a** formation is followed by a O-O bond heterolysis that generates a hypothetical Fe^V(O)(O₂CR) oxidant.³⁰ Que and co-worker, by replacing the TPA ligand with its more electron-donating TPA* (Figure 7), were able to characterize the low-spin acylperoxo iron(III) complex **6b*** by UV-Vis, Mössbauer, resonance Raman and electrospray mass spectrometric methods.³¹

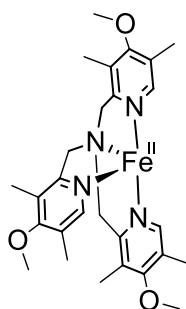


Figure 7. Structure of [(TPA*)Fe]²⁺.

This intermediate then undergoes, in a rate determining step, O-O bond cleavage forming an S=1/2 Fe^{IV}(O)(•OC(O)R) species which can convert by spin crossover to an S=3/2

$\text{Fe}^{\text{V}}(\text{O})(\text{OAc})$ active species.³² The species **6b***, can also be formed in comparable yields in the reactions of $[(\text{TPA}^*)\text{Fe}]$ with AcO_2H at $-40\text{ }^\circ\text{C}$.³¹

In contrast with the stability of $\text{Fe}(\text{IV})$ -oxo complexes that allows their full characterization, formation of $\text{Fe}(\text{V})$ -oxo complex is still controversial. The strong instability due to the high iron valence, did not allow, until now, the isolation and characterization of this interesting active species.

As outlined before, in comparison with the extensively studied nonheme iron complexes, less information are available on the mechanism and characterization of the oxidizing species for the manganese systems, despite an increasing attention to the design and the application of new highly efficient and selective manganese catalysts in the last few years.^{4c,6b,c} For the most promising Mn-catalytic systems containing tetradentate aminopyridine ligands, information on the structure and the reactivity of the active species is rather limited and the mechanistic conclusions are mainly supported by product analysis and kinetic data. Several X-ray structures for peroxo- or oxo-manganese complexes have been published, however very often are linked to relatively inert model systems.³³

Furthermore, characterization of $\text{Mn}(\text{III})$ hydroperoxo complexes is more complicated because they do not display characteristic EPR and UV-Vis signals and the synthetic $\text{Mn}^{\text{IV}}=\text{O}$ complexes with nonheme ligands demonstrate a much smaller oxidation reactivity in contrast to the iron analogs. The only exception, reported by Nam, is represented by $[(\text{BnTPEN})\text{Mn}^{\text{IV}}=\text{O}]^{2+}$ (see Figure 3 for the ligand structure) that showed a high reactivity in the oxidation of various substrates such as olefins, sulfides and aromatic compounds.³⁴ To date, interesting results have been obtained in the asymmetric alkene oxidation (*ee* up to 99%) with nonheme tetradentate aminopyridine Mn complexes like those reported in Figure 8.^{6f,1}

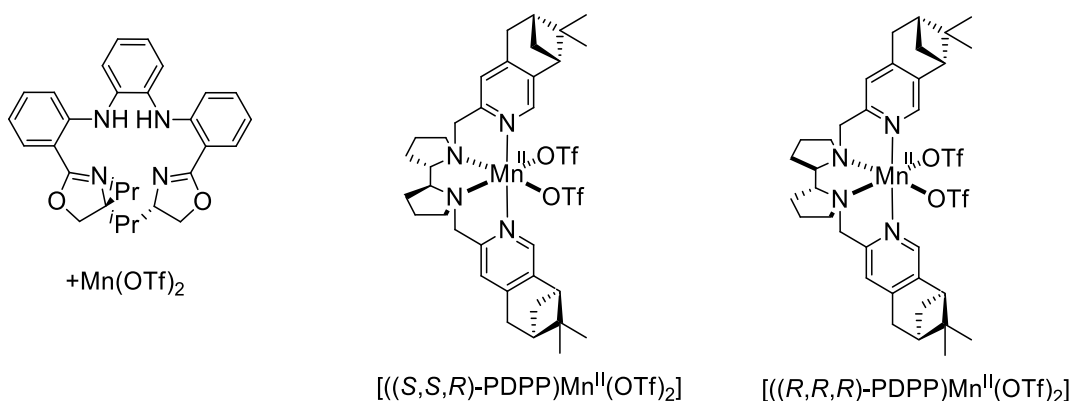


Figure 8. Nonheme Mn based asymmetric alkene oxidation catalysts.

Furthermore, the three catalysts shown in Figure 9 demonstrated unprecedented high selectivity and stereospecificity in presence of H₂O₂ and AcOH in the oxidation of aliphatic C-H bonds.^{6h}

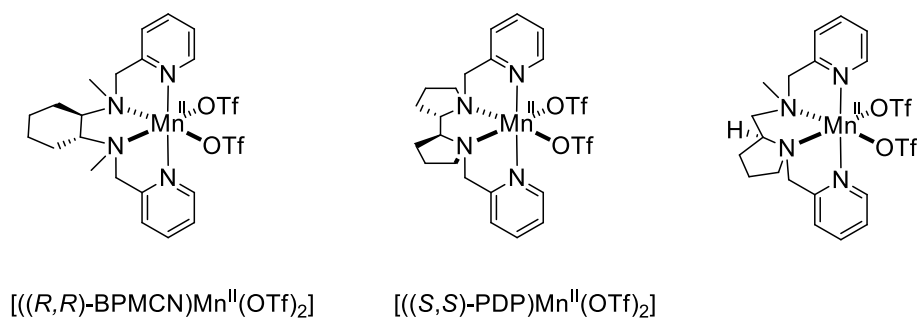


Figure 9. Nonheme Mn based aliphatic C-H oxidation catalysts.

Despite mechanistic data are very scarce, it is suggested that the active species in the catalytic systems $[(L)\text{Mn}^{\text{II}}]^{2+}/\text{H}_2\text{O}_2/\text{RCOOH}$ are manganese(V)-oxo intermediates $[(L)\text{Mn}^{\text{V}}=\text{O}(\text{OCOR})]^{2+}$ that are generated with a ‘water-assisted’ or ‘carboxylic acid-assisted’ mechanisms similar to those described for iron systems.^{6g,i,l}

Studies on nonheme amine based iron and manganese catalysts have been paralleled, in recent years, by investigations on nonheme imine based catalysts.³⁵ However, the latter have received less attention probably due to the idea that imines (or Schiff bases) are not robust enough to tolerate the typical oxidation conditions because they are generally subjected to hydrolysis and oxidation to amides. Catalytic activity is correlated with the stability of the complex, indeed the more stable is the catalyst, the higher is its activity.²⁶ Any ligand degradation causes a possible release of the metal ion with subsequent catalyst deactivation and trigger of radical reactions. Both degradation pathways have been observed, indeed, in a vast array of amine, amina and imine containing manganese catalytic systems by Browne’s group.³⁶ Notwithstanding a significant structural diversity, all the catalysts investigated displayed a very similar catalytic activity and selectivity. A closer investigation revealed that all these ligands oxidatively degrade to Mn(II)/picolinic acid complexes in the reaction conditions and this latter

species is responsible for the catalytic activity observed. To date, a large number of imine catalysts operate through a free-radical based mechanism, however some strategies have been developed to overcome the tendency of imine ligand systems to undergo degradation as the reinforcement of the ligand to metal binding. Thanks to these appropriate precautions, several imine-based complexes, described below, have been found to be stable enough to serve as oxidation catalysts and in many cases, the related imine ligands present the significant advantage of a much easier synthesis.^{35,37} Sometimes, both the ligand structure and the complex can be self-assembled directly *in situ* from simple building blocks, eliminating the need of pre-synthesizing the catalyst.^{35,37b}

Feringa and coworkers, for instance, investigated a series of tetradentate imino-pyridine iron complexes in the oxidation of ethylbenzene with H₂O₂ or O₂ as the terminal oxidant³⁸ and obtained the best results with H₂O₂ with Fe^{II} complexes of iminopyridine ligands bearing a 1,2-diimino motif (Figure 10, L₁, L₂). The A/K ratios (5.6-6.1) pointed to a metal-based reaction mechanism and the oxidation yields are dependent on the aromatic substituents (an increase in the electron density enhances the activity).

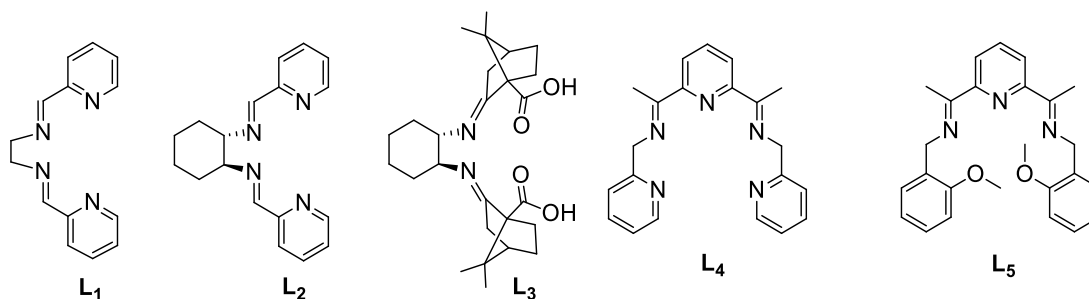


Figure 10. Example of imine based ligands promoting metal-based mechanism.

The tetradentate complex of Mn with ligand L₃ shown in Figure 10 was also found to catalyze the oxidation of activated C-H bonds with ^tBuOOH as the terminal oxidant in good to high yields (52-91%).³⁹ Furthermore the pentadentate iminopyridine iron complexes (Figure 11, L₄, L₅) and its related μ -oxo Fe^{III} dimer, act as C-H oxidation catalysts showing a metal-based mechanism.^{40,41}

Aim of the work

Over the last decades, there has been an extensively attention not only for the design and the synthetic application of new efficient and selective iron and manganese nonheme complexes, but also for the knowledge of the mechanistic details of these catalysts, including the isolation and characterization of the intermediates involved in the catalytic cycle. However several issues still hamper the application and the knowledge of these catalytic systems. In this thesis, some aspects related to the mechanistic analysis and catalytic activity of nonheme complexes have been investigated.

- In Chapter 2 an innovative approach consisting in the simultaneously use of time-resolved Energy Dispersive X-Ray Absorption (EDXAS) and UV/Vis spectroscopies with millisecond resolution, is tested. Excellent results have been obtained to follow the evolution of the oxidation state and of the local structure around the metal center in the oxidation of well known complex, $[(\text{TPA})\text{Fe}^{\text{II}}(\text{CH}_3\text{CN})_2]^{2+}$, with H_2O_2 and CH_3COOOH .

The remarkable variety of the oxidative processes promoted by nonheme iron and manganese complexes with high regio- and stereoselectivity, prompted us to employ three different nonheme catalytic systems (aminopyridine iron complexes, imine iron complexes and aminopyridine supramolecular iron and manganese complexes) in the oxidation of sulfides, alcohols, aromatic and aliphatic hydrocarbons.

- In Chapter 3 is described the studies aimed to solve the mechanistic dichotomy between a direct oxygen transfer and an electron transfer-oxygen rebound mechanism in the oxidation of a series of aryl sulfides (aryl 1-methyl-1-phenylethyl sulfides and aryl diphenylmethyl sulfides) catalyzed by two tetradentate ($[(\text{PDP})\text{Fe}^{\text{II}}(\text{SbF}_6)_2]$ and $[(\text{BPMC})\text{Fe}^{\text{II}}(\text{OTf})_2]$) and two pentadentate ($[(\text{N4Py})\text{Fe}^{\text{II}}(\text{OTf})_2]$ and $[(\text{Bn-TPEN})\text{Fe}^{\text{II}}(\text{OTf})_2]$) aminopyridine nonheme iron complexes.

- In Chapter 4 is studied the synthetic application of an iminopyridine iron(II) complex, easily prepared *in situ* by self-assembly of cheap and commercially available starting materials (2-picolylaldehyde, 2-picolylamine, and Fe(OTf)₂) in a 2:2:1 ratio in the oxidation of alcohols and aromatic compounds.

- In Chapter 5 the inhibition process of the Mn^{II}/PCA/butanedione catalytic system by catechol and guaiacol substrates has been studied in relation to the low efficiency of this catalytic system in the oxidation of electron rich benzylic alcohols.

- In Chapter 6 is presented a supramolecular and bioinspired approach to achieve site-selective C-H functionalization on C8 and C9 methylene positions of linear protonated primary amines thanks to reversible pre-association between ammonium moiety and the benzo-18-crown-6 ether used as receptor in the catalyst.

References

- (1) (a) J. T. Groves, *J. Inorg Biochem.*, **2006**, *100*, 434-447. (b) B. Meunier, S. P. De Visser, S. Shaik, *Chem. Rev.*, **2004**, *104*, 3947-3980. (c) I. G. Denisov, T. M. Makris, S. G. Sliger, I. Schlichting, *Chem. Rev.*, **2005**, *105*, 2253.
- (2) (a) M. Costas, M. P. Mehn, M. P. Jensen, L. Que Jr., *Chem. Rev.*, **2004**, *104*, 939-986. (b) C. Krebs, D. G. Fujimori, C. T. Walsh, M. Bollinger Jr., *Acc. Chem. Res.*, **2007**, *40*, 484-492. (c) P. C. A. Bruijninx, G. van Koten, R. J. M. Klein Gebbnk, *Chem. Soc. Rev.*, **2008**, *37*, 2716-2744.
- (3) (a) B. Meunier, *Chem. Rev.*, **1992**, *92*, 1411. (b) W. Nam *In Comprehensive Coordination Chemistry II*; L. Que Jr., W. Tolman, Vol. Eds.; J. A. McCleverty, T. J. Meyer, Series Eds.; Elsevier: San Diego, **2004**, *8*, 281-307. (c) W. Nam, *Acc. Chem. Res.*, **2007**, *40*, 522-531.
- (4) (a) L. Que Jr., *Acc. Chem. Res.* **2007**, *40*, 493-500. (b) W. Nam, Y.-M. Lee, S. Fukuzumi, *Acc. Chem. Res.*, **2014**, *47*, 1146-1154. (c) K. P. Bryliakov, E. P. Talsi, *Coord. Chem. Rev.*, **2014**, *276*, 73-96. (d) A. R. McDonald, L. Que Jr., *Coord. Chem. Rev.*, **2013**, *257*, 414-428.

- (5) For Fe complex: (a) L. Que, W. B. Tolman Jr., *Nature*, **2008**, *455*, 333-340. (b) M. Costas, *Coord. Chem. Rev.*, **2011**, *255*, 2912-2932. (c) P. Liu, Y. Liu, E. L. M. Wong, S. Xiang, C. M. Che, *Chem. Sci.*, **2011**, *2*, 2187-2195. (d) C. Pavan, J. Legros, C. Bolm, *Adv. Synth. Catal.*, **2005**, *347*, 703-705. (e) J. England, G. J. P. Britovsek, N. Rabadia, A. J. P. White, *Inorg Chem.*, **2007**, *46*, 3752-3767. (f) M. S. Chen, M. C. White, *Science*, **2010**, *327*, 566-571. (g) A. Company, L. Gómez, X. Fontrodona, X. Ribas, M. Costas, *Chem. Eur. J.*, **2008**, *14*, 5727-5731. (h) L. Gómez, I. Garcia-Bosch, A. A. Company, J. Benet-Buchholz, A. Polo, X. Sala, X. Ribas, M. Costas, *Angew. Chem. Int. Ed.* **2009**, *48*, 5720-5723. (i) T. Niwa, M. Nakada, *J. Am. Chem. Soc.*, **2012**, *134*, 13538-13541. (l) I. Prat, D. Font, A. Company, K. Junge, X. Ribas, M. Beller, M. Costas, *Adv. Synth. Catal.*, **2013**, *355*, 947-956.
- (6) For Mn complex (a) J. W. De Boer, J. Brinksma, W. R. Browne, A. Meetsma, P L. Alsters, R. Hage, B. L. Feringa, *J. Am. Chem. Soc.*, **2005**, *127*, 7990-7991. (b) E. P. Talsi, K. P. Bryliakov, *Coord. Chem. Rev.*, **2012**, *256*, 1418-1434. (c) P. Saisaha, J. W. de Boer, W. R. Browne, *Chem. Soc. Rev.*, **2013**, *42*, 2059-2074. (d) M. Wu, S. Wang, C. Xia, W. Sun, *Org. Lett.*, **2009**, *11*, 3622-3625. (e) B. Wang, C. Miao, S. Wang, C. Xia, W. Sun, *Chem. Eur. J.*, **2012**, *18*, 6750-6753. (f) I. Garcia-Borsch, L. Gómez, A. Polo, X. Ribas, M. Costas, *Adv. Synth. Catal.*, **2012**, *354*, 65-70. (g) O. Y. Lyakin, R. V. Ottenbacher, K. P. Bryliakov, E. P. Talsi, *ACS Catal.*, **2012**, *2*, 1196-1202. (h) R. V. Ottenbacher, D. G. Samsonenko, E. P. Talsi, K. P. Bryliakov, *Org. Lett.*, **2012**, *14*, 4310-4313. (i) R. V. Ottenbacher, D. G. Samsonenko, E. P. Talsi, K. P. Bryliakov, *ACS Catal.*, **2014**, *4*, 1599-1606. X. (l) X. Wang, C. Miao, S. Wang, C. Xia, W. Sun, *ChemCatChem*, **2013**, *5*, 2489-2494.
- (7) Y. Ashikawa, Z. Fujimoto, Y. Usami, K. Inoue, H. Noguchi, H. Yamane, H. Nojiri, *BMC Struct. Biol.*, **2012**, *12*, 15.
- (8) J. D. Lipscomb, L. Que Jr., *J. Biol. Inorg. Chem.*, **1998**, *3*, 331-336.
- (9) J. T. Groves, G. McClusky, *J. Am. Chem. Soc.*, **1976**, *98*, 859-861.
- (10) (a) M. H. Lim, J.-U. Rohde, A. Stubna, M. R. Bukowski, M. Costas, R. Y. N. Ho, E. Münck, W. Nam, L. Jr. Que, *Proc. Natl. Acad. Sci. U.S.A.* **2003**, *100*, 3665-3670. (b) J.-U. Rohde, J.-H. In, M. H. Lim, W. W. Brennessel, M.R. Bukowski, A. Stubna, E. Münck, W. Nam, L. Que Jr., *Science*, **2003**, *299*, 1037-1039. (c) V. Balland, M.-F. Charlot, F. Banse, J.-J. Girerd, T. A. Mattioli, E. Bill, J.-F. Bartoli, P. Battioni, D. Mansuy, *Eur. J. Inorg. Chem.*, **2004**, 301-308. (d) M.P. Jensen, M. Costas, R.Y.N. Ho, J. Kaizer, A. Mairatai Payeras, E. Münck, L. Que Jr., J.-U. Rohde, A. Stubna, *J. Am. Chem. Soc.*, **2005**, *127*, 10512-10525. (e) M. R. Bukowski,

- K. D. Koehntop, A. Stubna, E. L. Bominaar, J. A. Halfen, E. Münck, W. Nam, L. Que Jr., *Science*, **2005**, *310*, 1000-1002. (f) T. P. Paine, M. Costas, J. Kaizer, L. Que Jr., *J. Biol. Inorg. Chem.*, **2006**, *11*, 272-276.
- (11) C. Kim, K. Chen, J. H. Kim, L. Que Jr., *J. Am. Chem. Soc.*, **1997**, *119*, 5964-5965.
- (12) J. Kaizer, M. Costas, L. Que Jr., *Angew. Chem. Int. Ed.*, **2003**, *42*, 3671-3673.
- (13) (a) J. Kaizer, E. J. Klinker, N. Y. Oh, J.-U. Rohde, W. J. Song, A. Stubna, J. Kim, E. Münck, W. Nam, L. Que Jr., *J. Am. Chem. Soc.*, **2004**, *126*, 472-473. (b) C. V. Sastri, M. S. Seo, M. J. Park, K. M. Kim, W. Nam, *Chem. Commun.*, **2005**, 1405-1407.
- (14) O. Pestovsky, S. Stoian, E. L. Bominaar, X. Shan, E. Münck, L. Que Jr., A. Bakac, *Angew. Chem. Int. Ed.*, **2005**, *44*, 6871-6874.
- (15) S. O. Kim, C. V. Sastri, M. S. Seo, J. Kim, W. Nam, *J. Am. Chem. Soc.*, **2005**, *127*, 4178-4179.
- (16) M. S. Seo, T. Kamachi, T. Kouno, K. Murata, M. J. Park, K. Yoshizawa, W. Nam, *Angew. Chem. Int. Ed.*, **2007**, *46*, 2291-2294.
- (17) G. Olivo, O. Cussò, M. Costas, *Chem. - An Asian J.*, **2016**, *11*, 3148-3158.
- (18) M. Costas, K. Chen, L. Que Jr., *Coord. Chem. Rev.*, **2000**, 200-202, 517-544.
- (19) (a) K. Chen, L. Que Jr., *J. Am. Chem. Soc.*, **2001**, *123*, 6327-6337. (b) P. A. MacFaul, K. U. Ingold, D. D. M. Wayner, L. Que Jr., *J. Am. Chem. Soc.* **1997**, *119*, 10594-10598.
- (20) Bernadou, J.; Meunier, B. *Chem. Commun.*, **1998**, 2167-2173.
- (21) (a) W. N. Oloo, A. J. Fielding, L. Que Jr., *J. Am. Chem. Soc.*, **2013**, *135*, 6438-6441. (b) K. Ray, F. F. Pfaff, B. Wang, W. Nam, *J. Am. Chem. Soc.*, **2014**, *136*, 13942-13958.
- (22) K. Chen, M. Costas, J. H. Kim, A. K. Tipton, L. Que Jr., *J. Am. Chem. Soc.*, **2002**, *124*, 3026-3035.
- (23) I. Prat, J. S. Mathieson, M. Guell, X. Ribas, J. M. Luis, L. Cronin, M. Costas, *Nat. Chem.*, **2011**, *3*, 788-793.
- (24) K. Chen, M. Costas, L. Que, Jr., *J. Chem. Soc. Dalton Trans.*, **2002**, 672-679.
- (25) G. J. P. Britovsek, J. England, A. J. P. White, *Inorg. Chem.*, **2005**, *44*, 8125-8134.
- (26) J. England, C. R. Davies, M. Banaru, A. J. P. White, G. J. P. Britovsek, *Adv. Synth. Catal.*, **2008**, *350*, 883-897.
- (27) M. C. White, A. G. Doyle, E. N. Jacobsen, *J. Am. Chem. Soc.*, **2001**, *123*, 7194-7195.
- (28) O. Cussó, X. Ribas, J. Lloret-Fillol, M. Costas, *Angew. Chem. Int. Ed.*, **2015**, *54*, 2729-2733.

- (29) O. Cussó, I. Garcia-Bosch, X. Ribas, J. Lloret-Fillol, M. Costas, *J. Am. Chem. Soc.*, **2013**, *135*, 14871-14878.
- (30) R. Mas-Ballesté, L. Que Jr., *J. Am. Chem. Soc.*, **2007**, *129*, 15964-15972.
- (31) W. N. Oloo, K. K. Meier, Y. Wang, S. Shaik, E. Münck, L. Que Jr., *Nat. Commun.*, **2014**, *5*, 3046.
- (32) W. N. Oloo, L. Que Jr., *Acc. Chem. Res.*, **2015**, *48*, 2612-2621.
- (33) (a) R. B. VanAtta, C. E. Strouse, L. K. Hanson, J. S. Valentine, *J. Am. Chem. Soc.*, **1987**, *109*, 1425-1434. (b) N. Kitajima, H. Komatsuzaki, S. Hikichi, M. Osawa, Y. Moro-oka, *J. Am. Chem. Soc.*, **1994**, *116*, 11596-11597. (c) R. I. Shook, W. A. Gunderson, J. Greaves, J. W. Ziller, M. P. Hendrich, A. S. Borovik, *J. Am. Chem. Soc.*, **2008**, *130*, 8888-8889. (d) M. K. Coggins, J. A. Kovacs, *J. Am. Chem. Soc.*, **2011**, *133*, 12470-12473. (e) T. J. Collins, S. W. Gordon-Wylie, *J. Am. Chem. Soc.*, **1989**, *111*, 4511-4513. (f) T. J. Collins, R. D. Powell, C. Slebodnick, E. S. Uffelman, *J. Am. Chem. Soc.*, **1990**, *112*, 899-901.
- (34) X. Wu, M. S. Seo, K. M. Davis, Y. M. Lee, J. Chen, K. B. Cho, Y. N. Pushkar, W. Nam, *J. Am. Chem. Soc.*, **2011**, *133*, 20088-20091.
- (35) G. Olivo, O. Lanzalunga, S. Di Stefano, *Adv. Synth. Catal.*, **2016**, *358*, 843-863.
- (36) D. Pijper, P. Saisaha, J. W. de Boer, R. Hoen, C. Smit, A. Meetsma, R. Hage, R. P. van Summeren, P. L. Alsters, B. L. Feringa, W. R. Browne, *Dalton Trans.*, **2010**, *39*, 10375-10381.
- (37) (a) M. Ciaccia, S. Di Stefano, *Org. Biomol. Chem.*, **2015**, 646-654. (b) G. Olivo, G. Arancio, L. Mandolini, O. Lanzalunga, S. Di Stefano, *Catal. Sci. Technol.*, **2014**, *4*, 2900-2904. (c) B. Retcher, J. S. Costa, J. Tang, R. Hage, P. Gamez, J. Reedijk, *J. Mol. Catal. A Chem.*, **2008**, *286*, 1-5.
- (38) M. Klopstra, R. Hage, R. M. Kellogg, B. L. Feringa, *Tetrahedron Lett.*, **2003**, *44*, 4581-4584.
- (39) J. F. Pan, K. Chen, *J. Mol. Catal. A Chem.*, **2001**, *176*, 19-22.
- (40) S. Tanase, J. Reedijk, R. Hage, G. Rothenberg, *Top. Catal.*, **2010**, *53*, 1039-1044.
- (41) J. Tang, P. Gamez, J. Reedijk, *Dalton Trans.* **2007**, 4644-4646.

Chapter 2

Analysis of the ms timescale evolution of nonheme iron complexes oxidation by simultaneous X-Ray and UV/Vis spectroscopies

In this chapter an innovative approach aimed at disclosing the mechanism of the oxidation of a nonheme iron catalyst, $[(\text{TPA})\text{Fe}^{\text{II}}(\text{CH}_3\text{CN})_2]^{2+}$, occurring in solution in the ms time-scale, is presented. Time-resolved Energy Dispersive X-Ray Absorption and UV/Vis spectroscopies with millisecond resolution, are used simultaneously to directly follow the evolution of the oxidation state and the local structure of the metal center in the oxidation of the $[(\text{TPA})\text{Fe}^{\text{II}}(\text{CH}_3\text{CN})_2]^{2+}$ complex with H_2O_2 and CH_3COOOH . The former process involves the transformation of a Fe^{II} into two subsequent Fe^{III} species, while in the latter process a more complicate $\text{Fe}^{\text{II}}\text{-Fe}^{\text{III}}\text{-Fe}^{\text{IV}}\text{-Fe}^{\text{III}}$ sequence has been observed. The combined XAS - UV/Vis spectroscopic analysis has the potential to provide unique insights into reaction mechanisms in the liquid phase and represents a new powerful tool to characterize short-lived intermediates which are silent to common spectroscopic techniques.

Part of this work was carried out at the European Synchrotron Radiation Facility (Grenoble, France) under the supervision of Dr. Sakura Pascarelli

The results reported in this Chapter are published in:

G. Olivo, A. Barbieri, V. Dantignana, F. Sessa, V. Migliorati, M. Monte, S. Pascarelli, T. Narayanan, O. Lanzalunga, S. Di Stefano and P. D'Angelo, *J. Phys. Chem. Lett.*, **2017**, 8 (13), 2958-2963.

2.1 Introduction

The precise assignment of transient intermediates is of fundamental importance to elucidate mechanistic reaction pathways. Chemical reactions occur on a very large range of timescales, therefore it is necessary to find a proper technique that allows the detection of transient species.

Elementary steps involving valence-electron dynamics and single-bond rearrangements usually take place on femtosecond to picosecond timescales while bimolecular processes, including for instance redox reactions in liquid solution, occur on longer timescales (nano, micro, milliseconds and above). Several methods have been developed in the last decades to analyze the electronic and structural evolution involved in ultrafast chemical processes such as short-pulsed laser systems, time resolved methods using infrared and Raman spectroscopy,^{1,2} electron diffraction,^{3,4} X-Ray based techniques at synchrotrons (X-Ray diffraction^{5,6} and X-Ray absorption⁷⁻¹⁰) and X-Ray free electron laser.¹¹ On the contrary time-resolved structural dynamics techniques suitable to investigate processes involving cleavage and formation of covalent bonds in the millisecond timescale are less applied due to the rather demanding experimental setup. Our idea was to combine, for the first time, time-resolved energy dispersive X-Ray absorption spectroscopy (EDXAS) with UV/Vis spectroscopy to directly characterize the intermediates formed during a chemical reaction, by monitoring the structural and electronic changes occurring in solution in the millisecond (ms) timescale. UV/Vis spectroscopy is one of the most used technique to follow the electronic variations associated with a chemical transformation over a wide range of reaction times, but despite this, it can give only limited information on the structure of the reactive species. On the other hand, X-Ray absorption spectroscopy (XAS) is a very sensitive probe of both the local structure and oxidation state of an absorbing atom during a chemical reaction, but is generally used to characterize isolated intermediates in biological as well as in synthetic reactions. The combination of UV/Vis and time resolved XAS spectroscopies, thus, represents a new powerful strategy to provide essential mechanistic insights.

As reported in Chapter 1, the high regio- and stereoselectivity in oxidative processes promoted by bioinspired nonheme iron catalysts in association with the environmentally friendly terminal

oxidants H₂O₂,¹²⁻¹⁷, has prompted a great effort to elucidate the reaction mechanism of the oxidations of hydrocarbons, olefins, alcohols, etc. The key feature of such mechanisms lies in a controlled O-O bond activation that, without generation of free-diffusing radical intermediates (which undermines the oxidation selectivity), closely resembles the pathway observed in heme and nonheme iron oxygenases in nature.¹⁸⁻²⁴ The oxidation mechanism involves changes in the iron oxidation states during the catalytic cycle (from Fe^{II} up to Fe^{IV} or Fe^V) and is characterized by the formation of key intermediates that are very often elusive to conventional spectroscopies.¹⁸⁻²⁸

Fe^{II}(tris(2-pyridylmethyl)amine), [(TPA)Fe^{II}(CH₃CN)₂]²⁺ is probably one of the most widely investigated nonheme iron complexes and a lot of information about the iron oxidation state evolution during the catalytic cycle in presence of several terminal oxidants, are available in the literature.^{18,19,22,24,27,29} For this reason [(TPA)Fe^{II}(CH₃CN)₂]²⁺ represents a suitable nonheme iron complex probe to exploit the potentiality of our simultaneous EDXAS-UV/Vis technique in elucidating the structural and oxidation state evolution in the course of a chemical reaction in ms time-scale.

2.2 Results and Discussion

Time resolved EDXAS and UV/Vis spectroscopies have been combined to follow the oxidation of [(TPA)Fe^{II}(CH₃CN)₂]²⁺ in a stopped-flow apparatus that allowed fast injection of the reagents in the reaction cell. The principle of EDXAS is based on measuring the transmitted intensity from the sample and therefore the concentration of the photo absorber, in our case the iron present in the complex, has to be high enough for its detection in the transmission mode (> 30 mM). These concentrations would not seem compatible with UV/Vis detection, unless the reaction evolution is followed monitoring the spectral changes on the peak tails.

In order to assess the feasibility and reliability of the EDXAS experiment in the stopped flow cell, we compared the Fe K-edge EDXAS spectrum of a 35 mM solution of [(TPA)Fe^{II}(CH₃CN)₂]²⁺ in CH₃CN, collected in 40 ms in the stopped flow cell, with the spectrum collected on the same sample in transmission mode in 40 minutes on a standard XAS beamline. As shown in Figure 1, the two spectra are perfectly superimposable.

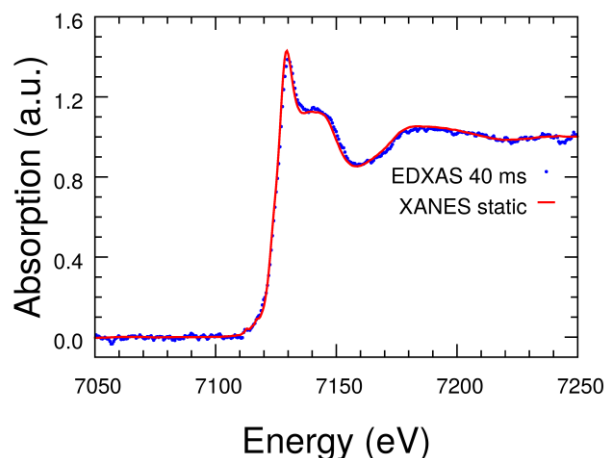


Figure 1. Comparison of the EDXAS spectrum of $[(\text{TPA})\text{Fe}^{\text{II}}(\text{CH}_3\text{CN})_2]^{2+}$ 35 mM in CH_3CN at 25 °C collected in 40 ms in the stopped flow cell with the XANES spectrum of the same compound collected in transmission mode in 40 min.

The reactions chosen to test the potentiality of our simultaneous EDXAS-UV/Vis technique in ms time-scale, are based on two different oxidative processes of $[(\text{TPA})\text{Fe}^{\text{II}}(\text{CH}_3\text{CN})_2]^{2+}$ with the two distinct terminal oxidants, namely H_2O_2 and peracetic acid ($\text{CH}_3\text{COO}_2\text{H}$).

In Figure 2A the evolution of the EDXAS spectra during the reaction of $[(\text{TPA})\text{Fe}^{\text{II}}(\text{CH}_3\text{CN})_2]^{2+}$ (35 mM) with H_2O_2 (70 mM) in $\text{CH}_3\text{CN}/\text{H}_2\text{O}$ 99.8:0.2 (v/v) at 25 °C is shown. The time resolved EDXAS spectra were recorded every 40 ms and the reaction was followed for 2 s. The normalized time resolved recorded X-Ray absorption near edge structure (XANES) spectra show both a fast increase of the Fe K-edge position in the first 104 ms and a modification of the structural oscillations, in accordance with an initial oxidation of Fe^{II} to Fe^{III} followed by a clear rearrangement of the local structure around the metal center, without further changes in the iron oxidation state.

The absorbance change at λ 524 nm, recorded simultaneously on the same reaction mixture, is shown in Figure 2B. The increase of absorbance at this wavelength, associated to the shift of the Fe K-edge position toward higher energy of 0.7 eV after 104 ms, points out a partial oxidation of the initial $[(\text{TPA})\text{Fe}^{\text{II}}(\text{CH}_3\text{CN})_2]^{2+}$ complex to $[(\text{TPA})\text{Fe}^{\text{III}}(\text{CH}_3\text{CN})(\text{OOH})]^{2+}$ species (λ_{max} 538 nm reported in literature).^{18,19,22,29} The subsequent absorbance decrease occurring between 104 and 704 ms, illustrates the conversion of such intermediate to the μ -oxo dimer $[(\text{TPA})_2\text{Fe}^{\text{III}}_2(\mu\text{-O})(\text{H}_2\text{O})_2]^{4+}$ as shown in Figure 2D and in accordance with the data

reported in literature.¹⁹ After 704 ms, no changes are observed neither in the EDXAS spectra nor in the visible absorbance at 524 nm, indicating that the reaction is completed. The XANES spectra collected at $t = 0, 104$ and 1984 ms are shown in Figure 2C with the edge region enlarged in the inset.

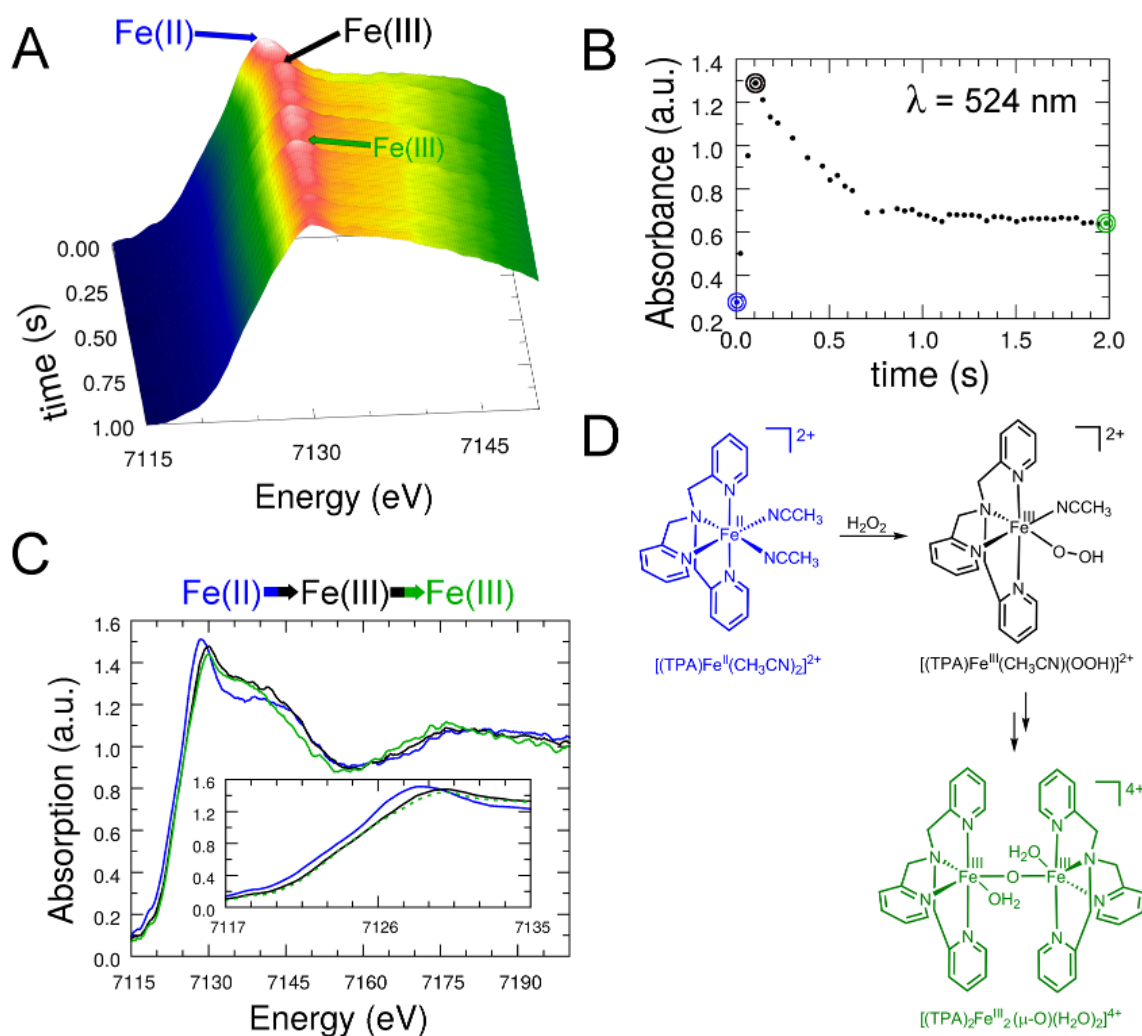


Figure 2 (A) Time evolution of the Fe K-edge EDXAS spectra of $[(\text{TPA})\text{Fe}^{\text{II}}(\text{CH}_3\text{CN})_2]^{2+}$ (35 mM) after addition of H_2O_2 (70 mM) in $\text{CH}_3\text{CN}/\text{H}_2\text{O}$ 99.8:0.2 (v/v) at 25°C . (B) Time evolution of the absorbance at λ 524 nm of the same reaction mixture of Figure 2A. EDXAS and UV/Vis spectra have been recorded simultaneously in the stopped-flow cell. (C) Selected EDXAS spectra of Figure 2A recorded at 0 ms (blue), 104 ms (black) and 1984 ms (green). A magnification of Fe K-edge region is shown in the inset. (D) Sequence of iron species compatible with the EDXAS-UV/Vis spectral evolution.

It can be noted that the XANES structural oscillations reported in Figure 2C are modified when an acetonitrile molecule coordinating the iron atom in $[(\text{TPA})\text{Fe}^{\text{II}}(\text{CH}_3\text{CN})_2]^{2+}$ is replaced by an oxygenated ligand in the $[(\text{TPA})\text{Fe}^{\text{III}}(\text{CH}_3\text{CN})(\text{OOH})]^{2+}$. The linear configuration of the acetonitrile molecule gives rise to strong multiple scattering contributions that decreases when one of the two acetonitrile molecules is replaced by a hydroperoxide ligand. The second step of the reaction does not involve any variation of the iron oxidation state as clearly shown by the position of the absorption edge that remains unchanged until the end of the reaction. However, the XANES oscillations around 7145 and 7170 eV move towards lower energies in the EDXAS spectra at the end of the reaction, pointing to an increase in the bond distance of some of the ligands. This is in agreement with the formation of a $[(\text{TPA})_2\text{Fe}^{\text{III}}_2(\mu\text{-O})(\text{H}_2\text{O})_2]^{4+}$ dimer where the iron atoms are connected through an oxygen bridge. In this case the higher frequency contribution could be due both to the presence of the Fe-Fe contact and to a slight increase of the Fe-O distances in the Fe-O-Fe configuration of $[(\text{TPA})_2\text{Fe}^{\text{III}}_2(\mu\text{-O})(\text{H}_2\text{O})_2]^{4+}$ as compared to the Fe-O and Fe-N distances in $[(\text{TPA})\text{Fe}^{\text{III}}(\text{OOH})(\text{CH}_3\text{CN})]^{2+}$. Therefore, the EDXAS and UV-Vis analysis fully confirms the mechanism proposed in literature for the oxidation of $[(\text{TPA})\text{Fe}^{\text{II}}(\text{CH}_3\text{CN})_2]^{2+}$ by H_2O_2 (Figure 2D).^{18,19,22,24,27,29}

In the presence of peroxyacetic acid the activation of the iron complex $[(\text{TPA})\text{Fe}^{\text{II}}(\text{CH}_3\text{CN})_2]^{2+}$ takes a different pathway leading to the generation of a relatively stable iron(IV)-oxo complex, $[(\text{TPA})\text{Fe}^{\text{IV}}(\text{O})]^{2+}$.²⁷ Therefore, a second reaction of $[(\text{TPA})\text{Fe}^{\text{II}}(\text{CH}_3\text{CN})_2]^{2+}$ (35 mM) and CH_3COOH (35 mM) as the oxidant, was carried out in $\text{CH}_3\text{CN}/\text{CH}_3\text{COOH}$ 99.6:0.4 (v/v) at 25 °C. Figure 3A shows the time-resolved XANES spectra collected each 40 ms during this reaction. The Fe K-edge position of the spectrum undergoes remarkable change during the reaction as reported in Figure 3C where the XANES spectra collected at $t = 0, 24, 264$ and 1964 ms are reported. The combination of EDXAS and UV/Vis techniques, allows us to follow the evolution of $[(\text{TPA})\text{Fe}^{\text{II}}(\text{CH}_3\text{CN})_2]^{2+}$ in the oxidative process. The first edge shift ($t = 24$ ms) of 0.7 eV has been indeed associated to the oxidation of $[(\text{TPA})\text{Fe}^{\text{II}}(\text{CH}_3\text{CN})_2]^{2+}$ to a first intermediate $[(\text{TPA})\text{Fe}^{\text{III}}(\kappa^2\text{-OOAc})]^{2+}$ (Figure 3D, path a). A further shift of 0.7 eV recorded at $t = 264$ ms is indicative of a partial oxidation to $[(\text{TPA})\text{Fe}^{\text{IV}}(\text{O})]^{2+}$ (Figure 3D, path b). In this respect it has to be remarked that the oxidation of Fe^{III} to Fe^{IV} is not quantitative (ca 70 %) at -40 °C and lower concentrations.²³

The final back movement of the Fe K-edge to lower energies occurring between 264 and 1964 ms, can be associated to the degradation of $[(\text{TPA})\text{Fe}^{\text{IV}}(\text{O})]^{2+}$ into the dimeric species $[(\text{TPA})_2\text{Fe}^{\text{III}}_2(\mu\text{-O})(\mu\text{-OAc})]^{3+}$ (Figure 3D, path c).

Interestingly, the Fe K-edge positions of the XANES spectra collected at 24 and 1964 ms are almost coincident.

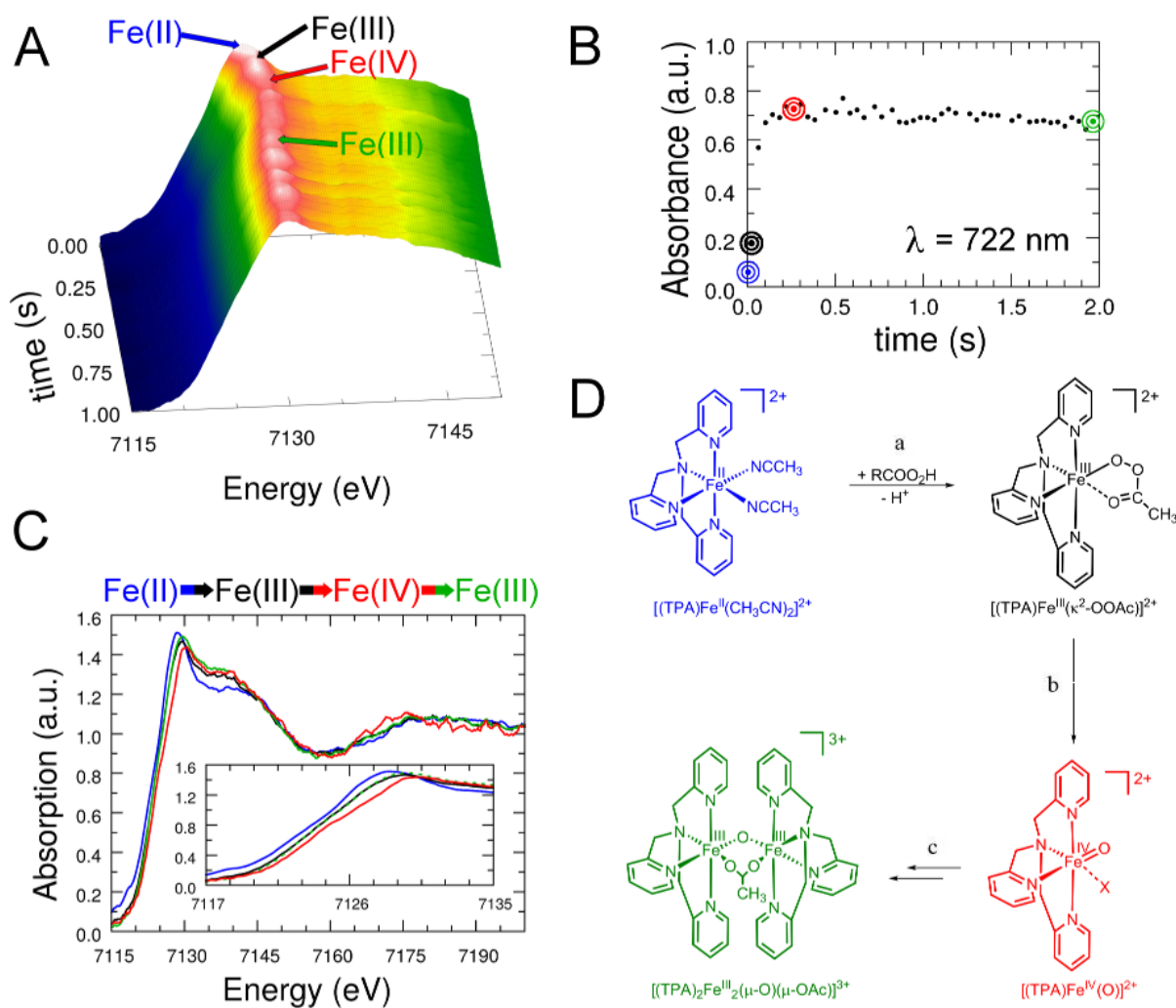


Figure 3. (A) Time evolution of the Fe K-edge EDXAS spectra of $[(\text{TPA})\text{Fe}^{\text{II}}(\text{CH}_3\text{CN})_2]^{2+}$ (35 mM) after addition of $\text{CH}_3\text{COO}_2\text{H}$ (35 mM) in $\text{CH}_3\text{CN}/\text{CH}_3\text{COOH}$ 99.6:0.4 (v/v) at 25 °C. (B) Time evolution of the absorbance at λ 722 nm of the same reaction mixture of Figure 3A. EDXAS and UV/Vis spectra have been recorded simultaneously in the stopped-flow cell. (C) Selected EDXAS spectra of Figure 3A recorded at 0 ms (blue), 24 ms (black), 264 ms (red) and

1964 ms (green). A magnification of Fe K-edge region is shown in the inset. (D) Sequence of iron species compatible with the EDXAS-UV/Vis spectral evolution ($X = \text{OAc}, \text{CH}_3\text{CN}$).

The absorbance at 722 nm has been simultaneously monitored on the same reaction mixture and its time evolution is shown in Figure 3B. This wavelength was chosen since the $[\text{Fe}^{\text{IV}}(\text{TPA})(\text{O})]^{2+}$ complex has a diagnostic pale green chromophore at $\lambda_{\text{max}} = 720$ nm, while none of its monomeric precursors shows absorption in this region.^{27,29} A significant increase of the absorbance is evident in the first phase of the reaction (0-264 ms), while a slight decrease is observed starting from 264 ms. Since the absorbance contribution of $[(\text{TPA})_2\text{Fe}^{\text{III}}_2(\mu\text{-O})(\mu\text{-OAc})]^{3+}$ at 720 nm is 4 times smaller than that of $[(\text{TPA})\text{Fe}^{\text{IV}}(\text{O})]^{2+}$,²⁷ the latter observation indicates that the decay of $[(\text{TPA})\text{Fe}^{\text{IV}}(\text{O})]^{2+}$ to $[(\text{TPA})_2\text{Fe}^{\text{III}}_2(\mu\text{-O})(\mu\text{-OAc})]^{3+}$ is not completed in the first 2 s. The partial conversion of $[(\text{TPA})\text{Fe}^{\text{IV}}(\text{O})]^{2+}$ to $[(\text{TPA})_2\text{Fe}^{\text{III}}_2(\mu\text{-O})(\mu\text{-OAc})]^{3+}$, less noticeable in the UV-Vis spectrophotometric analysis, is instead evident from the Fe K-edge energy shift of the XANES spectra. As a matter of fact, the two techniques have a different sensitivity towards the interconversion between the reactive intermediates and a clear picture of the reaction pathway can be gained only by the combination of the two techniques. The observed experimental evidences correctly reproduce the mechanistic sequence (Figure 3D) described before in literature. Furthermore, the reaction pathway is compatible with the variations of the XANES spectra. A clear modification of the structural oscillations is observed in the first phase of the reaction (0-24 ms), due to the change of the iron coordination sphere where two acetonitrile molecules in the first shell are replaced by a dioxygenated ligand. On the other hand the iron local coordination structures of the $[(\text{TPA})\text{Fe}^{\text{III}}(\kappa^2\text{-OOAc})]^{2+}$ and $[(\text{TPA})\text{Fe}^{\text{IV}}(\text{O})]^{2+}$ are very similar and this explains the close resemblance of the XANES oscillations collected at 24 and 264 ms. The main XANES features are also maintained in the EDXAS spectra collected at the end of the reaction. In this case most probably, the presence of the acetate bridge stretches the Fe-Fe distance in the $[(\text{TPA})_2\text{Fe}^{\text{III}}_2(\mu\text{-O})(\mu\text{-OAc})]^{3+}$ dimer so its contribution to the XANES spectrum becomes negligible.

2.3 Conclusion

This study demonstrates that bimolecular reactions in solution occurring in the ms time scale, can be profitably followed using a combined EDXAS-UV/Vis spectroscopic analysis. With this approach, it is possible to directly monitor the evolution of the oxidation state of an absorbing metal and the changes in the local coordination geometry taking place during chemical reaction. In particular, we showed the transformation of a Fe^{II} species into two subsequent Fe^{III} species and a more complex evolution Fe^{II}-Fe^{III}-Fe^{IV}-Fe^{III} for the [(TPA)Fe^{II}(CH₃CN)₂]²⁺ in the oxidations promoted by H₂O₂ and CH₃COO₂H, respectively.^{13,25} The information collected from the combined EDXAS-UV/Vis experimental data, are in perfect agreement with the mechanisms reported in literature and acquired using different approaches.^{18,19,23,24,27,29} We envisage that such technique will provide unique insights into chemical reaction mechanisms involving transition metals, for which the direct and unambiguous assignment of the metal oxidation state as well as the definition of its first coordination sphere, is a crucial step to discriminate among different mechanistic hypotheses. Moreover, it may represent a powerful tool to characterize intermediates which are silent to common spectroscopic techniques. A definite improvement of this approach will be the adoption of a stopped-flow apparatus able to reach low temperatures and to work in presence of organic solvents allowing in this way a slowdown of the reaction kinetics. It would give the opportunity of detecting and quantitatively monitoring some elusive species, such as Fe^V intermediates, that represent one of the most exciting challenges in the study of the catalytic processes promoted by nonheme iron complexes.

2.4 Experimental Section

[(TPA)Fe^{II}(OTf)₂] was prepared by metallation of the ligand TPA with Fe(OTf)₂×2CH₃CN³⁰ in dry CH₃CN and crystallization was carried out by slow diffusion of dry diethyl ether in a dry dichloromethane solution according to a literature method.³¹ Preparation and handling of air-sensitive materials were carried out under an inert atmosphere by using either standard Schlenk and vacuum line techniques or a glove-bag under N₂ atmosphere. The complex was then stored

under inert atmosphere. When the $[(\text{TPA})\text{Fe}^{\text{II}}(\text{OTf})_2]$ complex is dissolved in CH_3CN , two solvent molecules enter the iron first coordination sphere giving rise to the $[(\text{TPA})\text{Fe}^{\text{II}}(\text{CH}_3\text{CN})_2](\text{OTf})_2$ complex.

2.4.1 Reaction details

Reaction of $[(\text{TPA})\text{Fe}^{\text{II}}(\text{CH}_3\text{CN})_2]^{2+}$ with H_2O_2 For each stopped-flow mixing experiment, mother solutions of 70 mM $[(\text{TPA})\text{Fe}^{\text{II}}(\text{CH}_3\text{CN})_2]^{2+}$ in CH_3CN and 140 mM H_2O_2 in CH_3CN (diluted from the commercially available 50 wt. H_2O_2 solution in H_2O), were inserted into the reservoirs of the stopped-flow instrument. They were mixed in a 1:1 volume ratio at room temperature to obtain final concentrations of 35 mM and 70 mM for $[(\text{TPA})\text{Fe}^{\text{II}}(\text{CH}_3\text{CN})_2]^{2+}$ and H_2O_2 respectively. For each measurement, 100 μL of both solutions were shot by the instrument into the cell.

Reaction of $[(\text{TPA})\text{Fe}^{\text{II}}(\text{CH}_3\text{CN})_2]^{2+}$ with $\text{CH}_3\text{COO}_2\text{H}$ For each stopped-flow mixing experiment, mother solutions of 70 mM $[(\text{TPA})\text{Fe}^{\text{II}}(\text{CH}_3\text{CN})_2]^{2+}$ in CH_3CN and 70 mM $\text{CH}_3\text{COO}_2\text{H}$ in CH_3CN (diluted from the commercially available 36-40 wt. % $\text{CH}_3\text{COO}_2\text{H}$ solution in acetic acid), were inserted into the reservoirs of the stopped-flow instrument. They were mixed in a 1:1 volume ratio at room temperature to obtain final concentrations of 35 mM and 35 mM for $[(\text{TPA})\text{Fe}^{\text{II}}(\text{CH}_3\text{CN})_2]^{2+}$ and $\text{CH}_3\text{COO}_2\text{H}$, respectively. For each measurement, 100 μL of both solutions were shot by the instrument into the cell.

References

- (1) M. N. W. Matthias, R. Groß, C. Schumann, J. A. Wolny, V. Schünemann, A. Døssing, H. Paulsen, J. J. McGarvey, R. Rolf Diller, *Phys. Chem. Chem. Phys.*, **2008**, *10*, 4264-4273.
- (2) R. Zhang, Y. Zhang, Z. C. Dong, S. Jiang, C. Zhang, L. G. Chen, L. Zhang, Y. Liao, J. Aizpurua, Y., Luo, *Nature*, **2013**, *498*, 82-86.
- (3) B. J. Siwick, J. R. Dwyer, R. E. Jordan, D. R. J. Miller, *Science*, **2003**, *302*, 1382-1385.
- (4) P. Reckenthaeler, M. Centurion, W. Fuß, S. A. Trushin, F. Krausz, E. E. Fill, *Phys. Rev. Lett.*, **2009**, *102*, 213001.
- (5) C. Y. Ruan, V. A. Lobastov, F. Vigliotti, S. Chen, A. H. Zewail, *Science*, **2004**, *304*, 80-84.

- (6) A. Barty, S. Boutet, M. J. Bogan, S. Hau-Riegel, S. Marchesni, K. Sokolowski-Tinten, N. Stojanovic, R. Tobey, H. Ehrke, A. Cavalleri, *Nature Photon*, **2008**, 2, 415-419.
- (7) J. A. van Bokhoven, C. Lamberti, *X-Ray Absorbption and X-Ray Emission Spectroscopy*, (Wiley, **2016**).
- (8) J. Kern, R. Alonso-Mori, R. Tran, J. Hattne, R. J. Gildea, N. Echols, C. Glöckner, J. Hellmich, H. Laksmono, R. G. Sierra, *Science*, **2013**, 340, 491-495.
- (9) C. Bressler, C. Milne, V.-T. Pham, A. ElNahas, R. M. van der Veen, W. Gawelda, S. Johnson, P. Beaud, D. Grolimund, M. Kaiser, *Science*, **2009**, 323, 489-492.
- (10) Y. Pertot, C. Schmidt, M. Matthews, A. Chauvet, M. Huppert, V. Svoboda, A. von Conta, A. Tehlar, D. Baykusheva, J.-P. Wolf, *Science*, **2017**, 355, 264-267.
- (11) K. Hirata, K. Shinzawa-Itoh, N. Yano, S. Takemura, K. Kato, M. Hatanaka, M. Muramoto, T. Kawahara, T. Tsukihara, E. Yamashita, *Nature Methods*, **2014**, 11, 734-736.
- (12) M. S. Chen, M. C. White, *Science*, **2007**, 318, 783-787.
- (13) M. S. Chen, M. C. White, *Science*, **2010**, 327, 566-571.
- (14) M. C. White, *Science* **2012**, 335, 807-809.
- (15) O. Cussó, X. Ribas, J. Lloret-Fillol, M. Costas, *J. Am. Chem. Soc.*, **2013**, 135, 14871-14878.
- (16) E. P. Talsi, K. P. Bryliakov, *Coord. Chem. Rev.*, **2012**, 256, 1418-1434.
- (17) (a) G. Olivo, O. Cussò, M. Costas, *Chem. - An Asian J.* **2016**, 11, 3148. (b) G. Olivo, O. Lanzalunga, S. Di Stefano, *Adv. Synth. Catal.*, **2016**, 358, 843-863.
- (18) K. Chen, L. Que Jr., *J. Am. Chem. Soc.*, **2001**, 123, 6327-6337.
- (19) K. Chen, M. Costas, J. Kim, A. K. Tipton, L. Que Jr., *J. Am. Chem. Soc.*, **2002**, 124, 3026-3035.
- (20) Y. Dong, H. Fujii, M. P. Hendrich, R. A. Leising, G. Pan, C. R. Randall, E. C. Wilkinson, Y. Zang, L. Que Jr., B. G. Fox, *J. Am. Chem. Soc.*, **1995**, 117, 2778-2792.
- (21) R. Mas-Ballesté, L. Jr. Que, *J. Am. Chem. Soc.*, **2007**, 129, 15964-15972.
- (22) W. N. Oloo, A. J. Fielding, L. Que Jr. *J. Am. Chem. Soc.*, **2013**, 135, 6438-6441.
- (23) W. N. Oloo, K. K. Meier, Y. Wang, S. Shaik, E. Münck, L. Que Jr., *Nat. Commun.*, **2014**, 5, 3046-3049.
- (24) W. N. Oloo, L. Que Jr., *Acc. Chem. Res.*, **2015**, 48, 2612-2621.
- (25) W. Nam, Y. -M. Lee, S. Fukuzumi, *Acc. Chem. Res.*, **2014**, 47, 1146-1154.
- (26) K. P. Bryliakov, E. P. Talsi, *Coord. Chem. Rev.*, **2014**, 276, 73-96.

- (27) M. H. Lim, J.-U. Rohde, A. Stubna, M. R. Bukowski, M. Costas, R. Y. N. Ho, E. Münck, W. Nam, L. Que Jr., *Proc. Nat. Acad. Sci.*, **2003**, 100, 3665-3670.
- (28) J.-U. Rohde, J.-H. In, M. H. Lim, W. W. Brennessel, M. R. Bukowski, A. Stubna, E. Münck, W. Nam, L. Que Jr., *Science*, **2003**, 299, 1037-1039.
- (29) C. Kim, K. Chen, J. Kim, L. Que Jr., *J. Am. Chem. Soc.*, **1997**, 119, 5964-5965.
- (30) A. Diebold, A. Elbouadili, K. S. Hagen, *Inorg. Chem.*, **2000**, 39, 3915-3923.
- (31) A. Diebold, K. S. Hagen, *Inorg. Chem.*, **1998**, 37, 215-223.

Chapter 3

Electron transfer mechanism in the oxidation of aryl sulfides promoted by nonheme iron complexes

The oxidation of a series of aryl sulfides (aryl 1-methyl-1-phenylethyl sulfides and aryl diphenylmethyl sulfides) catalyzed by two tetradentate ($[(\text{PDP})\text{Fe}^{\text{II}}(\text{SbF}_6)_2]$ and $[(\text{BPMC})\text{Fe}^{\text{II}}(\text{OTf})_2]$) and two pentadentate ($[(\text{N4Py})\text{Fe}^{\text{II}}(\text{OTf})_2]$ and $[(\text{Bn-TPEN})\text{Fe}^{\text{II}}(\text{OTf})_2]$) nonheme iron complexes, occurs by an electron transfer-oxygen transfer (ET-OT) mechanism as supported by the observation of products deriving from fragmentation of the corresponding radical cations in association with *S*-oxidation products (sulfoxides). For the first time the rate constants of the oxygen rebound process (k_{OT}) from the reduced nonheme iron-oxo complexes to the sulfide radical cations were determined for the oxidation of aryl 1-methyl-1-phenylethyl sulfides from the fragmentation rate constants of the radical cations (k_f) and the *S*-oxidation/fragmentation products ratios.

The laser flash photolysis (LFP) experiments were carried out in the laboratories of Prof. Massimo Bietti at the University of Rome “Tor Vergata”.

The results reported in this Chapter are published in:

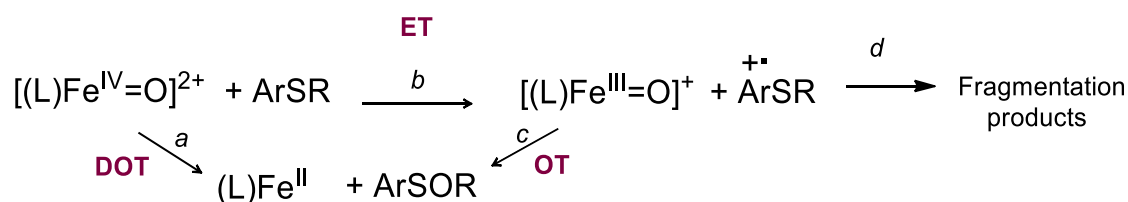
-A. Barbieri, R. Chimenti De Carlo, T. Del Giacco, S. Di Stefano, O. Lanzalunga, A. Lapi, M. Mazzonna, G. Olivo, M. Salamone, *J. Org. Chem.*, **2016**, *81*, 2513-2520.

-A. Barbieri, T. Del Giacco, O. Lanzalunga, A. Lapi, M. Mazzonna, G. Olivo, *J. Org. Chem.*, **2016**, *81*, 12382-12387.

-A. Barbieri, S. Di Stefano, O. Lanzalunga, A. Lapi, M. Mazzonna, G. Olivo, *Phosphorus Sulfur Silicon Relat. Elem.*, **2017**, *192*, 241-244.

3.1 Introduction

Among the oxidative processes promoted by heme and nonheme enzymes, the oxidation of sulfides has attracted a special attention not only for its relevance in biology¹ but also in organic synthesis. Accordingly, the main products deriving from *S*-oxidation, i.e. sulfoxides, are involved in a variety of synthetically useful procedures.² A great number of heme and nonheme model systems, able to mimic the enzymatic catalytic activity, were found to efficiently catalyze the *S*-oxidation process.³⁻¹⁰ Oxidation of sulfides to sulfoxides promoted by heme enzymes, like cytochrome P450 and peroxidases, as well as their biomimetic model compounds, has been the subject of intense mechanistic investigation by several research groups at the end of last century.³⁻⁹ More recently the mechanism of sulfoxidation of thioanisoles promoted by high-valent iron-oxo species in nonheme iron oxygenases and their synthetic nonheme models, has been analysed in detail.^{10a-h} These studies aimed in particular to clarify the mechanistic dichotomy that characterizes the oxidation of sulfides by high-valent iron(IV)-oxo complexes: “direct oxygen transfer” vs “electron transfer-oxygen rebound” mechanisms. In the direct oxygen transfer or “oxene process”, an oxygen atom is transferred in one step from the iron(IV)-oxo complex to the sulfide (DOT, Scheme 1, path a). In the two-step electron transfer-oxygen rebound process, an initial electron transfer from the sulfide to the iron(IV)-oxo complex leads to the formation of a sulfide radical cation and the reduced iron-oxo complex, this step is then followed by the oxygen transfer from the reduced iron-oxo complex to the radical cation (ET-OT, Scheme 1, paths b-c).^{4-7,10,11}



Scheme 1

Product analysis of the oxidation of sulfides whose corresponding radical cations undergo very fast fragmentation processes (Scheme 1, path d)¹²⁻¹⁶ in competition with the formation of sulfoxides through oxygen-rebound, may represent a useful tool to solve the mechanistic dichotomy DOT vs ET-OT. If the operating mechanism is DOT, we should not observe any fragmentation product, instead if the oxidation proceeds by ET-OT, in addition to the S-oxidation products (sulfoxides), we should observe the presence of fragmentation products, if the fragmentation of sulfide radical cations is sufficiently fast to compete with the oxygen rebound process.

This approach has been previously applied for the oxidation of aryl alkyl and dialkyl sulfides promoted by chloroperoxidase (CPO) and iron-porphyrin biomimetic heme models in organic solvents. In these systems it was observed that the oxidation led to the exclusive formation of sulfoxides, while in the horseradish peroxidase (HRP) and *Coprinus cinereus* peroxidase (CiP) catalyzed oxidations, sulfoxides were accompanied by fragmentation products thus indicating that the sulfide radical cation formed after the initial ET step, undergoes partitioning between the oxygen rebound (OT in Scheme 1) and the fragmentation processes (Scheme 1, path d).^{4,6} Moreover from the fragmentation rate constants of the sulfide radical cations and the product distribution in the reaction of aryl benzyl sulfides catalyzed by HRP, it was also possible to estimate the rate of the oxygen rebound process.⁶

In this respect, we deemed it worthwhile to extend the mechanistic analysis of the sulfide oxidation promoted by nonheme iron complexes, so far limited to thioanisoles,^{10a-h} to other model substrates which are characterized by fast fragmentation processes of the corresponding radical cations.

Aryl diphenylmethyl sulfides **1-4** and aryl 1-methyl-1-phenylethyl sulfides **5-9** (Figure 1) represent two classes of suitable substrates to test the intermediacy of radical cations in biomimetic oxidation processes.⁴

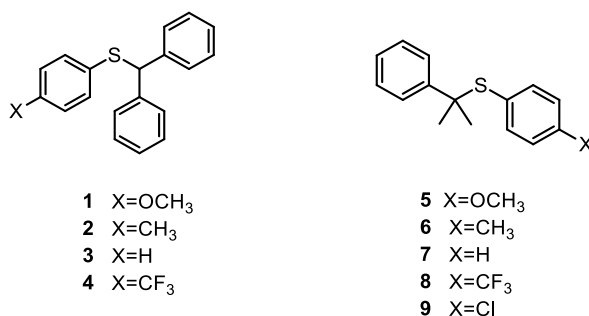


Figure 1. Aryl diphenylmethyl sulfides (**1-4**) and aryl 1-methyl-1-phenylethyl sulfides **5-9**.

Previous studies of the oxidation of aryl diphenylmethyl sulfides and aryl 1-methyl-1-phenylethyl sulfides promoted by chemical and photochemical oxidants,^{4,13,15,17} indicated that the corresponding radical cations undergo very fast and efficient fragmentation processes.

On these basis, I have carried out a detailed product and kinetic study of the oxidation of a series of aryl diphenylmethyl sulfides (**1-4**) and aryl 1-methyl-1-phenylethyl sulphides (**5-8**) by two nonheme iron(IV)-oxo pentadentate complexes, [(N4Py)Fe^{IV}(O)]²⁺ [N4Py = *N,N*-bis(2-pyridylmethyl)-*N*-bis(2-pyridyl)methylamine] and [(Bn-TPEN)Fe^{IV}(O)]²⁺ [Bn-TPEN = *N*-benzyl-*N,N',N'*-tris(2-pyridylmethyl)-1,2-diaminoethane)] in CH₃CN (Figure 2).

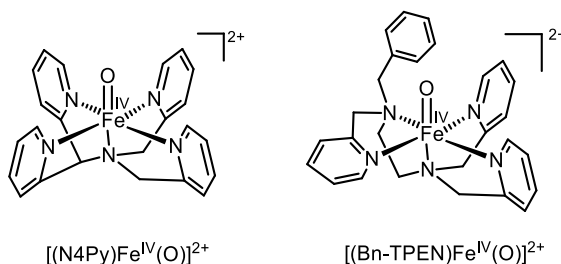
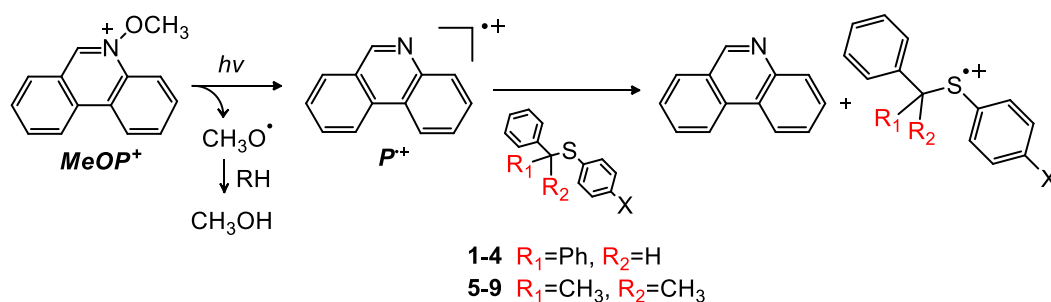


Figure 2 Nonheme iron(IV)-oxo complexes [(N4Py)Fe^{IV}(O)]²⁺ and [(Bn-TPEN)Fe^{IV}(O)]²⁺.

This study has been integrated by a steady state and laser flash photolysis (LFP) analysis of the photochemical oxidation of the same substrates carried out in the presence of *N*-methoxyphenanthridinium hexafluorophosphate (MeOP⁺PF₆⁻) which allowed us to investigate the fragmentation processes of the radical cations **1^{+•}**-**9^{+•}** and to determine their fragmentation rate constants.¹⁴⁻¹⁶

After the irradiation of a solution of *N*-methoxyphenanthridinium cation (MeOP^+) in CH_3CN , the N-O bond cleavage occurs with the formation of the phenanthridinium radical cation ($\text{P}^{+\bullet}$)¹⁸ which is a quite powerful oxidant that can be used in subsequent bimolecular reactions, to generate the radical cations of added donors with $E^\circ < 1.9 \text{ V vs SCE}$ in a exergonic processes (Scheme 2).



Scheme 2. Generation of radical cations $1^{+\bullet}$ - $9^{+\bullet}$ by photolysis of MeOP^+

Since all the sulfides investigated are characterized by oxidation potentials $< 1.9 \text{ V vs SCE}$,¹⁵ this approach resulted well suited for the generation of sulfides radical cations and for the study of the fragmentation reactions that no longer have to compete with the back electron-transfer process (an endergonic reaction).

When an ET-OT mechanism is operating, it is also possible to estimate the rate of the oxygen rebound step from the fragmentation rate constants of the sulfide radical cations and the product distribution (fragmentation products *vs* sulfoxides) as shown in the oxidation of aryl benzyl sulfides with H_2O_2 catalyzed by horseradish peroxidase.⁶ In this chapter, for the first time, the rate constants of the oxygen rebound process (k_{OT}) from the two reduced nonheme iron-oxo complexes, $[(\text{N4Py})\text{Fe}^{\text{III}}=\text{O}]^+$ and $[(\text{Bn-TPEN})\text{Fe}^{\text{III}}=\text{O}]^+$ to the aryl sulfide radical cations, will be described.

Finally, in order to gain more information both on the role of ET processes in the reactions promoted by nonheme iron complexes and on the dependence between the rate constants of the oxygen rebound process on the nature of the ligand, I have extended the mechanistic analysis to the oxidation of aryl 1-methyl-1-phenylethyl sulfides catalyzed by two tetradentate nonheme iron complexes $[(\text{PDP})\text{Fe}^{\text{II}}(\text{SbF}_6)_2]$ and $[(\text{BPMC})\text{Fe}^{\text{II}}(\text{OTf})_2]$ (Figure 3)

in presence of H_2O_2 as terminal oxidant. In these reactions a nonheme iron(V)-oxo complex has been proposed as the active species (see the proposed mechanism in Figure 5, Chapter 1).¹⁹⁻²¹

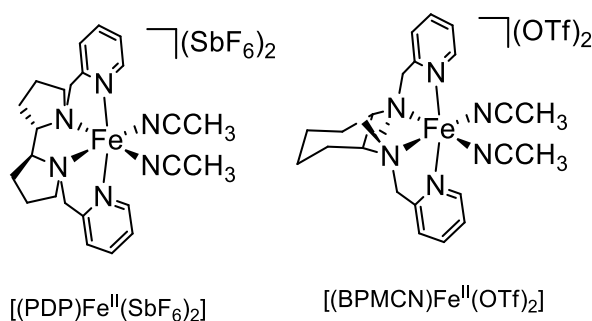


Figure 3 Tetradentate nonheme iron complexes $[(\text{PDP})\text{Fe}^{\text{II}}(\text{SbF}_6)_2]$ and $[(\text{BPMCNC})\text{Fe}^{\text{II}}(\text{OTf})_2]$.

3.2 Results and Discussion

3.2.1 Oxidation of aryl diphenylmethyl sulfides promoted by



3.2.1.1 Photochemical Oxidation

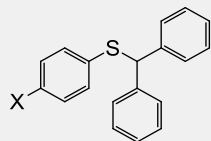
As described above, diphenylmethyl phenyl sulfide (**3**) represents a useful mechanistic probe to distinguish the intermediacy of sulfide radical cations in biomimetic and enzymatic oxidation processes.⁴ This substrate, indeed, has been used as a probe in some photochemical and biomimetic oxidation, showing different mechanistic pathways. Products deriving from the C-S bond cleavage were formed as major products in the photochemical oxidation of **3** with tetranitromethane¹³, while the exclusive formation of diphenylmethyl phenyl sulfoxide and diphenylmethyl phenyl sulfone was observed in the oxidation of **3** with H_2O_2 catalyzed by the iron-porphyrin $\text{TPPFe}^{\text{III}}\text{Cl}$ in CH_3CN , fully supporting the occurrence of a direct oxygen transfer (DOT) mechanism.⁴

In order to investigate in detail the fragmentation processes of aryl diphenylmethyl sulphide radical cations $\mathbf{1}^{\bullet+}$ - $\mathbf{4}^{\bullet+}$ and to determine their fragmentation rate constants, I have analysed the

photochemical oxidation of sulphides **1-4** in the presence of *N*-methoxyphenanthridinium hexafluorophosphate by both steady state and laser flash photolysis.

In a typical steady state photolysis experiments, a solution of **1-4** (2.5×10^{-2} M) and MeOP⁺PF₆⁻ (5.5×10^{-3} M) in N₂-saturated CH₃CN, was irradiated in a photoreactor at 355 nm (see Experimental Section). The fragmentation products diphenylmethanol, benzophenone and diaryl disulfide, formed after photolysis, were identified and quantified by GC, GC-MS and ¹H-NMR analysis, by comparison with authentic specimens. No products were detected in the absence of the sensitizer.

Table 1. Products and yields formed in the photooxidation of aryl diphenylmethyl sulfides (**1-4**) sensitized by MeOP⁺ in CH₃CN a 25 °C.^a

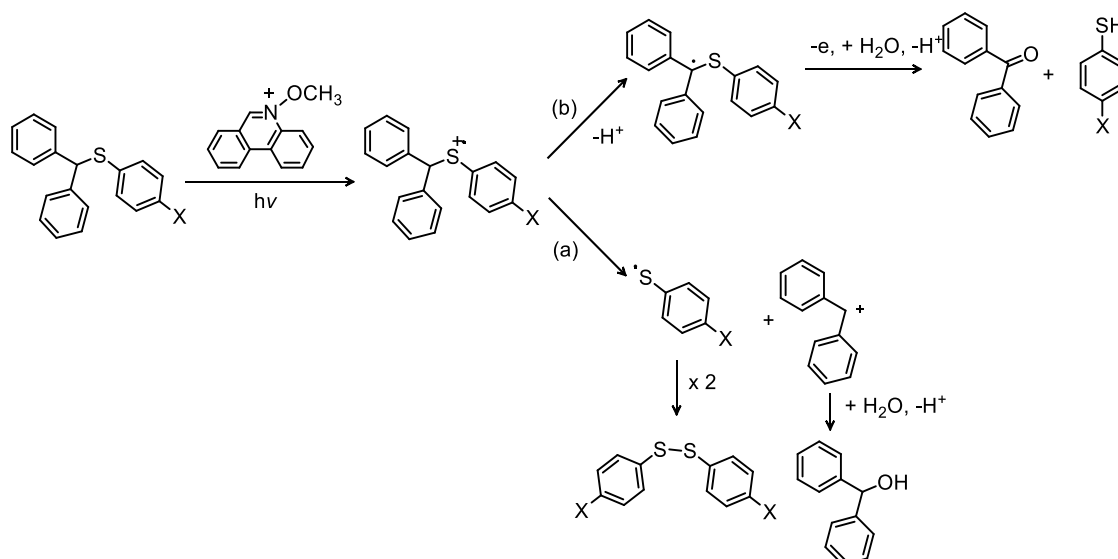
	Products (Yield %) ^b			Ratio
	(C ₆ H ₅) ₂ CHOH	(C ₆ H ₅) ₂ CO	ArSSAr	[CO]/[OH]
1 X=OCH ₃	13	17	16	1.3
2 X=CH ₃	9.0	20	14	2.2
3 X=H	7.1	26	17	3.7
3-d	13	15	11	1.2
4 X=CF ₃	5.5	31	15	5.5

^aMeOP⁺PF₆ (5.5 μmol), sulfide (25 μmol) in CH₃CN (1 mL) under nitrogen. ^bYields are referred to the amount of sensitizer. Average of at least three determinations, the error is $\pm 5\%$.

The yields, based on the amount of sensitizer, are reported in Table 1. In the last column of this table are also reported the benzophenone/diphenylmethanol molar ratios.

Formation of diphenylmethanol and diaryl disulfide in the steady state photolysis experiments, can be rationalized on the basis of C_α-S bond cleavage in the intermediate radical cations **1^{•+}**-**4^{•+}** producing the diphenylmethyl cation and the arylsulfenyl radical, as described in Scheme 3

(path a). The cation by reaction with traces of water present in CH_3CN ²² leads to diphenylmethanol, while arylsulfenyl radicals dimerize to diaryl disulfides.



Scheme 3. Formation of fragmentation products from competitive $\text{C}_{\alpha}\text{-H}$ vs $\text{C}_{\alpha}\text{-S}$ bond cleavage in radical cations $1^{+\bullet}$ - $4^{+\bullet}$.

Benzophenone can be formed by further oxidation of diphenylmethanol under the reaction conditions, even though it cannot be excluded that it might derive by $\text{C}_{\alpha}\text{-H}$ deprotonation of the radical cation (Scheme 3, path b) by the base phenanthridine, in a process that competes efficiently with $\text{C}_{\alpha}\text{-S}$ bond cleavage in aryl sulfide radical cations.^{4,6,13,23} Oxidation, followed by reaction with water of the α -sulfenyl carbon radical, leads to benzophenone and arylthiols. The occurrence of a competition between $\text{C}_{\alpha}\text{-H}$ vs $\text{C}_{\alpha}\text{-S}$ bond fragmentation in radical cations $1^{+\bullet}$ - $4^{+\bullet}$ is in accordance with the significant decrease of the benzophenone/diphenylmethanol product ratio in the oxidation of the deuterated sulfide $\text{C}_6\text{H}_5\text{SCD}(\text{C}_6\text{H}_5)_2$ (**3-d**) (see Table 1). The presence of electron withdrawing aryl substituents should favor both the fragmentation pathways, by effect of the increase of the $\text{C}_{\alpha}\text{-H}$ bond acidity, as well as the $\text{C}_{\alpha}\text{-S}$ bond cleavage rate constants in radical cations $1^{+\bullet}$ - $4^{+\bullet}$.^{14,15,23c} The increase of the benzophenone/diphenylmethanol ratio observed on going from $1^{+\bullet}$ (4-OCH₃) to $4^{+\bullet}$ (4-CF₃), clearly indicates that the substituent effect mainly influences the acidity of the $\text{C}_{\alpha}\text{-H}$ over the $\text{C}_{\alpha}\text{-S}$ bond fragmentation.

In order to determine the fragmentation rate constants of radical cations $1^{\bullet+}$ - $4^{\bullet+}$, I have investigated the photochemical oxidation of sulphides **1-4** in the presence of MeOP^+ by laser flash photolysis. After the laser irradiation ($\lambda_{\text{exc}} = 355 \text{ nm}$) of N_2 saturated solutions of sulfides **1-4** (0.01 M) and MeOP^+ ($1.6 \times 10^{-4} \text{ M}$) in CH_3CN , a broad absorption bands with maxima in the 480-590 nm region of the spectrum, depending on the substrate, were observed (see the Experimental Section). In Figure 4 is shown, as example, the time resolved absorption spectra observed after laser irradiation in the **3**/ MeOP^+ system.

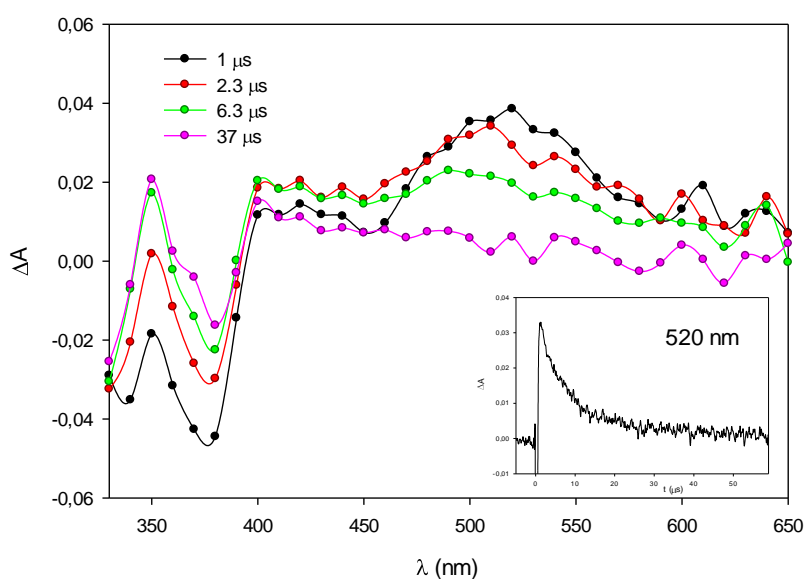


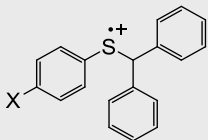
Figure 4. Time-resolved absorption spectra of the MeOP^+ ($1.6 \times 10^{-4} \text{ M}$)/ $(\text{C}_6\text{H}_5)_2\text{CHSC}_6\text{H}_5$ (**3**) ($1.0 \times 10^{-2} \text{ M}$) system in N_2 -saturated CH_3CN recorded 1 (●), 2.3 (●), 6.3 (●) and 37 μs (●) after the laser pulse. Inset: decay kinetics recorded at 520 nm. The negative absorption is due to the depletion of the ground state of MeOP^+ .

The time-evolution of the absorption spectra showed a second order decay of the transients absorbing at 480-590 nm, as shown for example in the insets of Figure 4 for the LFP experiments with the **3**/ MeOP^+ system, which can be attributed to the main decay process consisting in the deprotonation of $1^{\bullet+}$ - $4^{\bullet+}$ by phenanthridine produced after ET from **1-4** to $\text{P}^{\bullet+}$ (see Scheme 3). The decays are always coupled with the growth of an absorption at 340-360 nm which can be assigned to the C-centered radicals $4\text{-X-C}_6\text{H}_4\text{SC}^{\bullet}(\text{C}_6\text{H}_5)_2$. Clearly, the observation of $4\text{-X-C}_6\text{H}_4\text{SC}^{\bullet}(\text{C}_6\text{H}_5)_2$ indicates that, in accordance with the results of the steady-

state photolysis experiments, the decay of $\mathbf{1}^{\bullet+}\text{-}\mathbf{4}^{\bullet+}$ is due to the fast fragmentation reaction involving the heterolytic C-H bond cleavage.

The k_d/ε values (s^{-1}cm) for $\mathbf{1}^{\bullet+}\text{-}\mathbf{4}^{\bullet+}$ were determined at the maximum absorption wavelengths of the radical cations (590 nm for $\mathbf{1}^{\bullet+}$, 540 nm for $\mathbf{2}^{\bullet+}$, 520 nm for $\mathbf{3}^{\bullet+}$ and 480 nm for $\mathbf{4}^{\bullet+}$). The k_d/ε values are reported in Table 2.

Table 2. Maximum absorption wavelengths (λ_{max}) and k_d/ε values of aryl diphenylmethyl sulfide radical cations ($\mathbf{1}^{\bullet+}\text{-}\mathbf{4}^{\bullet+}$) generated by photooxidation of $\mathbf{1}\text{-}\mathbf{4}$ sensitized by $\text{MeOP}^+\text{PF}_6^-$ ($\lambda_{\text{exc}} = 355 \text{ nm}$)^a and peak oxidation potentials (E_p) of $\mathbf{1}\text{-}\mathbf{4}$.

	λ_{max} (nm)	k_d/ε (s^{-1}cm) ^b	E_p ^c
$\mathbf{1}^{\bullet+}$ X=OCH ₃	590	2.3×10^5	1.41
$\mathbf{2}^{\bullet+}$ X=CH ₃	540	3.1×10^5	1.56
$\mathbf{3}^{\bullet+}$ X=H	520	7.1×10^6	1.65
$\mathbf{4}^{\bullet+}$ X=CF ₃	480	1.6×10^7	1.86

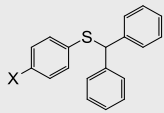
^aFrom LFP experiments ($\lambda_{\text{exc}} = 355 \text{ nm}$) in N_2 -saturated CH_3CN . $[\text{sulfide}] = 1.0 \times 10^{-2} \text{ M}$, $[\text{MeOP}^+\text{PF}_6^-] = 1.6 \times 10^{-4} \text{ M}$. ^bSecond order decay rate constants/ ε values recorded at the maximum of absorption of the radical cations. ^cPeak oxidation potentials E_p (V vs SCE in CH_3CN) from cyclic voltammetry.

3.2.1.2 Biomimetic Oxidation by $[(\text{N4Py})\text{Fe}^{\text{IV}}(\text{O})]^{2+}$

The iron(IV)-oxo complex $[(\text{N4Py})\text{Fe}^{\text{IV}}=\text{O}]^{2+}$ was prepared by oxidation of the corresponding iron(II) complex, $[(\text{N4Py})\text{Fe}^{\text{II}}(\text{OTf})_2]$ (2.5 μmol) with an excess of PhIO (12.5 μmol) in CH_3CN as reported in previous studies.^{10g,24} After 10 min from the addition of 50 μmol of sulfides $\mathbf{1}\text{-}\mathbf{4}$ to the solution of $[(\text{N4Py})\text{Fe}^{\text{IV}}=\text{O}]^{2+}$ in CH_3CN at 0 °C (see Experimental

Section), product analysis revealed that sulfoxides 4-X-C₆H₄SOCH(C₆H₅)₂ were always accompanied by significant amounts of fragmentation products, i.e. diphenylmethanol, benzophenone and diaryl disulfides. No products were observed in the absence of PhIO, while very small amounts of sulfoxides (< 1 %, referred to the amount of oxidant) were formed in presence of the oxidant and in absence of the complex [(N4Py)Fe^{II}(OTf)₂]. Using aryl diphenylmethyl sulfoxides as substrates, under the same reaction conditions, no products were formed and the recovery of the sulfoxides was quantitative, thus indicating that fragmentation products diphenylmethanol and benzophenone cannot originate from sulfoxide degradation. Products and the yields, based on the amount of oxidant, are reported in Table 3. In the last column of this table are also reported the alkyl fragmentation products (diphenylmethanol + benzophenone) / sulfoxide molar ratios.

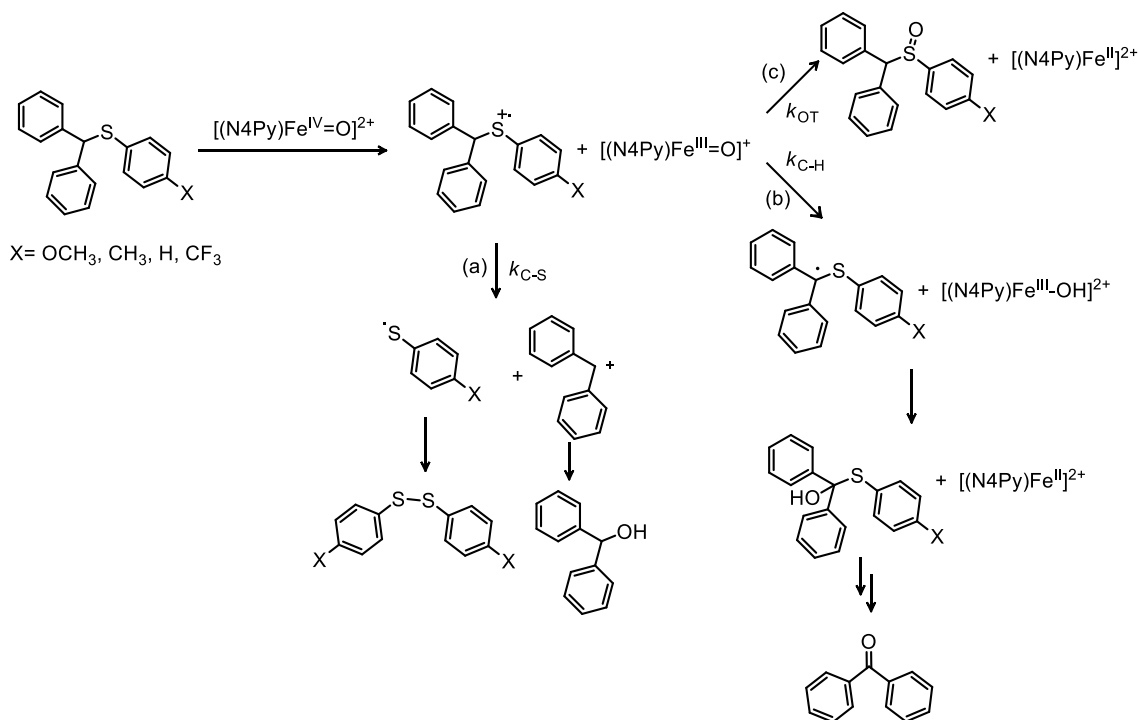
Table 3. Products and yields in the oxidation of aryl diphenylmethyl sulfides (**1-4**) by [(N4Py)Fe^{IV}=O]²⁺ in CH₃CN at 0 °C.^a

	Products (Yield %) ^b				Ratio [OH+CO]/ [SO]
	(Ph) ₂ CHOH	(Ph) ₂ CO	ArSOCH(Ph) ₂	ArSSAr	
1 X=OCH ₃	14	2	73	6	0.22
2 X=CH ₃	12	6	48	8	0.38
3 X=H	15	7	30	9	0.73
3-d	16	-	43	5	0.37
4 X=CF ₃	18	15	7	14	4.7

^aIodosylbenzene (12.5 μmol), [(N4Py)Fe^{II}(OTf)₂] (2.5 μmol) and 4-X-C₆H₄SCH(C₆H₅)₂ (50 μmol) in CH₃CN (500 μL). ^bYields (mol %) refers to the amount of oxidant PhIO. Average of at least three determinations. The error is $\pm 5\%$.

The formation of fragmentation products is a clear indication of the occurrence of an ET process from the sulfides **1-4** to [(N4Py)Fe^{IV}=O]²⁺.

Diphenylmethanol and diaryl disulfides are formed after C_{α} -S bond cleavage in radical cations $1^{+\bullet}$ - $4^{+\bullet}$ as described in path a of Scheme 3 for the steady state photolysis of the $1-4/\text{MeOP}^+$ systems and in path a of Scheme 4 for the oxidation of $1-4$ by $[(\text{N4Py})\text{Fe}^{\text{IV}}=\text{O}]^{2+}$.



Scheme 4. C_{α} -S and C_{α} -H bond fragmentation vs oxygen rebound processes in the oxidation of sulfides $1-4$ by $[(\text{N4Py})\text{Fe}^{\text{IV}}(\text{O})]^{2+}$ in CH_3CN .

Formation of benzophenone might be attributed, in analogy to the steady state photolysis of the $1-4/\text{MeOP}^+$ systems, either to the C_{α} -H fragmentation in radical cations $1^{+\bullet}$ - $4^{+\bullet}$ likely promoted by the reduced iron(III)-oxo complex $[(\text{N4Py})\text{Fe}^{\text{III}}=\text{O}]^+$ (Scheme 4, path b), or to the oxidation of diphenylmethanol. The former process is in accordance with the almost constant diphenylmethanol/benzophenone product ratio observed by increasing the reaction time from 1 min to 10 min and with the disappearance of benzophenone among the reaction products accompanied by increased yields of diphenylmethanol and diphenylmethyl phenyl sulfoxide observed when the oxidation is carried out in presence of deuterated sulfide $3-d$ under the same reaction conditions (see Table 3). This result can be attributed to a reduced deprotonation rate of $3-d^{+\bullet}$ by $[(\text{N4Py})\text{Fe}^{\text{III}}=\text{O}]^+$ and to a complete suppression of path b in Scheme 4.

The results shown in Table 3 indicate that the yields of diaryl disulfides are less than half of those of diphenylmethanol and benzophenone probably due to a further oxidation of the disulfides under the reaction conditions.

Kinetic studies of the reaction of $[(\text{N4Py})\text{Fe}^{\text{IV}}(\text{O})]^{2+}$ with diphenylmethyl aryl sulfides were carried out by monitoring spectrophotometrically the decrease of the absorbance at 695 nm (λ_{max} for $[(\text{N4Py})\text{Fe}^{\text{IV}}(\text{O})]^{2+}$)^{24a} in the presence of an excess of **1-4** (at least ten times) (see Experimental Section). The rate obeyed pseudo-first-order kinetics and the pseudo-first-order rate constant (k_{obs}) increased linearly with increasing concentration of diphenylmethyl aryl sulfides. The second-order rate constants (k_2), reported in Figure 5 (left side) were obtained from the slope of the linear correlation of k_{obs} vs the substrate concentrations.

The total yields of oxidation products increased from 40 % for **4** to 89 % for the most reactive **1** and, in accordance with the electrophilic nature of the oxidizing species $[(\text{N4Py})\text{Fe}^{\text{IV}}=\text{O}]^{2+}$ ^{10a}, a negative ρ value (-0.4) was determined in the Hammett correlation when the $\log(k_X/k_H)$ values were plotted vs the substituent constants σ_p^+ . (Figure 5, right side).

Sulfide	k_2 ($\text{M}^{-1}\text{s}^{-1}$) ^a
1	0.17
2	0.12
3	8.6×10^{-2}
4	3.9×10^{-2}
Thioanisole	0.20

^a $[(\text{N4Py})\text{Fe}^{\text{IV}}=\text{O}]^{2+}$ (1.2 mM), substrate (8-30 mM) in CH_3CN (1 mL) at 8 °C .

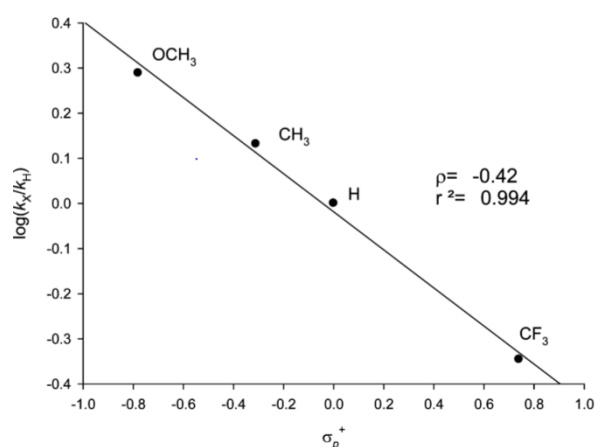


Figure 5. Second order rate constants (k_2) for the oxidation of aryl diphenylmethyl sulfides (**1-4**) and thioanisole by $[(\text{N4Py})\text{Fe}^{\text{IV}}=\text{O}]^{2+}$ in CH_3CN at 8 °C^a and Hammett plot for the oxidation of **1-4** by $[(\text{N4Py})\text{Fe}^{\text{IV}}=\text{O}]^{2+}$

The occurrence of an ET process from sulfides **1-4** to $[(N4Py)Fe^{IV}=O]^{2+}$, indicates that sulfoxides are likely formed after the oxygen rebound (OT) process from the reduced iron(III)-oxo complex to the radical cations **1^{+•}-4^{+•}**. Thus, the C_α-S and C_α-H bond fragmentation of radical cations **1^{+•}-4^{+•}** occur in competition with the oxygen rebound as shown in Scheme 4 (paths a, b and c, respectively). The competition between S-oxidation and fragmentation pathways for radical cations **1^{+•}-4^{+•}** is in full agreement with the marked dependence of the product distribution and in particular of the sulfoxide/fragmentation product ratios, reported in the last column of Table 3 and in the histogram of Figure 6, on the nature of the aryl substituents.

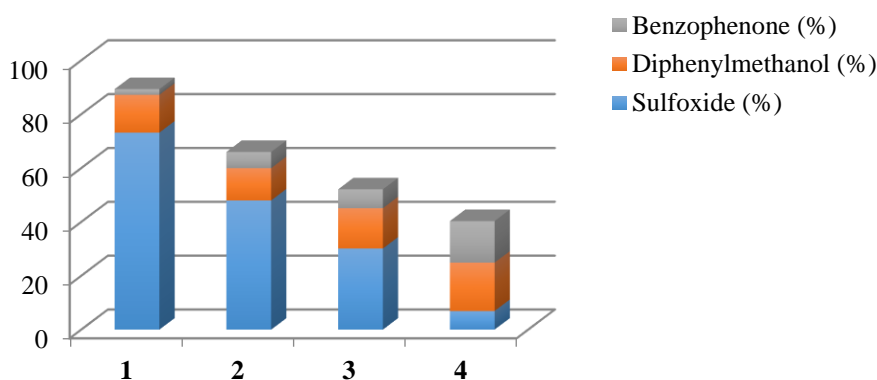


Figure 6. Yields (% referred to the amount of oxidant) of fragmentation products (benzophenone and diphenylmethanol) and sulfoxides in the oxidation of sulfides **1-4** by $[(N4Py)Fe^{IV}=O]^{2+}$ in CH_3CN at 0 °C.

The relative amount of fragmentation products regularly increase by decreasing the electron donating effect of the aryl substituents i.e. by increasing the fragmentation rate constants of the radical cations, as indicated by the results of the LFP experiments (Table 2). In the oxidation of 4-OCH₃-C₆H₄SCH(C₆H₅)₂ by $[(N4Py)Fe^{IV}=O]^{2+}$ the sulfoxide is by far the major product since the corresponding radical cation **1^{+•}** is characterized by a relatively low C_α-S fragmentation rate constant. On the opposite, the oxidation of 4-CF₃-C₆H₄SCH(C₆H₅)₂ by the same iron(IV)-oxo complex, leads to higher amounts of diphenylmethanol and benzophenone. In this case the fragmentation process competes efficiently with the oxygen rebound in accordance with the relatively fast C_α-S bond cleavage of **4^{+•}**.

3.2.2 Oxidation of aryl 1-methyl-1-phenylethyl sulfides promoted by [(N4Py)Fe^{IV}(O)]²⁺ and [(Bn-TPEN)Fe^{IV}(O)]²⁺: the rate of the oxygen rebound process

As discussed previously in the Introduction, when an ET-OT mechanism is operating, it is possible to estimate the rate of the oxygen rebound step from the fragmentation rate constants of the sulfide radical cations and the product distribution (fragmentation products *vs* sulfoxides). Though aryl diphenylmethyl sulfides represent suitable substrates to test the intermediacy of radical cations in biomimetic oxidation processes,⁴ the occurrence of both C-S and C-H bond cleavage in the radical cations represents a limitation when the rate of the oxygen rebound process has to be determined. The rates of C-H bond cleavage in sulfide radical cations are dependent on the nature of the deprotonating base so it was not possible to directly compare the fragmentation rates of the radical cation in the biomimetic oxidation with those determined by laser flash photolysis (LFP) analysis for the photochemical oxidation of the same substrates carried out in the presence of *N*-methoxyphenanthridinium hexafluorophosphate (MeOP⁺PF₆⁻) due to the different bases involved in the C-H bond cleavage processes ([[(N4Py)Fe^{III}=O]⁺ and phenanthridine, respectively).

Moreover from the data reported in Tables 1 and 3, and in particular from the benzophenone/diphenylmethanol product ratios, it can be noted that the photochemical oxidations are characterized by a higher contribution of the C_α-H bond cleavage to the overall fragmentation process, while the C_α-S bond cleavage prevails in the biomimetic oxidations. Even considering the difference in the relative contribution of the C_α-H and C_α-S bond cleavage processes, an increase of the fragmentation rate constants in the biomimetic oxidations should be expected through a decrease in the electron-donating power of the aryl substituent, that is, by decreasing the stability of the radical cation.

To this purpose, in order to determine the rate of the oxygen rebound process from reduced nonheme iron-oxo complexes to aryl sulfide radical cations (Scheme 1, path c), I have investigated the oxidation of a series of aryl 1-methyl-1-phenylethyl sulfides (**5-8**) promoted by two nonheme iron(IV)-oxo complexes: [(N4Py)Fe^{IV}=O]²⁺ and [(Bn-TPEN)Fe^{IV}=O]²⁺. In this series of substrates no cleavable benzylic C-H bonds in the α position with respect to the S atom is present, so the fragmentation of radical cations **5⁺**-**8⁺** exclusively involves the cleavage of

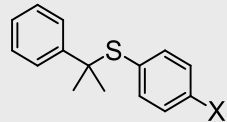
C $_{\alpha}$ -S bond, as observed in the photochemical oxidations of aryl 1-methyl-1-arylethyl sulfides with MeOP⁺PF₆⁻ and 9,10-dicyanoanthracene/O₂ systems.¹⁵⁻¹⁷

3.2.2.1 Laser Flash Photolysis Studies

The rate of the C $_{\alpha}$ -S bond cleavage of a series of aryl 1-methyl-1-arylethyl sulfide radical cations, including **6**⁺ and **7**⁺, have been previously determined by laser flash photolysis (LFP) in the photochemical oxidation of the sulfides carried out in the presence of MeOP⁺PF₆⁻ in CH₃CN at 25 °C (the fragmentation rate constant of **5**⁺, instead, was too low to be determined in the LFP experiments and only an upper limit could be given).¹⁵ In the same way, I have determined the rate constants for fragmentation of **6**⁺-**8**⁺ (k_f) at 0 °C by fitting the exponential decays at the maximum absorption wavelengths (see Table 4 and Experimental Section).

Table 4 shows that fragmentation rates increase regularly from **6**⁺ to **8**⁺, that is, by increasing the electron withdrawing (EW) properties of the aryl substituents.

Table 4. Maximum absorption wavelengths and C $_{\alpha}$ -S fragmentation rate constants (k_f) of aryl 1-methyl-1-phenylethyl sulfide radical cations (**5**⁺-**8**⁺) generated by photooxidation of **5-8** sensitized by MeOP⁺PF₆⁻ ($\lambda_{exc}=355\text{nm}$) in CH₃CN at 0 °C.

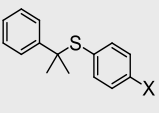
	λ_{MAX}	$k_f(10^4 \text{ s}^{-1})^a$
5 X=OCH ₃	570	< 1
6 X=CH ₃	550	3.0
7 X=H	530	3.4
8 X=CF ₃	510	6.7

^aFrom LFP experiments in N₂-saturated CH₃CN, [sulfide]=1.0×10⁻² M, [MeOP⁺PF₆⁻]=1.6×10⁻⁴ M.

3.2.2.2 Biomimetic Oxidation by $[(\text{N4Py})\text{Fe}^{\text{IV}}(\text{O})]^{2+}$ and $[(\text{Bn-TPEN})\text{Fe}^{\text{IV}}(\text{O})]^{2+}$

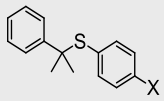
For the product analysis of the biomimetic oxidations, aryl 1-methyl-1-phenylethyl sulfides (**5-8**) (50 μmol) were added to a solution of the iron(IV)-oxo complex prepared by oxidation of $[(\text{N4Py})\text{Fe}^{\text{II}}]^{2+}$ or $[(\text{Bn-TPEN})\text{Fe}^{\text{II}}]^{2+}$ (2.5 μmol) with $\text{PhIO}^{10\text{g},24}$ (12.5 μmol) in CH_3CN (0.5 mL) and stirred at 0°C for 90 min and 30 min respectively (see Experimental Section). The reaction products, identified by GC, GC-MS, HPLC and ^1H NMR analyses, were 2-phenyl-2-propanol, diaryl disulfides, aryl 1-methyl-1-phenylethyl sulfoxides. In all cases material recovery was satisfactory (>95%). No products were formed in the absence of PhIO , while small amounts of aryl 1-methyl-1-phenylethyl sulfoxides (< 1 %, referred to the amount of oxidant) were observed in the oxidation with PhIO in the absence of the nonheme complexes $[(\text{N4Py})\text{Fe}^{\text{II}}]^{2+}$ or $[(\text{Bn-TPEN})\text{Fe}^{\text{II}}]^{2+}$. Products and yields, referred to the amount of oxidant, are reported in Table 5 and in Table 6 for the oxidations promoted by $[(\text{N4Py})\text{Fe}^{\text{IV}}(\text{O})]^{2+}$ and $[(\text{Bn-TPEN})\text{Fe}^{\text{IV}}=\text{O}]^{2+}$, respectively.

Table 5. Products and yields in the oxidation of aryl 1-methyl-1-phenylethyl sulfides (**5-8**) by $[(\text{N4Py})\text{Fe}^{\text{IV}}=\text{O}]^{2+}$ in CH_3CN at 0°C .^a

	Products (Yields %) ^b			Ratio [OH]/[SO]
	(Ph)C(CH ₃) ₂ OH	ArSSAr	ArSOC(CH ₃) ₂ (Ph)	
5 X=OCH ₃	31±2	14±1	64±5	0.48
6 X=CH ₃	39±2	15±1	44±4	0.89
7 X=H	40±4	16±2	25±2	1.6
8 X=CF ₃	48±5	22±2	8.4±0.5	5.7

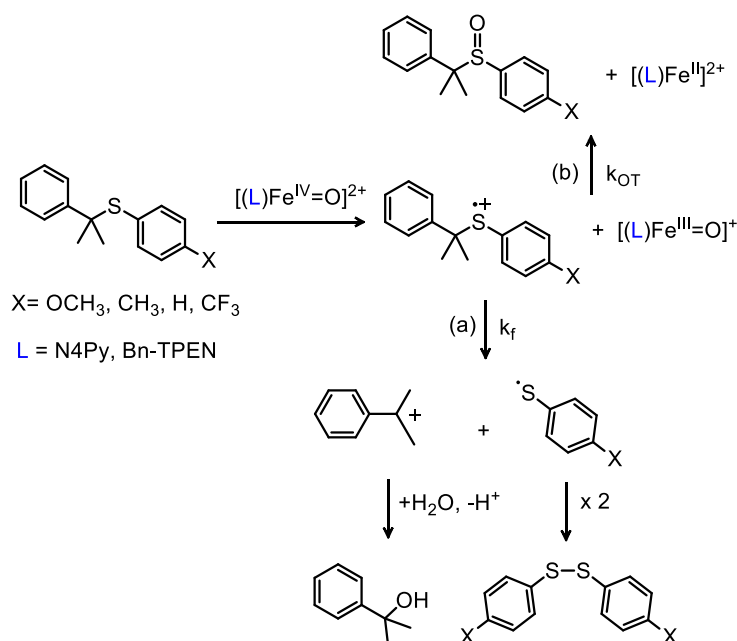
^aIodosylbenzene (12.5 μmol), $[(\text{N4Py})\text{Fe}^{\text{II}}(\text{OTf})_2]$ (2.5 μmol) and aryl 1-methyl-1-phenylethyl sulfides (50 μmol) in CH_3CN (500 μL). ^b Yields (mol %) refer to the amount of oxidant PhIO .

Table 6. Products and yields in the oxidation of aryl 1-methyl-1-phenylethyl sulfides (**5-8**) by $[(\text{Bn-TPEN})\text{Fe}^{\text{IV}}=\text{O}]^{2+}$ in CH_3CN at 0°C .^a

	Products (Yields %) ^b			Ratio [OH]/[SO]
	(Ph)C(CH ₃) ₂ OH	ArSSAr	ArSOC(CH ₃) ₂ (Ph)	
5 X=OCH ₃	56±4	27±2	44±4	1.3
6 X=CH ₃	62±5	25±2	33±2	1.9
7 X=H	64±6	28±4	18±2	3.6
8 X=CF ₃	70±5	27±3	10±1	7.0

^aIodosylbenzene (12.5 μmol), [(Bn-TPEN)Fe^{II}(OTf)₂] (2.5 μmol) and aryl 1-methyl-1-phenylethyl sulfides (50 μmol) in CH₃CN (500 μL). ^b Yields (mol %) refer to the amount of oxidant PhIO.

From the data reported in Tables 5-6, it can be readily noted that higher yields of oxidation products are observed in the oxidations promoted by [(Bn-TPEN)Fe^{IV}=O]²⁺ with respect to those promoted by [(N4Py)Fe^{IV}(O)]²⁺, in accordance with the higher oxidizing ability of the former iron(IV)-oxo complex also reported for the oxidation of *para*-substituted thioanisoles.^{10g} As observed for the oxidation of sulfides **1-4** by [(N4Py)Fe^{IV}(O)]²⁺, a regular increase of the total yields of oxidation products are detected with both the iron-oxo complexes by increasing the electron releasing power of the aryl substituents, in accordance with the electrophilic nature of the oxidizing species [(N4Py)Fe^{IV}=O]²⁺ and [(Bn-TPEN)Fe^{IV}=O]²⁺.^{10g} Moreover the *S*-oxygenation products (sulfoxides) are always accompanied by significant amounts of fragmentation products (2-phenyl-2-propanol and diaryl disulfides). Again the oxidation of **5-8** promoted by [(N4Py)Fe^{IV}=O]²⁺ and [(Bn-TPEN)Fe^{IV}=O]²⁺ involves an ET process with formation of radical cations **5⁺**-**8⁺**. C_α-S bond cleavage of **5⁺**-**8⁺** leads to the 2-phenyl-2-propyl cation and an arylsulfenyl radical as described in path a of Scheme 5. The cation leads to 2-phenyl-2-propanol by reaction with traces of water present in CH₃CN, while arylsulfenyl radicals dimerize to diaryl disulfides.¹⁵⁻¹⁷



Scheme 5. Fragmentation vs oxygen rebound processes in the oxidation of aryl 1-methyl-1-phenylethyl sulfides (**5-8**) by $[(\text{N4Py})\text{Fe}^{\text{IV}}=\text{O}]^{2+}$ and $[(\text{Bn-TPEN})\text{Fe}^{\text{IV}}=\text{O}]^{2+}$ in CH_3CN .

The presence of the two competitive pathways for **5⁺-8⁺** (oxygen rebound and $\text{C}_\alpha\text{-S}$ fragmentation) is in accordance with a regular increase of the 2-phenyl-2-propanol / aryl 2-phenyl-2-propyl sulfoxide product ratios (Tables 5-6) on increasing the EW effect of the aryl substituents as shown in Figure 7.

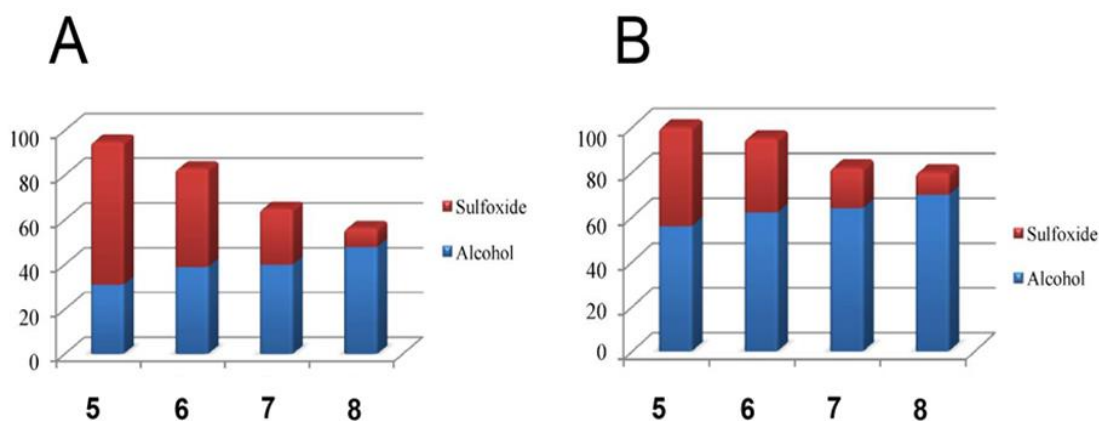


Figure 7. Yields (% referred to the amount of oxidant) of aryl 1-methyl-1-phenylethyl sulfoxides and 2-phenyl-2-propanol in the oxidation of aryl 1-methyl-1-phenylethyl sulfides **5-8** by (a) [(N4Py)Fe^{IV}=O]²⁺ and (b) [(Bn-TPEN)Fe^{IV}=O]²⁺ in CH₃CN at 0 °C.

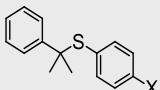
The increase of the relative amount of the C_α-S fragmentation products observed by increasing the EW power of the X substituents, results from the enhancement of fragmentation rate constants of the radical cations on going from **5**^{•+} to **8**^{•+}, as already reported for the oxidation of aryl diphenylmethyl sulfides by [(N4Py)Fe^{IV}=O]²⁺.

3.2.2.3 Determination of oxygen rebound rate constants (*k*_{OT})

Since the radical cations **5**^{•+}-**8**^{•+} produced in the oxidations of **5-8** by [(N4Py)Fe^{IV}=O]²⁺ and [(Bn-TPEN)Fe^{IV}=O]²⁺ undergo partitioning between the oxygen rebound and the C_α-S bond fragmentation shown in Scheme 5, it is possible to estimate the rate of the oxygen rebound step (*k*_{OT}) from the fragmentation rate (*k*_f) of the radical cations and the ratio of the yields of the sulfoxides and the fragmentation product 2-phenyl-2-propanol according to eq 1 (see Tables 5-6). It is not possible to calculate *k*_{OT} for **5**^{•+} since the fragmentation rate constant is too low to be determined in the LFP experiments (see Table 4). The values of *k*_{OT} are reported in Table 7.

$$k_{OT} = k_f [\text{ArSOC}(\text{CH}_3)_2\text{C}_6\text{H}_5]/[\text{C}_6\text{H}_5\text{C}(\text{CH}_3)_2\text{OH}] \quad (1)$$

Table 7. Oxygen rebound rate constants (*k*_{OT}) for the oxidation of **5-8** by [(N4Py)Fe^{IV}=O]²⁺ and [(Bn-TPEN)Fe^{IV}=O]²⁺ in CH₃CN at 0 °C.

	$k_{OT}(10^4 \text{ s}^{-1})^a$	
	$[(\text{N4Py})\text{Fe}^{\text{IV}}=\text{O}]^{2+}$	$[(\text{Bn-TPEN})\text{Fe}^{\text{IV}}=\text{O}]^{2+}$
5 X=OCH ₃	< 2.1	< 0.8
6 X=CH ₃	3.5	1.6
7 X=H	2.0	1.0
8 X=CF ₃	1.2	0.9

^aCalculated from eq 1.

Interestingly, the k_{OT} values for all the sulfides and both the nonheme iron(IV)-oxo complexes are of the same order of magnitude (see Table 7), thus supporting a common ET-OT oxidation mechanism involving a competition between the oxygen rebound (OT) and C $_{\alpha}$ -S fragmentation of radical cations **5**⁺-**8**⁺. The lower k_{OT} values found with $[(\text{Bn-TPEN})\text{Fe}^{\text{III}}=\text{O}]^+$ can be reasonably explained on the basis of a higher steric hindrance of the Bn-TPEN with respect to the N4Py iron ligand. Finally, it has to be noted that the k_{OT} values are slightly higher than those determined in the oxidation of aryl benzyl sulfides with H₂O₂ catalyzed by horseradish peroxidase,⁶ where the OT process involves the reaction of aryl sulfide radical cations with a heme iron(IV)-oxo complex.

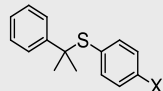
3.2.3 Oxidation of aryl 1-methyl-1-phenylethyl sulfides promoted by $[(\text{PDP})\text{Fe}^{\text{II}}(\text{SbF}_6)_2]$ and $[(\text{BPMCN})\text{Fe}^{\text{II}}(\text{OTf})_2]$: the rate of the oxygen rebound process

Oxidations of aryl sulfides promoted by tetradentate nonheme iron complexes were carried out with the series of substrates (aryl 1-methyl-1-phenylethyl sulfides) that allowed to estimate the oxygen rebound rate constants. Oxidations of aryl 1-methyl-1-phenylethyl sulfides **5-7, 9** by H₂O₂ catalysed by $[(\text{PDP})\text{Fe}^{\text{II}}(\text{SbF}_6)_2]$ and $[(\text{BPMCN})\text{Fe}^{\text{II}}(\text{OTf})_2]$ were carried out by addition of the oxidant (60 μmol) to a solution of the substrate (60 μmol) and the iron complex (1.5 μmol) in CH₃CN (600 μL) stirred at 0 °C for 6 min (see Experimental Section). Reaction

products were identified by ^1H NMR analyses (comparison with authentic specimens). 2-Phenyl-2-propanol and diaryl disulfides were the main products accompanied by minor amounts of aryl 1-methyl-1-phenylethyl sulfoxides. Aryl 1-methyl-1-phenylethyl sulfones were also observed in trace amounts ($< 1\%$). No products were formed in the absence of H_2O_2 while small amounts of aryl sulfoxides ($< 1\%$, referred to the amount of oxidant) were observed in the oxidation with H_2O_2 in the absence of the nonheme complexes $[(\text{PDP})\text{Fe}^{\text{II}}(\text{SbF}_6)_2]$ and $[(\text{BPMCN})\text{Fe}^{\text{II}}(\text{OTf})_2]$.

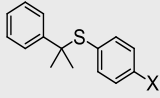
Products and yields of the fragmentation product 2-phenyl-2-propanol and of the *S*-oxidation products aryl 1-methyl-1-phenylethyl sulfoxides, referred to the amount of oxidant, are reported in Table 8 and in Table 9 for the oxidations catalyzed by $[(\text{PDP})\text{Fe}^{\text{II}}(\text{SbF}_6)_2]$ and $[(\text{BPMCN})\text{Fe}^{\text{II}}(\text{OTf})_2]$, respectively.

Table 8. Products and yields in the oxidation of aryl 1-methyl-1-phenylethyl sulfides (**5-7, 9**) with H_2O_2 catalysed by $[(\text{PDP})\text{Fe}^{\text{II}}(\text{SbF}_6)_2]$ in CH_3CN at $0\text{ }^\circ\text{C}$.^a

	Products (Yields %) ^b		Ratio
	(Ph)C(CH ₃) ₂ OH	ArSOC(CH ₃) ₂ (Ph)	[OH]/[SO]
5 X=OCH ₃	5.7	2.7	2.1
6 X=CH ₃	19	1.8	11
7 X=H	25	1.7	15
9 X=Cl	27	1.0	26

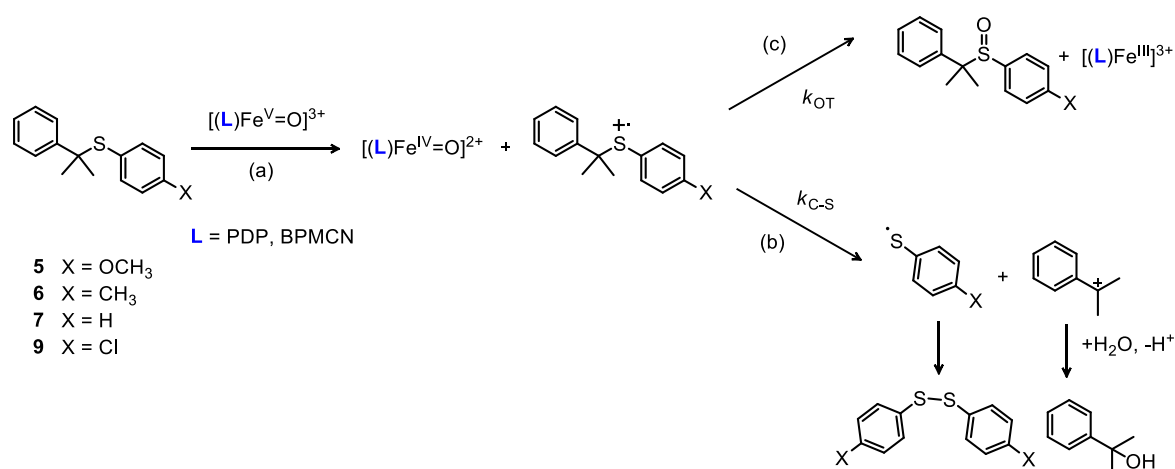
^a H_2O_2 (60 μmol), $[(\text{PDP})\text{Fe}^{\text{II}}(\text{SbF}_6)_2]$ (1.5 μmol) and aryl 1-methyl-1-phenylethyl sulfides (60 μmol) in CH_3CN (600 μL) at 0°C in 6 min. ^b Yields (mol %) refer to the amount of oxidant.

Table 9. Products and yields in the oxidation of aryl 1-methyl-1-phenylethyl sulfides (**5-7, 9**) with H_2O_2 catalysed by $[(\text{BPMCN})\text{Fe}^{\text{II}}(\text{OTf})_2]$ in CH_3CN at $0\text{ }^\circ\text{C}$.^a

	Products (Yields %) ^b		Ratio
	(Ph)C(CH ₃) ₂ OH	ArSOC(CH ₃) ₂ (Ph)	[OH]/[SO]
5 X=OCH ₃	19	2.6	7.3
6 X=CH ₃	38	2.4	16
7 X=H	49	1.4	35
9 X=Cl	44	0.7	68

^aH₂O₂ (60 μmol), [(BPMCN)Fe^{II}(OTf)₂] (1.5 μmol) and aryl 1-methyl-1-phenylethyl sulfides (60 μmol) in CH₃CN (600 μL) at 0°C in 6 min. ^b Yields (mol %) refer to the amount of oxidant.

The formation of fragmentation products is a clear indication, also in this case, of the occurrence of an ET process from the sulfides to [(PDP)Fe^V=O]³⁺ and [(BPMCN)Fe^V=O]³⁺ (Scheme 6, path a) and the generation of 2-phenyl-2-propanol and diaryl disulfides follows the same mechanism described for the oxidation promoted by [(N4Py)Fe^{IV}=O]²⁺ and [(Bn-TPEN)Fe^{IV}=O]²⁺ (Scheme 5, path b).^{15-17,25-27} In accordance with the presence of the two competitive decay pathways for **5**^{•+}-**7**^{•+}, **9**^{•+} (C-S fragmentation and oxygen rebound), a regular increase of the 2-phenyl-2-propanol / aryl sulfoxide product ratios (Tables 7-8) is observed by increasing the electron withdrawing effect of the aryl substituents.

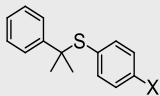


Scheme 6. Competition between C-S fragmentation and oxygen rebound in the oxidation of aryl 1-methyl-1-phenylethyl sulfides **5-7, 9** promoted by the iron(V)-oxo complexes $[(PDP)Fe^V=O]^{3+}$ and $[(BPMCN)Fe^V=O]^{3+}$.

The rate constants of the oxygen rebound step (k_{OT}) can be calculated, as described above, from the fragmentation rate (k_f) of the radical cations and the ratio of the yields of the sulfoxides and the fragmentation product 2-phenyl-2-propanol by the equation 1 (Table 10).

It is interesting to note that the k_{OT} values reported in Table 10 show that the oxygen rebound process promoted by $[(PDP)Fe^{IV}=O]^{2+}$ with all the substrates investigated, is significantly faster than that promoted by $[(BPMCN)Fe^{IV}=O]^{2+}$.

Table 10. C-S Fragmentation rate constants (k_f) of aryl 1-methyl-1-phenylethyl sulfide radical cations (**5^{+•}**-**7^{+•}**, **9^{+•}**) and oxygen rebound rate constants (k_{OT}) for the oxidation of **5-7, 9** by $[(PDP)Fe^V=O]^{3+}$ and $[(BPMCN)Fe^V=O]^{3+}$.

	$k_f(10^4 \text{ s}^{-1})^a$	$k_{OT}(10^3 \text{ s}^{-1})^a$	
		$[(PDP)Fe^V=O]^{3+}$	$[(BPMCN)Fe^V=O]^{3+}$
5 X=OCH ₃	< 1	< 4.7	< 1.4
6 X=CH ₃	3.0	2.8	1.9
7 X=H	3.4	2.3	0.97
9 X=Cl	3.7	1.4	0.59

^aFrom LFP experiments.

3.3 Conclusion

The observation of products deriving from C_α-S and C_α-H fragmentation of radical cations **1^{+•}**-**4^{+•}** (diphenylmethanol, benzophenone and diaryl disulfides) and from C_α-S fragmentation of radical cations **5^{+•}**-**9^{+•}** (2-phenyl-2-propanol, diaryl disulfides) in association

with sulfoxides in the oxidation of aryl diphenylmethyl sulfides and aryl 1-methyl-1-phenylethyl sulfides respectively, promoted by the nonheme iron active species, clearly demonstrates with no doubt that an electron transfer-oxygen transfer (ET-OT) mechanism takes place. The ET-OT process is also supported by the increase of the fragmentation/*S*-oxidation product ratios observed by decreasing the electron donating power of the aryl substituents i.e. by increasing the fragmentation rate constants of the radical cations **1^{•+}**-**9^{•+}**, as indicated by the results of LFP experiments of the photochemical oxidation of **1-9** by MeOP⁺. A substrate structural dependence in the oxidation mechanism can be evinced comparing the results obtained for the oxidation of aromatic sulfides and thioanisoles promoted by the same iron(IV)-oxo complex, [(N4Py)Fe^{IV}=O]²⁺. The more bulky substituents in sulfides **1-9** could hamper the direct transfer of the oxygen atom from [(N4Py)Fe^{IV}(O)]²⁺ to the sulfur atom making possible an endergonic and relatively slow ET process with respect to a DOT pathway which would require a closer approach to the iron-oxo moiety.

The rate constant for the oxygen rebound step associated to the oxidative process of sulfides **5-8** promoted by the pentadentate iron(IV)-oxo complexes, [(N4Py)Fe^{IV}(O)]²⁺ and [(Bn-TPEN)Fe^{IV}(O)]²⁺, has been determined for the first time and range between $<0.8 \times 10^4$ and 3.5×10^4 s⁻¹, with values very close to the ones measured for the heme enzyme horseradish peroxidase. Furthermore, the rate constants for the oxygen rebound step between **5^{•+}**-**7^{•+}**, **9^{•+}** and the two reduced iron(IV) oxo tetradentate complexes, [(PDP)Fe^{IV}(O)]²⁺ and [(BPMCN)Fe^{IV}(O)]²⁺, resulted ca. one order of magnitude lower with respect to those determined for the reduced iron(III) oxo pentadentate complexes. These results indicate that the rate of the oxygen rebound process from reduced nonheme iron-oxo complexes is clearly dependent on the nature of the nonheme iron ligand.

3.4 Experimental Section

N-methoxyphenanthridinium tetrafluoroborate was prepared according to a literature procedure.¹⁸ Iodosylbenzene was prepared by a literature method and stored at 0 °C under inert atmosphere.²⁸ (N4Py)Fe(OTf)₂ and (Bn-TPEN)Fe(OTf)₂ were prepared by metalation of the ligand N4Py^{24b} and Bn-TPEN²⁹ with Fe(OTf)₂ according to a literature method.^{24a}

[(N4Py)Fe^{IV}=O] and [(Bn-TPEN) Fe^{IV}=O] were prepared by reacting [(N4Py)Fe(OTf)₂] and [(Bn-TPEN)Fe(OTf)₂] with an excess solid of PhIO.^{24a}

Aryl diphenylmethyl sulfides **1-4** and aryl 1-methyl-1-phenylethyl sulfides **5-7, 9** were prepared by acid catalyzed reaction of 4-X-thiophenols with diphenylmethanol or 2-phenyl-2-propanol according to literature method³⁰ and characterized according to the published data.^{15,31-34}

4-Trifluoromethylphenyl 1-methyl-1-phenylethyl sulfide **8** was prepared by a procedure reported in the literature³⁵ with some modification. A solution of 500 mg (2.8 mmol) of 4-trifluoromethylthiophenol in 0.8 mL of dry diethyl ether was added to phenylmagnesium bromide prepared from 420 mg (2.7 mmol) of bromobenzene and 68 mg (2.8 mmol) of magnesium in 5 ml of dry diethyl ether. The mixture was refluxed for 15 min, then 456 mg (2.3 mmol) of 2-phenyl-2-propyl bromide was added. The resulting mixture was refluxed for 3.5 h. A standard aqueous workup followed by purification by silica gel column chromatography with hexane as eluent, gave 450 mg (67 %) of **8**.

8. White solid, mp 25-36 °C. ¹H NMR (300MHz, CDCl₃): δ 1.75 (s, 6H), 7.19-7.36 (m, 5H), 7.41-7.49 (m, 4H). ¹³C NMR (75MHz, CDCl₃): δ 30.4, 52.3, 119.2-130.9 (q, *J* = 270 Hz), 125.5-125.6 (q, *J* = 3.7 Hz), 127.1, 127.4, 128.7, 130.4-131.3 (q, *J* = 1.1 Hz), 136.1, 138.6-138.7 (q, *J* = 1.4 Hz), 146.5. GC-MS: *m/z* (rel. intensity) M⁺ 77 (7), 91 (35), 103 (9), 115 (5), 119 (100), 178 (9), 296 (1). Anal. Calcd. for C₁₆H₁₅F₃S: C, 64.85; H, 5.10; S, 10.82. Found: C, 65.04; H, 5.07; S, 10.95.

3.4.1 Reaction details

Steady state photolysis. Photooxidation reactions were carried out in a photoreactor equipped with 2 phosphor coated Hg lamps (360 nm; 14 W each). 1 mL solution containing the aryl diphenylmethyl sulfide **1-4** (25 μmol) and MeOP⁺ (5.5 μmol) in N₂-saturated CH₃CN was irradiated in a rubber cap-sealed jacketed tube for 5 min, thermostated at 25 °C. After addition of an internal standard, the mixtures were analysed by GC and ¹H NMR. All products formed were identified by comparison with authentic specimens: diphenylmethanol, benzophenone, diaryl disulfides, protonated phenanthridine and methanol. The material balance was always satisfactory (> 90%).

Laser Flash Photolysis Studies. N₂-saturated CH₃CN solutions of MeOP⁺PF₆⁻ (1.6 × 10⁻⁴ M) and sulfides (1.0 × 10⁻² M) were employed under magnetic stirring. The transient spectra of the MeOP⁺/**1-4**, MeOP⁺/**6**, MeOP⁺/**8** and MeOP⁺/**9** systems (for the transient spectra of MeOP⁺/**5** and MeOP⁺/**7** systems see ref. 15) were obtained at 25 ± 0.5 °C by a point-to-point technique, monitoring the change of absorbance (ΔA) after the laser flash at intervals of 10 nm over the spectral range of 390–650 nm. Rate constants for the decay of radical cations **1^{•+}-4^{•+}** were obtained by monitoring the change of absorbance at the maximum absorption wavelengths (480-590 nm) at 25 ± 0.5 °C while the first-order rate constants for the fragmentation of radical cations **6^{•+}-9^{•+}** (*k_f*) were obtained by fitting the absorbance decay data at the maximum absorption wavelengths (510–570 nm) to the exponential equation at 0 ± 0.5 °C. Five to seven kinetic runs were performed with each solutions and the rate constants averaged. The error estimated on the rate constants was ±10%.

Kinetic studies for the oxidation of 1-4 by [(N4Py)Fe^{IV}=O]²⁺. Kinetic measurements were performed on a diode array UV-vis spectrophotometer using a quartz cuvette (10 mm path length) at 8 °C. A solution of [(N4Py)Fe^{IV}=O]²⁺ (1.2 mM in CH₃CN) was prepared by oxidation of the corresponding iron(II) complex [(N4Py)Fe^{II}(OTf)₂] with an excess of solid PhIO (2.5 equiv.). After 30 min, the solution was filtered and aryl diphenylmethyl sulfides (8-30 mM) were added. The rates of oxidation of **1-4** were monitored following the decay of the [(N4Py)Fe^{IV}=O]²⁺ absorption band at 695 nm.^{24a} The second-order rate constants (*k₂*) were obtained from the slope of the linear correlation of the pseudo-first-order rate constant (*k_{obs}*) vs the substrate concentrations.

Product Analysis of the Oxidation of 1-4, 5-8 by [(N4Py)Fe^{IV}=O]²⁺. [(N4Py)Fe^{IV}=O]²⁺ was generated in situ at room temperature by adding iodosylbenzene (12.5 μmol) to a stirred solution of [(N4Py)Fe^{II}(OTf)₂] (2.5 μmol) in acetonitrile (500 μL).^{24a} The mixture was vigorously stirred at room temperature for 15 min, then the solution was cooled down at 0 °C and 50 μmol of aryl diphenylmethyl sulfides (**1-4**) or aryl 1-methyl-1-phenylethyl sulfides (**5-8**) were added. After 10 min of vigorous stirring or 90 min respectively at 0 °C, 25 μmol of a Na₂S₂O₅ aqueous solution and the internal standard were added. The mixture was extracted with Et₂O, the organic layer was dried over Na₂SO₄ and analyzed by HPLC, GC and ¹H NMR. All products formed (diphenylmethanol, benzophenone, diaryl disulfides, aryl diphenylmethyl sulfoxides or 2-

phenyl-2-propanol, aryl disulfides, aryl 1-methyl-1-phenylethyl sulfoxides) were identified by comparison with authentic specimens.

Product Analysis of the Oxidation of 5–8 by [(Bn-TPEN)Fe^{IV}=O]²⁺. [(Bn-TPEN)Fe^{IV}=O]²⁺ was generated in situ at room temperature by adding iodosylbenzene (12.5 μmol) to a stirred solution of [(Bn-TPEN)Fe^{II}(OTf)₂] (2.5 μmol) in acetonitrile (500 μL).^{24a} The mixture was cooled down at 0 °C and vigorously stirred for 5 min, then 50 μmol of aryl 1-methyl-1-phenylethyl sulfides (**5–8**) were added. After 30 min of vigorous stirring, 25 μmol of a Na₂S₂O₅ aqueous solution and the internal standard were added. The mixture was extracted with Et₂O, the organic layer was dried over Na₂SO₄ and analyzed by HPLC, GC and ¹H NMR. Reaction products were identified as reported above for the oxidation promoted by [(N4Py)Fe^{IV}=O].

Product Analysis of the Oxidation of 5-7, 9 by [(PDP)Fe^V=O]³⁺ and [(BPMCN)Fe^V=O]³⁺ [(PDP)Fe^{II}(SbF₆)₂] or [(BPMCN)Fe^{II}(OTf)₂] (1.5 μmol) was solubilized in acetonitrile (600 μL). The solution was cooled down at 0 °C and 60 μmol of aryl 1-methyl-1-phenylethyl sulfides (**5–7, 9**) were added. 60 μmol of H₂O₂ (diluted from 35% w/w H₂O₂ commercial solution) were added over 6 min by syringe pump under vigorous stirring. At this point an internal standard was added and the reaction mixture was filtered over a short pad of SiO₂ with 2 mL of ethyl acetate and analyzed by ¹H NMR. All products formed (2-phenyl-2-propanol, aryl disulfides, aryl 1-methyl-1-phenylethyl sulfoxides) were identified by comparison with authentic specimens.

References

- (1) (a) C. Schoneich, D. Pogocki, G. L. Hug, K. Bobrowski, *J. Am. Chem. Soc.*, **2003**, *125*, 13700. (b) D. A. Butterfield, J. Kanski, *Peptides*, **2002**, *23*, 1299. (c) C. Schoneich, *Arch. Biochem. Biophys.*, **2002**, *397*, 370. (d) B. L. Miller, K. Kuczera, C. Schoneich, *J. Am. Chem. Soc.* **1998**, *120*, 3345. (e) K. Bobrowski, G. L. Hug, B. Marciniak, B. L. Miller, C. Schoneich, *J. Am. Chem. Soc.*, **1997**, *119*, 8000. (f) S. Ozaki, P. R. Ortiz de Montellano, *J. Am. Chem. Soc.*, **1995**, *117*, 7056. (g) B. Marciniak, G. L. Hug, J. Rozwadowski, K. Bobrowski, *J. Am. Chem. Soc.*, **1995**, *117*, 127 (h) R. Z. Harris, S. L. Newmyer, P. R. Ortiz de Montellano, *J. Biol. Chem.*,

- 1993**, 268, 1637. (i) Y. Watanabe, T. Numata, T. Iyanagi, S. Oae, *Bull. Chem. Soc. Jpn.*, **1981**, 54, 1163.
- (2) (a) H. Pellissier, *Tetrahedron*, **2006**, 62, 5559-5601. (b) I. Fernandez, N. Khiar, *Chem. Rev.*, **2003**, 103, 3651-3705. (c) M. C. Carreno, *Chem. Rev.*, **1995**, 95, 1717-1760. (c) J. Legros, J. R. Dehli, C. Bolm, *Adv. Synth. Catal.*, **2005**, 347, 19-31. (d) R. Bentley, *Chem.Soc.Rev.*, **2005**, 34, 309-324. (e) J. M. Shin, Y. M. Cho, G. Sachs, *J. Am. Chem. Soc.*, **2004**, 126, 7800-7811. (f) M. Caligaris, O. Carugo, *Coord. Chem. Rev.*, **1996**, 153, 83-154.
- (3) (a) S. Shaik, Y. Wang, H. Chen, J. Song, R. Meir, *Faraday Discuss.*, **2010**, 145, 49. (b) C. S. Porro, M. J. Sutcliffe, S. P. de Visser, *J. Phys. Chem. A*, **2009**, 113, 11635. (c) D. Kumar, S. P. de Visser, P. K. Sharma, H. Hirao, S. Shaik, *Biochemistry*, **2005**, 44, 8148. (d) P. K. Sharma, S. P. de Visser, S. Shaik, *J. Am. Chem. Soc.*, **2003**, 125, 8698. (e) E. Baciocchi, M. F. Gerini, P. J. Harvey, O. Lanzalunga, S. Mancinelli, *Eur. J. Biochem.*, **2000**, 267, 2705-2710. (f) H. B. Dunford, in *Heme Peroxidase*, John Wiley & Sons, New York, **1999**. (g) A. Tuynman, M. K. S. Vink, H. L. Dekker, H. E. Schoemaker, L. Weber, *Eur. J. Biochem.*, **1998**, 258, 906-913. (h) *Peroxidases in Chemistry and Biology* (Eds.: J. Everse, K. E. Everse, M. B. Grisham.), CRC Press, Boca Raton, **1991**. (i) E. Baciocchi, O. Lanzalunga, B. Pirozzi, *Tetrahedron*, **1997**, 53, 12287-12289. (j) D. R. Doerge, N. M. Cooray, M. E. Bewster, *Biochemistry*, **1991**, 30, 8960-8964. (k) S. Kobayashi, M. Nakano, T. Kimura, A. P. Schaap, *Biochemistry*, **1987**, 26, 5019-5022. (l) *Cytochrome P450: Structure, Mechanism, and Biochemistry* (Ed.: P. R. Ortiz de Montellano), 2nd ed., Plenum, New York, **1986**.
- (4) A. B. Peñeñory, J. E. Argüello, M. Puiatti, *Eur. J. Org. Chem.*, **2005**, 114-122.
- (5) E. Baciocchi, M. F. Gerini, O. Lanzalunga, A. Lapi, M. G. Lo Piparo, *Org. Biomol. Chem.*, **2003**, 1, 422.
- (6) E. Baciocchi, O. Lanzalunga, S. Malandrucco, M. Ioele, S. Steenken, *J. Am. Chem. Soc.*, **1996**, 118, 8973-8974.
- (7) Y. Goto, T. Matsui, S. Ozaki, Y. Watanabe, S. Fukuzumi, *J. Am. Chem. Soc.*, **1999**, 121, 9497.
- (8) S. Oae, Y. Watanabe, K. Fujimori, *Tetrahedron Lett.*, **1982**, 23, 1189.
- (9) D. Kumar, G. N. Sastry, S. P. de Visser, *Chem. Eur. J.*, **2011**, 17, 6196.
- (10) (a) W. Nam, Y.-M. Lee, S. Fukuzumi, *Acc. Chem. Res.*, **2014**, 47, 1146. (b) J. Park, Y. Morimoto, Y.-M. Lee, W. Nam, S. Fukuzumi, *Inorg. Chem.*, **2014**, 53, 3618-3628. (c) J. Park, Y. Morimoto, Y.-M. Lee, W. Nam, S. Fukuzumi, *J. Am. Chem. Soc.*, **2012**, 134, 3903-3911. (d)

- J. Park, Y. Morimoto, Y.-M. Lee, W. Nam, S. Fukuzumi, *J. Am. Chem. Soc.*, **2011**, *133*, 5236-5239. (e) C. Krebs, D. G. Fujimori, C. T. Walsh, J. M. Bollinger Jr., *Acc. Chem. Res.*, **2007**, *40*, 484. (f) W. Nam, *Acc. Chem. Res.*, **2007**, *40*, 522. (g) J. Park, J. Lee, Y. Suh, J. Kim, W. Nam, *J. Am. Chem. Soc.*, **2006**, *128*, 2630-2634. (h) C. V. Sastri, M. S. Seo, M. J. Park, K. M. Kim, W. Nam, *Chem. Commun.*, **2005**, 1405-1407. (i) J. Legros, C. Bolm, *Angew. Chemie, Int. Ed.* **2003**, *42*, 5487. (l) J. Legros, C. Bolm, *Angew. Chemie, Int. Ed.*, **2004**, *43*, 4225.
- (11) (a) A. M. Khenkin, G. Leitun, R. Neumann, *J. Am. Chem. Soc.*, **2010**, *132*, 11446. (b) A. Kumar, I. Goldberg, M. Botoshansky, Y. Buchman, Z. Gross, *J. Am. Chem. Soc.*, **2010**, *132*, 15233.
- (12) (a) O. Lanzalunga, A. Lapi, *J. Sulfur Chem.*, **2011**, *33*, 101-129. (b) E. Baciocchi, T. Del Giacco, P. Giombolini, O. Lanzalunga, *Tetrahedron*, **2006**, *62*, 6566-6573. (c) R. S. Glass, *Top. Curr. Chem.*, **1999**, *205*, 1.
- (13) W. Adam, J. E. Argüello, A. B. Peñeñory, *J. Org. Chem.*, **1998**, *63*, 3905-3910.
- (14) T. Del Giacco, O. Lanzalunga, M. Mazzonna, P. Mencarelli, *J. Org. Chem.*, **2012**, *77*, 1843-1852.
- (15) E. Baciocchi, M. Bettoni, T. Del Giacco, O. Lanzalunga, M. Mazzonna, P. Mencarelli, *J. Org. Chem.*, **2011**, *76*, 573-582.
- (16) E. Baciocchi, T. Del Giacco, M. F. Gerini, O. Lanzalunga, *Org. Lett.*, **2006**, *8*, 641-644.
- (17) E. Baciocchi, C. Crescenzi, O. Lanzalunga, *Tetrahedron*, **1997**, *53*, 4469.
- (18) D. Shukla, L. Guanghua, J. P. Dinnocenzo, S. Farid, *Can. J. Chem.*, **2003**, *81*, 744.
- (19) W. N. Oloo, L. Que Jr., *Acc. Chem. Res.*, **2015**, *48*, 2612-2621.
- (20) O. Y. Lyakin, A. M. Zima, D. G. Samsonenko, K. P. Bryliakov, E. P. Talsi, *ACSCatal.*, **2015**, *5*, 2702-2707.
- (21) I. Prat, A. Company, V. Postils, X. Ribas, L. Que Jr., J. M. Luis, M. Costas, *Chem. Eur. J.*, **2013**, *19*, 6724-6738.
- (22) E. Baciocchi, T. Del Giacco, O. Lanzalunga, P. Mencarelli, B. Procacci, *J. Org. Chem.*, **2008**, *73*, 5675.
- (23) (a) E. Baciocchi, O. Lanzalunga, F. Marconi, *Tetrahedron Lett.*, **1994**, *35*, 9771-9774. (b) E. Baciocchi, E. Fasella, O. Lanzalunga, M. Mattioli, *Angew. Chem. Int. Ed. Engl.*, **1993**, *32*, 1071. (c) E. Baciocchi, C. Rol, E. Scamosci, G. V. J. Sebastiani, *Org. Chem.*, **1991**, *56*, 5498.

- (24) (a) J. Kaizer, E. J. Klinker, N. Y. Oh, J.-U. Rohde, W. J. Song, A. Stubna, J. Kim, E. Münck, W. Nam, L. Que Jr., *J. Am. Chem. Soc.*, **2004**, *126*, 472. (b) M. Lubben, A. Meetsma, E. C. Wilkinson, B. Feringa, L. Que Jr., *Angew. Chem. Int. Ed.*, **1995**, *34*, 1512.
- (25) E. Baciocchi, M. Bietti, O. Lanzalunga, *J. Phys. Org. Chem.*, **2006**, *19*, 467.
- (26) O. Lanzalunga, A. Lapi, *J. Sulfur Chem.*, **2012**, *33*, 101.
- (27) O. Lanzalunga, *Phosphorous, Sulfur, and Silicon*, **2013**, *188*, 322.
- (28) H. J. Salzman, G. Sharefkin, *Organic Syntheses*, Wiley: New York, **1973**; Vol. V, p 658.
- (29) L. Duelund, R. Hazell, C. J. McKenzie, L. P. Nielsen, H. Toftlund, *J. Chem. Soc. Dalton Trans*, **2001**, 152.
- (30) C. G. Screttas, M. Micha-Screttas, *J. Org. Chem.*, **1977**, *42*, 1462.
- (31) Y. Guo, W. S. Jenks, *J. Org. Chem.*, **1997**, *62*, 857.
- (32) H. Firouzabadi, N. Iranpoor, A. A. Jafari, *Tetrahedron Lett.*, **2005**, *46*, 2683-2686.
- (33) G. Frensh, N. Hussain, F. A. Marques, P. J. Walsh, *Adv. Synth. Catal.*, **2014**, *356*, 2517.
- (34) C. Y. Meyers, R. Chan-Yu-King, D. H. Hua, V. M. Kolb, W. S. Matthews, T. E. Parady, T. Horii, P. B. Sandrock, Y. Hou, S. Xie, *J. Org. Chem.*, **2003**, *68*, 500.
- (35) X. Creary, *J. Org. Chem.*, **1985**, *50*, 5080.

Chapter 4

Oxidation of alcohols and aromatics with H₂O₂ catalyzed by a nonheme imine based iron complex

In this chapter is described the application of an iminopyridine iron(II) complex, easily prepared *in situ* by self-assembly of cheap and commercially available starting materials, 2-picolylaldehyde, 2-picolylamine, and Fe(OTf)₂, in a 2:2:1 ratio, in the oxidation of alcohols and aromatic compounds. Oxidation of aliphatic alcohols to carbonyl products proceeds smoothly, while that of benzylic alcohols is more challenging with an unprecedented selectivity toward the aromatic ring instead of the alcohol moiety. This selectivity has been exploited in the oxidation of aromatic substrates where the catalyst shows a marked preference for aromatic ring hydroxylation over side-chain oxidation, both in intramolecular and intermolecular competitions. The selectivity pattern of this reaction closely matches that of electrophilic aromatic substitutions with a metal-based S_EAr pathway, without a significant involvement of free diffusing radical pathways, as supported by kinetic isotope effect studies and by the use of radical scavengers.

The results in this Chapter are published:

-G. Olivo, M. Nardi, D. Vidal-Sanchez, A. Barbieri, A. Lapi, L. Gómez, O. Lanzalunga, M. Costas, S. Di Stefano, *Inorg. Chem*, **2015**, *54*, 10141-10152.

-G. Olivo, S. Giosia, A. Barbieri, O. Lanzalunga, S. Di Stefano, *Org. Biomol. Chem.*, **2016**, *14*, 10630-10635.

- G. Capocasa, G. Olivo, A. Barbieri, O. Lanzalunga, S. Di Stefano, *Catal. Sci. Technol.*, **2017**, *7*, 5677.

4.1 Introduction

During the past decade, nonheme iron(II) complexes of tetradentate or pentadentate amine ligands have shown high levels of regio- and chemo-selectivity in the oxidations of a broad range of organic compounds.¹ Many efforts have been made not only in the comprehension of the catalytic mechanism but also in the identification of the intermediates involved in such oxidative transformations as described in Chapter 1 and in Chapter 2.^{1a,2}

The selectivity in the oxidations promoted by nonheme iron complexes is dictated primarily by electronic and steric effects indeed, the most electron-rich and sterically accessible bonds in the substrate are the most easily oxidized.³⁻⁵ Moreover, structural features of the catalyst might also play a key role. The increase of the catalyst steric hindrance and consequent decrease of accessibility to the active iron-oxo moiety, can even switch the reactivity in favor of the least sterically encumbered positions.⁶ However, these bulky and sophisticated catalysts usually require rather elaborate ligands that limit their applicability.

With the aim of simplifying ligand structures, we have started to explore the activity of imine-based iron complexes.⁷ Despite the imines preparation is much easier in comparison with amines, many imine-based complexes explored recently in the oxidations of simple cycloalkanes showed reactivity patterns characteristic of free-diffusing radicals and moderate TONs, as explained in Chapter 1.⁸⁻¹⁰ Nevertheless, few years ago, my research group, reported^{7,11} that simple imine-based nonheme iron(II) complexes (Figure 1), prepared just by simply mixing commercially available, non-expensive reagents (2-aminopicoline and 4-substituted-2-picolyl aldehydes) in the reaction vessel, with no prior synthesis and isolation, catalyzed alkane hydroxylation with efficiencies (TONs in the range of 15-48) comparable to those obtained with much more sophisticated amine-based catalysts.^{3,4,6,8,12}

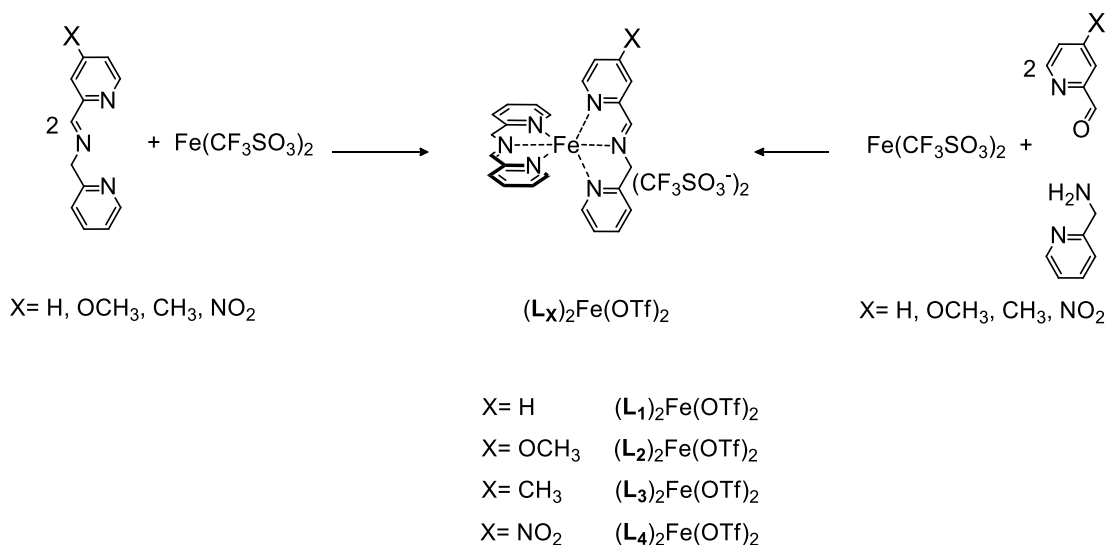


Figure 1. Imine-based iron complexes $[(\text{L}_1)_2\text{Fe}(\text{OTf})_2]$ - $[(\text{L}_4)_2\text{Fe}(\text{OTf})_2]$

The solid-state structures of $[(\text{L}_1)_2\text{Fe}(\text{OTf})(\text{ClO}_4)]$ and $[(\text{L}_3)_2\text{Fe}(\text{OTf})_2]$ showed a low-spin slightly distorted octahedral geometry around the iron center with the ligands arranged in a meridional fashion and the two iminic N atoms in *trans* to each other.¹¹ A detailed mechanistic study provided evidence that C-H oxidations were metal-based indeed reactions occurred with high stereoretention at the hydroxylated carbon. Moreover the selectively at tertiary over secondary C-H bonds, alcohol ketone ratio and KIE (Figure 2) were in accordance with the values obtained with other nonheme amine-based iron complexes for which the involvement of a metal-based oxidant has been demonstrated.¹¹

Moreover isotopic labeling analyses showed that oxygen atoms present in the oxygenated product, came from H_2O_2 .¹¹

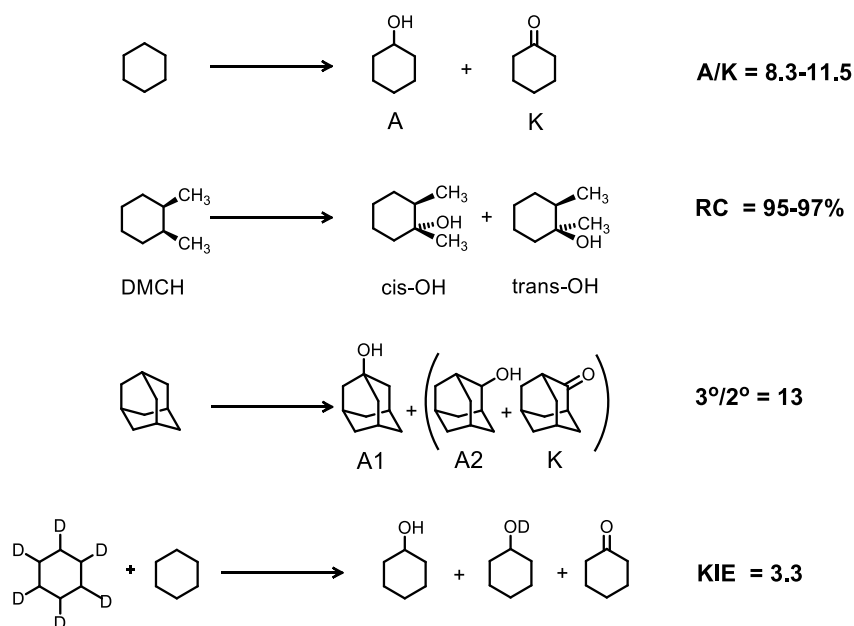
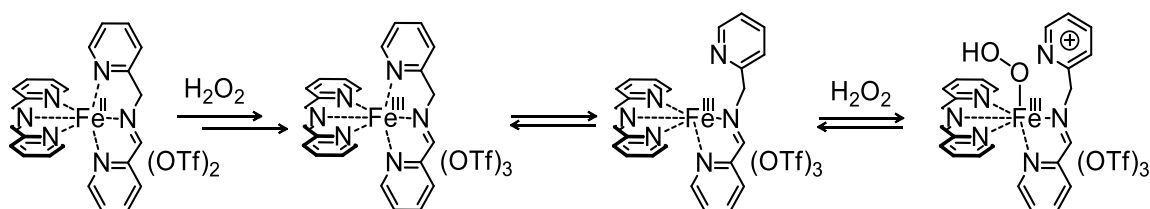


Figure 2. Oxidation of mechanistic probes used to distinguish between a metal-based and a free radical-based oxidation with H_2O_2 catalyzed by $[(L_1-L_4)_2Fe(OTf)_2]$.

Indirect experimental evidences prompted us to suggest that the reaction involved initial oxidation of the complex to the ferric state followed by a ligand arm dissociation that enabled the H_2O_2 binding and activation (Scheme 1).¹¹ Selectivity patterns and isotopic labeling studies strongly suggested that activation of hydrogen peroxide occurred by heterolytic O-O cleavage, through the probable intermediacy of a pentadentate oxidizing species, without the assistance of a *cis*-binding water or carboxylic acid.¹¹



Scheme 1. First transformations in the catalytic cycle of $[(L_1)_2Fe(OTf)_2]$ showing the hydrogen peroxide coordination.

The interesting results obtained in the aliphatic C-H hydroxylation^{7,11}, encouraged us to expand the application of this catalyst to the oxidation of alcohols.

Oxidation of alcohols is a fundamental reaction in organic synthesis, since it converts available substrates into carbonyl compounds prone to further functionalization. Several methodologies have been developed over the years to perform such reaction but most of them employed toxic reactive oxidants such as CrO₃ or hypervalent iodine,^{13,14} so the use of a non-polluting catalyst in combination with a cheap and environmentally friendly terminal oxidant as H₂O₂ or O₂, is an optimal alternative. Recently, some non-toxic systems (Cu/air/TEMPO¹⁵ or tungsten oxide/phase transfer catalysts¹⁶) gave brilliant results, however the large availability and low environmental impact of the iron coupled with the high atom-economy of H₂O₂,¹⁷ make the latter catalytic systems highly attractive. In the last years, it has been demonstrated that aminopyridine iron complexes are able to promote effective and highly selective oxidation reactions, mimicking natural nonheme iron oxygenases^{3,12c,18} in presence of H₂O₂ and *t*-BuOOH.^{19,10b} Also manganese-based catalysts in combination with H₂O₂ provided promising results in alcohol oxidation as, for instance, the catalytic system obtained *in situ* by combination of a Mn (II) salt, pyridine-2-carboxylic acid (PCA) and substoichiometric 1,2-diketones proposed by Browne and his research group.²⁰

The surprising observation of some byproducts deriving from oxidation of the aromatic C-H bonds in the oxidation of benzylic alcohols, prompted us to investigate also the oxidation of aromatic substrates with H₂O₂ promoted by [(L₁)₂Fe(OTf)₂]. It is well known that the synthesis of phenol by direct hydroxylation of aromatic compounds is very challenging²¹ due to the high stability towards oxidation of the aromatic ring and to the great strength of the C-H bonds. Moreover it is usually difficult to limit the oxidation at the desired phenol stage, since the latter is more reactive than the parent substrate (*chemoselectivity* issue) or to discriminate among different oxidation sites (*regioselectivity* issue).

Oxygen-centered radicals can effectively hydroxylate aromatic rings,²² but they generally suffer the poor selectivity of the process.^{21b} Combination of metal complexes and peroxide oxidants is also possible, indeed several Ni,^{21f} Cu^{1a,23} and Fe²⁴ complexes have been tested as catalysts with H₂O₂. However, most of these systems were found to involve the formation of reactive HO•^{24a,b,25} or slightly more stable HOO•^{23a,26} through Fenton-type processes. A remarkable

exception to this mechanistic scenario is the Ni-TPEA/H₂O₂ system described by Itoh,^{21f} which works through a genuine metal-based mechanism.

The nonheme iron complexes are able to promote the hydroxylation of aromatic rings,²⁷ but irreversible phenol binding to these tetracoordinated Fe^{III} species usually prevents catalytic turnover.^{24a,27e,28} Nonetheless, careful modification of the ligand architecture aimed at disfavoring such coordination (for instance pentadentate complexes^{24d,24e}), may avoid inhibition and allow catalytic oxidations in few cases^{24c,24d} but, very often, doubly oxidized quinones are the main products.^{24e,29} The probable intermediacy of a pentadentate oxidizing species in the [(L₁)₂Fe(OTf)₂] catalytic cycle, together with the encouraging results obtained in the benzyl alcohol oxidations, indicate that this imine-based iron complex may represent a suitable catalyst for the efficient and selective oxidations of aromatic compounds.

4.2 Results and Discussion

4.2.1 Oxidation of alcohols with H₂O₂ catalyzed by [(L₁)₂Fe(OTf)₂]

Before to investigate the efficiency of the complex [(L₁)₂Fe(OTf)₂] in the oxidations of a broad range of cyclic and linear aliphatic alcohols, we selected the oxidation of cyclohexanol to cyclohexanone to find the optimized reaction conditions consisting in the slow addition of 2.5 molar equivalents of H₂O₂ and 1 mol % catalyst [(L₁)₂Fe(OTf)₂], (generated in situ by self-assembly of 2-picolylaldehyde and 2-picolylamine) at 25 °C in CH₃CN for 90 min (Figure 3).

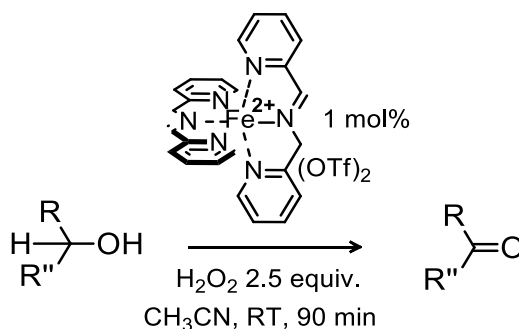
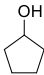
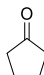
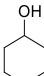
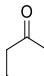
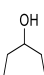
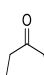
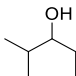
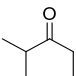
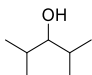
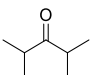
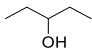
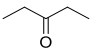
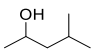
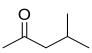


Figure 3. Alcohol Oxidation catalyzed by $[(L1)_2Fe(OTf)_2]$ in CH_3CN at 25 °C.

At first, the effect of the alcohol ring size and substrate steric hindrance on the catalytic efficiency was evaluated (see Experimental Section). Cyclopentanol and cycloheptanol are oxidized slightly less efficiently than cyclohexanol. Oxidation of 2-methylcyclohexanol and 2,6-dimethylcyclohexanol also led to lower yields of ketones with respect to cyclohexanol as an effect of the steric hindrance around the hydroxyl function (Table 1).

Table 1. Oxidation of aliphatic alcohols to the corresponding ketones with H_2O_2 catalyzed by $[(L1)_2Fe(OTf)_2]$ in CH_3CN at 25 °C.^a

substrate	conv(%)	product	yield (%)
	77		54
	93		74
	67		56
	73		54
	51		38
	80		76
	57		50 ^b



^aReaction condition, determination of yields and conversions, are reported in the Experimental Section. Yield and TON coincide.

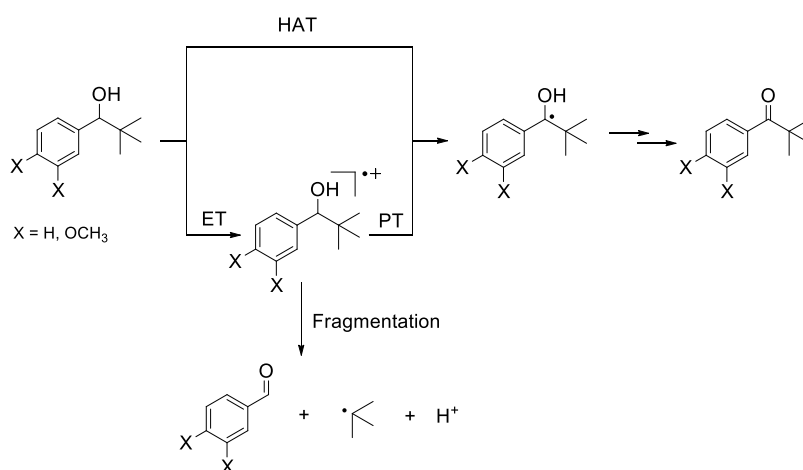
^breaction carried out in CH₃CN/CH₂Cl₂ 80:20. ^cKetone product is accompanied by lower amounts of C-H oxidation products.

^dCarboxylic acid is also detected.

The oxidation of linear alcohol 3-pentanol to 3-pentanone proceeded smoothly (Table 1) and, also in this case, the presence of a methyl group in the β position (4-methyl-2-pentanol) led to a marked decrease in ketone yield.

Primary alcohols were less prone to oxidation, as expected on the basis of electronic effects and this is reflected in the low yield of aldehyde obtained in 1-decanol oxidation. Oxidation of cyclohexanol to cyclohexanone and cycloheptanol to cycloheptanone were carried out in preparative scale (500 mg of substrate) under the optimized conditions (see Experimental Section). The reaction proceeded smoothly with no loss in efficiency, yielding 67% and 50% of ketone products, respectively and the ketone could be easily obtained pure after a quick filtration on an inch SiO₂ layer with dichloromethane, demonstrating the good potential of such catalyst for synthetic purpose (unreacted alcohol remains on the silica layer).

In order to gain more information about the reaction mechanism, we carried out the oxidation of a substrate probe, 1-phenyl-2,2-dimethylpropanol under the same conditions. The occurrence of an electron transfer (ET) mechanism would form a radical cation which undergoes rapid fragmentation to yield benzaldehyde, in competition with proton transfer and ketone formation (Scheme 2).³⁰ In our case, no trace of benzaldehyde was detected even when the more easily oxidizable 1-(3,4-dimethoxy)-phenyl-2,2-dimethylpropanol was used as a substrate. Therefore, an ET oxidation mechanism can be reasonably excluded in favour of hydrogen atom transfer (HAT). Interestingly, a similar mechanism has been proposed also for the oxidation of the same substrate promoted by the active species of cytochrome P450.³¹



Scheme 2. Oxidation of 1-aryl-2,2-dimethylpropanol with H₂O₂ catalyzed by [(L₁)₂Fe(OTf)₂].

We then turned our attention to benzylic alcohol substrates because it is well known that the oxidation of benzyl alcohols to carbonyl compounds is usually easier than oxidation of aliphatic ones. Accordingly a HAT process from the benzylic α -C-H(OH) bond to the metal-based oxidant, is facilitated not only by the relatively low BDE of this bond³² but also by the stabilization of the partial positive charge developing on the benzylic carbon in the TS due to polar effects.^{33,34} Surprisingly, disappointing results have been obtained in the oxidation of these substrates with H₂O₂ catalyzed by [(L₁)₂Fe(OTf)₂]. Primary benzyl alcohol and secondary 1-phenylethanol are sluggishly oxidized into the corresponding carbonyl compounds with poor selectivity (Table 2).

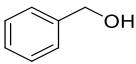
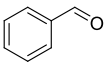
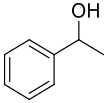
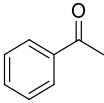
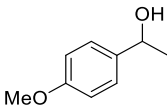
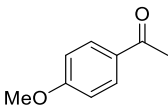
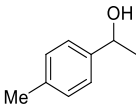
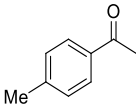
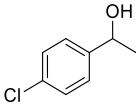
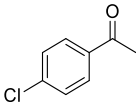
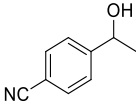
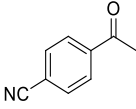
As a possible explanation, we have proposed that the highly electrophilic oxidizing species formed by reaction of [(L₁)₂Fe(OTf)₂] with H₂O₂, is able to hydroxylate the aromatic ring in a process occurring in competition with the side-chain benzylic oxidation (this hypothesis is supported by the observation of GC peaks assigned to phenolic oxidation byproducts in amounts comparable to those of aromatic ketones).

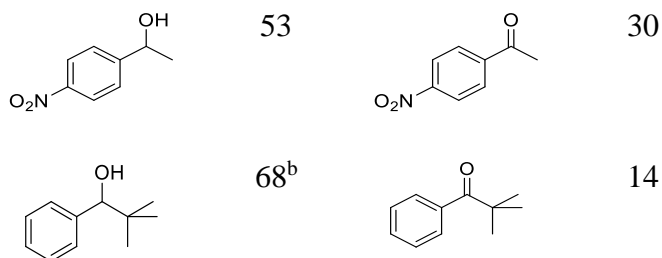
The oxidation of a series of 4-substituted-1-phenylethanols, revealed that the yields of the ketone products regular increased on increasing the electron withdrawing power of the substituents. The more electron donating is the substituent, the more prone to oxidation is the aromatic ring, with respect to the alcoholic moiety. The withdrawal of electron density from the aromatic ring tends to switch the preferential oxidation site

from the arene to the benzylic position. A similar behavior has been observed in the oxidation of alkylaromatic substrates.²⁸

Moreover, when cyclohexanol oxidation was carried out in the presence of equimolar amounts of toluene or benzene, catalytic activity dramatically dropped down (10% and 11% cyclohexanone yield, respectively), reinforcing the idea of competitive aromatic ring oxidation. Some iron-based catalysts have been recently reported to efficiently convert benzylic alcohols into the corresponding carbonyl compounds,^{19a,e,f,10b} as for instance [(TPA)Fe(OTf)₂].

Table 2. Oxidation of benzylic alcohols to carbonyl products with H₂O₂ catalyzed by [(L₁)₂Fe(OTf)₂] in CH₃CN at 25 °C.^a

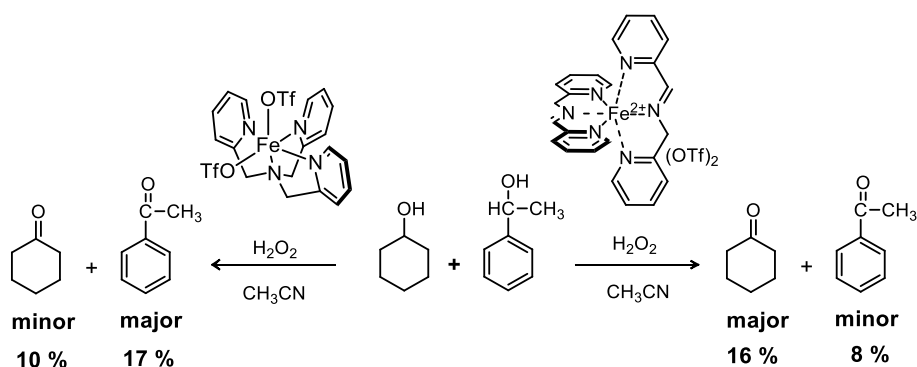
substrate	conv(%)	product	yield (%)
	51 ^b		21
	58 ^b		9
	80 ^b		5
	65 ^b		6
	36 ^b		11
	55		29



^aReaction condition, determination of yields and conversions, are reported in the Experimental Section. Yield and TON coincide.

^bdihydroxyl derivatives appear in the mass spectra of the product mixture.

At this point, a competitive oxidation experiment between equimolar amounts of 1-phenylethanol and cyclohexanol was carried out in presence of $[(\mathbf{L}_1)_2\text{Fe}(\text{OTf})_2]$ or $[(\text{TPA})\text{Fe}(\text{OTf})_2]$ (see Experimental Section). In the oxidation catalyzed by $[(\text{TPA})\text{Fe}(\text{OTf})_2]$, the acetophenone yield (17 %) was much higher than that of cyclohexanone (10 %) as expected on the basis of an enthalpic (BDEs of $\alpha\text{-C-H}(\text{OH})$ bonds are 92.8 and 85.1 kcal/mol for cyclohexanol and 1-phenylethanol, respectively)³² and polar effects in HAT processes. The cyclohexanone yield (16 %) was much higher than that of acetophenone (8 %) in the oxidation catalyzed by $[(\mathbf{L}_1)_2\text{Fe}(\text{OTf})_2]$ confirming the peculiar selectivity displayed by this catalyst (Scheme 3).



Scheme 3. Competitive oxidations of 1-phenylethanol and cyclohexanol with H_2O_2 catalyzed by $[(\mathbf{L}_1)_2\text{Fe}(\text{OTf})_2]$ or $[(\text{TPA})\text{Fe}(\text{OTf})_2]$ in CH_3CN .

4.2.2 Oxidation of aromatic compounds with H₂O₂ catalyzed by [(L₁)₂Fe(OTf)₂]

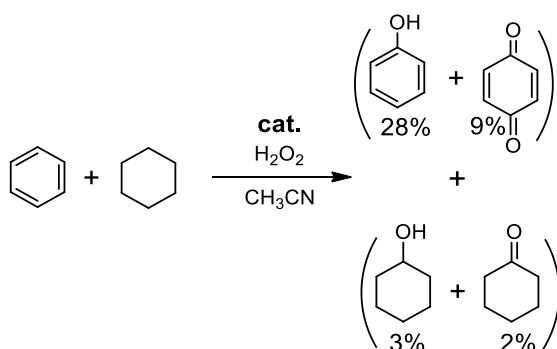
The surprising oxidation selectivity observed with benzylic alcohols, prompted us to carry out a detailed investigation of the oxidation of aromatic substrates with H₂O₂ promoted by [(L₁)₂Fe(OTf)₂].

We began our investigation by focusing on the oxidation of the simplest yet challenging aromatic substrate benzene and, after a careful search for the best reaction conditions, we realized that the optimal set-up was very similar to that employed for the alcohols oxidation (see Experimental Section). Increase in the reaction time or in the amount of oxidant led to an increase of the benzoquinone yield, strongly suggesting that the latter compound derived from phenol overoxidation. Slow addition of H₂O₂, generally used in the oxidations mediated by nonheme iron complexes in order to keep its concentration low and avoid unproductive disproportionation,^{18a,35} was unnecessary and almost the same product yields were obtained by adding the oxidant all at once at the beginning of the reaction.

It was interesting to note that benzene oxidation could be easily scaled up (0.5 g) without losses in efficiency (26% yield), highlighting the attractiveness of this approach.

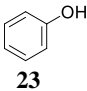
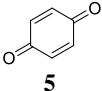
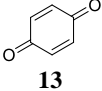
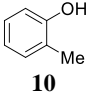
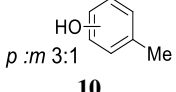
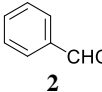
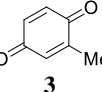
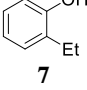
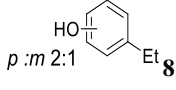
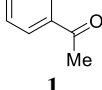
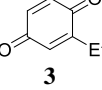
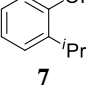
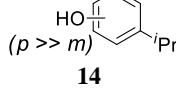
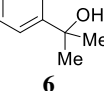
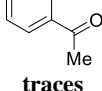
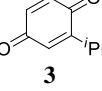
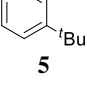
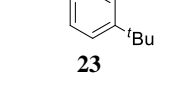
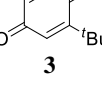
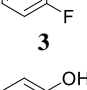
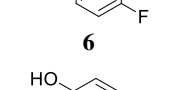
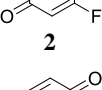
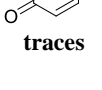
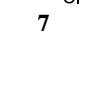
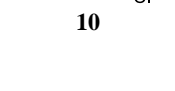
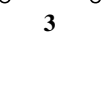
We extended then our study to the oxidation of alkylbenzenes. Oxidation of toluene catalyzed by [(L₁)₂Fe(OTf)₂] produced three cresols (20 %, *ortho* + *para* + *meta* in a 10:7.5:2.5 ratio) in a total yield comparable to the one obtained in the benzene oxidation (Table 3). Remarkably, only low amounts of products deriving from aliphatic hydrogen atom abstraction (benzaldehyde 2%, bibenzyl <1%) were detected, indicating that [(L₁)₂Fe(OTf)₂] is highly selective for aromatic over aliphatic oxidation (84% selectivity). Even with aromatic compounds containing more easily oxidable secondary or tertiary aliphatic C-H bonds such as ethylbenzene and cumene, the oxidations occur preferentially in the aromatic ring (15% *para* + *meta* + *ortho* ethylphenols and 1% of acetophenone for ethylbenzene and 21% *ortho* + *meta* + *para* isopropylphenols, 3% of 2-phenyl-2-propanol and 3% of 2-isopropyl-1,4-benzoquinone for cumene oxidation).

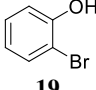
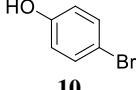
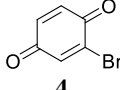
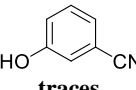
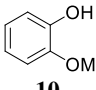
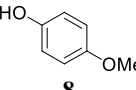
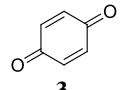
Preference for aromatic over aliphatic oxidation is further confirmed in the intermolecular competitive oxidation of benzene and cyclohexane (see Scheme 4). Aromatic hydroxylation (combined 37% yield) is clearly favored over alkane oxidation (combined 5% yield), in line with the results obtained in intramolecular competitions.



Scheme 4. Competitive oxidation of benzene and cyclohexane (1:1 ratio) catalyzed by $[(\text{L}1)_2\text{Fe}(\text{OTf})_2]$

Table 3. Oxidation of aromatic compounds with H_2O_2 by complex $[(\text{L}1)_2\text{Fe}(\text{OTf})_2]$ in CH_3CN at $25\text{ }^\circ\text{C}$.^a

Sub Ph-X	Unreacted sub	Product 1	Product 2	Product 3	Product 4	Product 5	Product 6	Selectivity for aromatic oxidation
H	55	 23				 5		-
OH	52					 13		-
CH_3	47	 10	 <i>p:m</i> 3:1 10		 2	 3		92%
Et	47	 7	 <i>p:m</i> 2:1 8		 1	 3		92%
<i>i</i> Pr	65	 7	 <i>(p >> m)</i> 14	 6	 traces	 3		80%
^t Bu	48	 5	 23			 3		100%
F	73	 3	 6			 2	 traces	-
Cl	76	 7	 10			 3		-

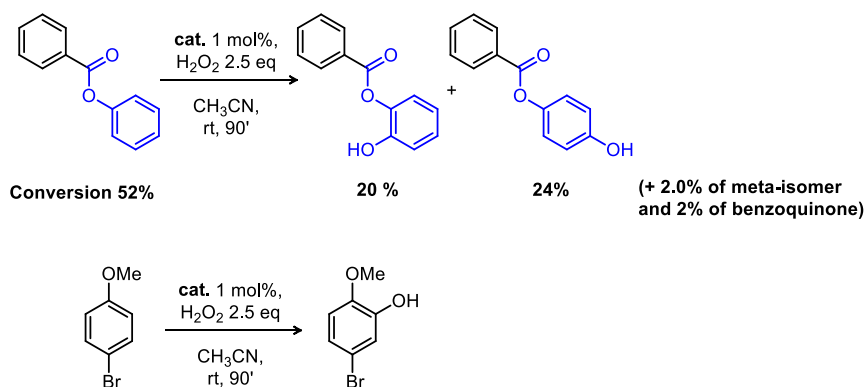
Br	65				-
CN	100		 traces		-
OCH ₃	58				-

^aReaction condition, determination of yields and conversions, are reported in the Experimental Section. GC conversions and yields are an average of at least two determinations (relative error within 5%, within 10% for yields).

Such selective preference for arene hydroxylation is inconsistent with the involvement of HO[•] radicals^{21b,36} and it is higher than what generally reported for iron catalysts.^{24b,c,37,38} This results show that our system could be one of the most selective reported in the literature.^{21f,g} Oxidation of *tert*-butylbenzene by complex [(L₁)₂Fe(OTf)₂] and H₂O₂ gave the best results among the alkylaromatic substrates with a 28% yield of phenols and 3% of *tert*-butyl-1,4-benzoquinone as the only byproduct. In all these cases, hydroxylation mostly occurs on the *ortho* and *para* positions of the alkylbenzenes, showing a selectivity pattern resembling that of electrophilic aromatic substitutions moreover the distribution of phenol products is sensitive to the steric hindrance of the lateral chain, accordingly the ratio (*meta+para*)/*ortho* steadily increases going from methyl (toluene), ethyl (ethylbenzene), isopropyl (cumene), *t*-butyl (*tert*-butylbenzene) (1.0, 1.14, 2.0 and 4.6 respectively).

Fluoro, chloro and bromobenzenes are smoothly oxidized to *ortho* and *para* phenols with some 1,4-benzoquinone byproducts, in accordance with the *ortho-para* directing effects of the halogens substituents in electrophilic aromatic substitution reactions. Moreover, electron-withdrawing groups (-CN) deactivated the aromatic rings towards electrophiles, while, on the other hand, electron-releasing groups enhanced the electron-density of the aromatic ring and thus favor its oxidation (Table 3).

In support of an electrophilic aromatic substitution reactions are also the results of the oxidation of phenyl benzoate where the two arenes have different electronic features. The most electron rich phenolic moiety is preferentially hydroxylated over the benzoyl ring (see Scheme 5, top). Moreover in the oxidation of 5-bromo-2-methoxyphenol only the formation of the 5-bromo-2-methoxyphenol, guided by the most electron-releasing group, was observed (see Scheme 5, bottom).



Scheme 5. Oxidation selectivity in the presence of substituents with different electronic properties.

4.2.2.1 Mechanistic outlook

The results reported above, would suggest an electrophilic aromatic substitution, but in principle, other possible mechanistic pathways are feasible (Figure 4). The oxidation could be promoted by oxygen-centered radicals formed through Fenton-type reactions of the iron complex with H_2O_2 (path *a*) or alternatively can be promoted by a high-valent iron species (metal-based mechanism, paths *b-e*) in a hydrogen atom abstraction from the aromatic substrate (path *b*), electrophilic aromatic substitution (path *c*), radical aromatic substitution (path *d*) and arene epoxidation followed by rearrangement (path *e*).

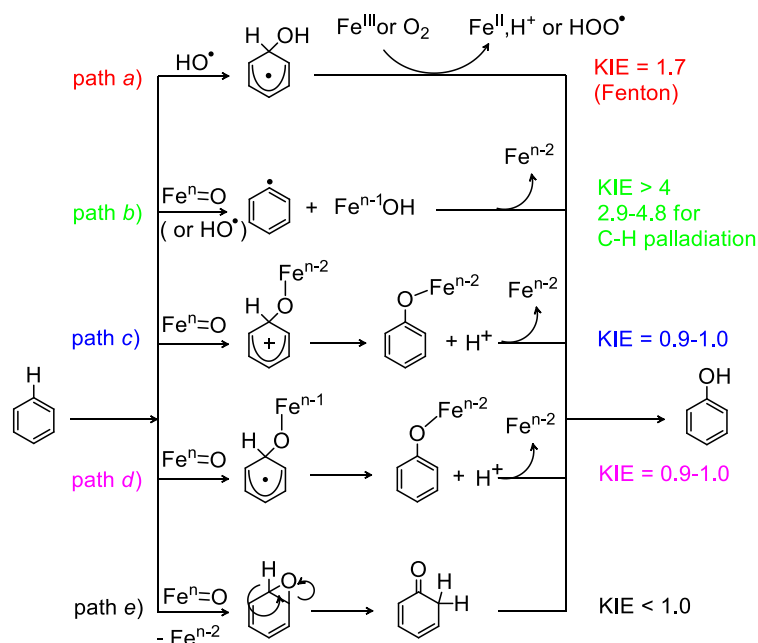


Figure 4. Alternative mechanisms in the aromatic oxidation with H_2O_2 catalyzed by complex $[(L_1)_2Fe(OTf)_2]$.

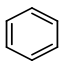
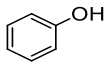
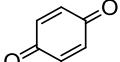
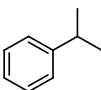
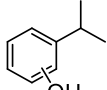
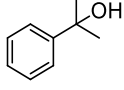
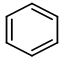
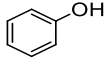
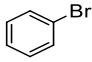
The good selectivity observed in the oxidation of substituted benzene derivatives as well as the high sensitivity to the electronic properties of the substituent, are generally not consistent with a free radical reaction, but point to a metal-based oxidation mechanism mediated by an electrophilic species. Indeed, Fenton-type oxidations are less sensitive to the electronic effects of the substituent and afford comparable yields of lateral chain oxidation.^{36b,39}

The scarce effect of O_2 , that strongly affects the efficiency and the selectivity in radical processes,^{36b,39,40} coupled with the absence of biphenyl dimerization products, that should be favored over phenol production in the absence of O_2 in Fenton-type systems,^{36b} are also in support of a metal-based mechanism in the oxidation of benzene and cumene with H_2O_2 catalyzed by $[(L_1)_2Fe(OTf)_2]$ (Table 4).

Furthermore, no traces of bromobenzene have been observed when the benzene oxidation was carried out in the presence of the radical trap $CBrCl_3$.^{35,41} On the other hand, Fenton-type benzene oxidation, i.e. with simple $Fe(OTf)_2(CH_3CN)_2$ salt as the catalyst in presence of H_2O_2 , carried out in the presence of $CBrCl_3$, formed significant amounts of bromobenzene byproduct, likely derived from Br atom abstraction by an intermediate carbon-centered radical. All these pieces of evidence consistently point to an aromatic hydroxylation fully devoid of free radical

intermediates, allowing us to confidently discard the radical path *a*. We cannot entirely rule out the path *d* in Figure 4, since the very short-lived radical Wheland intermediate might form phenols before undergoing reaction with radical scavengers.

Table 4. Evidences in favor of a metal-based mechanism in the oxidation of benzene and cumene with H₂O₂ catalyzed by [(L₁)₂Fe(OTf)₂].^a

catalyst	additive	substrate	Product	Product
cat.	under air		 23%	 5%
cat.	under argon	“	26%	4%
cat.	under air		 21% ^b	 6%
cat.	under argon	“	27% ^c	7%
cat.	CBrCl ₃ ^d		 20% ^e	 n.d.
Fe ²⁺ ^f	CBrCl ₃ ^d	“	3%	1%
Fe ²⁺ ^f	-	“	4%	-

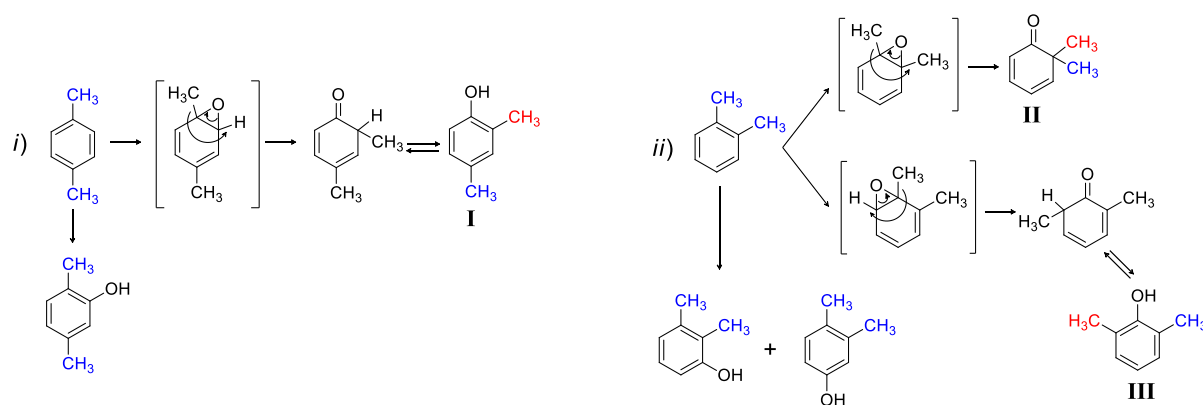
^aConditions as in Table 2. ^b+3% *p*-quinone. ^c+4% *p*-quinone. ^dAdded as 0.1 molar equivalent with respect to the substrate. ^e+3% *p*-quinone. ^fAdded as Fe(OTf)₂(CH₃CN)₂ salt.

Kinetic isotope effects, determined as the ratio between phenol and pentadeuterophenol *d*₅-PhOH in competitive oxidation of benzene and perdeuterated benzene, represents a powerful tool to discriminate among different aromatic oxidation mechanisms, since almost each pathway is reported to have a different and diagnostic KIE value (see Figure 4). The KIE value obtained, 0.98 ± 0.02, clearly rules out both a direct HAT process (path *b*, which typically furnishes much higher values) and radical reactions (a KIE of 1.7 has been reported for caged HO•/Fe^{IV}=O mediated aromatic hydroxylations, in which the first step is probably the addition

of the caged HO[•] radical to the aromatic ring^{24a}), and is consistent with a trigonal→tetrahedral change in the configuration of carbon atom directly involved in the reaction (paths *c*, *d*, and *e*). The KIE value is in line with those observed in natural iron oxygenases^{42,43} and in single-turnover oxidation experiments mediated by other nonheme^{24c,27d,e} or phthalocyanin⁴⁴ iron catalysts.

In order to distinguish between the two remaining pathways, i.e. electrophilic aromatic substitution (path *c*) or arene epoxidation (path *e*), we investigated the oxidation of *o*-xylene and *p*-xylene.

Oxidation of *o*-xylene led to the formation of a rearranged byproduct 2,2-dimethyl cyclohexadienone **II** (Scheme 6ii) deriving from methyl migration in an epoxide intermediate suggesting the occurrence of the arene epoxidation mechanism. However no traces of the other expected rearrangement product 2,6-dimethylphenol **III** (Scheme 6ii) were detected in the reaction mixture. Moreover, no parallel 1,2 alkyl shift was observed in the oxidation of *p*-xylene (no formation of 2,4-dimethylphenol **I**, Scheme 6i). Therefore, a general conclusion on the two mechanistic alternatives, path *c* or path *e*, cannot be drawn, since the rearrangement observed may be due to some specific properties of the *ortho*-xylene substrate (for instance, a certain character of double bond exerted by the two *ortho* methyl groups).



Scheme 6. Methyl rearrangements that can follow the direct oxygen transfer from the iron based active species to the aromatic rings of *p*-xylene and *o*-xylene.

4.3 Conclusion

The oxidation of aliphatic alcohols with H₂O₂ catalyzed by the complex [(L₁)₂Fe(OTf)₂], proceeded with moderate-to-good yields in the case of aliphatic secondary alcohols, depending on substrate steric hindrance and with moderate-to-low yields for the primary alcohols. Surprisingly benzylic alcohols are oxidized to aromatic ketones with low efficiency due to competitive aromatic hydroxylation.

The remarkable selectivity for the oxidation of the aromatic ring in benzyl alcohols is supported by the results of the oxidation of aromatic compounds with H₂O₂ catalyzed by the complex [(L₁)₂Fe(OTf)₂].

Gratifying results in terms of yields and selectivity have been obtained particularly when electron-releasing groups are present in the aromatic ring. In the presence of an aliphatic chain, catalyst [(L₁)₂Fe(OTf)₂] is highly selective for the aromatic nucleus hydroxylation, independently of the aliphatic C-H bond strength. Moreover, the regioselectivity of the phenol products is mainly dictated by the electronic effects of the substituents, although also steric factors play a key role. The selectivity of the reaction, its insensitivity towards the addition of radical scavengers and the KIE measured, lead to exclude a radical mechanism and strongly point to a metal-based S_EAr mechanism, although an arene epoxidation mechanism similar to the one of iron and copper oxygenases^{24,43} cannot be completely ruled out.

4.4 Experimental Section

General procedure for the oxidation reactions by [(L₁)₂Fe(OTf)₂]

Fe(CF₃SO₃)₂(CH₃CN)₂ (1.09 mg, 2.50 μmol), picolylamine (from a 0.1 M CH₃CN solution, 5.0 μmol) and picolylaldehyde (from a 0.1 M CH₃CN solution, 5.0 μmol) were mixed in a vial at 25°C. Substrate (250 μmol) and CH₃CN were then added up to a total volume of 700 μL. In the alcohol oxidation a 0.7 M CH₃CN solution of H₂O₂ (diluted from a 35% w/w H₂O₂ commercial solution) was added over 30 minutes by syringe pump under vigorous stirring, and left reacting for additional 60 minutes. While in the aromatic oxidation the same amount of H₂O₂ was added one shot and the reaction was

left under vigorous stirring for 90 minutes. At this point an internal standard was added (bibenzyl or nitrobenzene, 125 μ mol) and the reaction mixture was filtered over a short pad of SiO₂ with 2 mL of AcOEt. The filtered solution was subjected to GC, GC-MS and ¹H NMR.

The oxidation of phenyl benzoate was performed as described above and at the end of the reaction, the solvent was removed by rotatory evaporation and column chromatography gave the unreacted substrates and the products that have been analyzed by GC-MS, ¹H NMR, ¹³C NMR and COSY.

All the competitive reactions have been carried out following the same procedure, except for that promoted by [(TPA)Fe(OTf)₂] where 0.5 eq. of AcOH have been added.

In the 0.5-gram scale oxidation of cyclohexanol and cycloheptanol, the same procedure reported above has been followed. The solvent is removed by rotatory evaporation and the residue dissolved in CH₂Cl₂, dried over Na₂SO₄ and filtered over SiO₂. After solvent evaporation, pure cyclohexanone and cycloheptanone have been obtained (67% and 49% respectively). In the 0.5-gram scale oxidation of benzene, the mixture was filtered over a short pad of SiO₂ with AcOEt, concentrated to roughly half of the initial volume and extracted with a 1M NaOH solution. The combined aqueous phases were neutralized with a 2M H₂SO₄ solution and extracted with ethyl acetate. The combined organic layers were washed with a saturated NaHCO₃ aqueous solution and brine, dried over Na₂SO₄ and the solvent was removed by rotatory evaporation. Pure phenol was obtained with 26% yield.

GC conversions and yields are defined as (mol unrecovered substrate/mol substrate)×100 and (mol product/mol substrate) respectively and are an average of three determinations (error \pm 2%, unless written otherwise in the main text).

References

- (1) (a) L. Que Jr., W. B. Tolman, *Nature*, **2008**, *455*, 333-340. (b) M. C. White, *Science*, **2012**, *335*, 807-809. (c) E. P. Talsi, K. P. Bryliakov, *Coord. Chem. Rev.*, **2012**, *256*, 1418-1434. (d) A. Company, J. Lloret-Fillol, L. Gómez, M. Costas, *In Alkane C-H Activation by Single-Site Metal Catalysis*; Perez, P. J., Ed.; Springer: Dordrecht, The Netherlands, **2013**; Vol. 38.

- (2) (a) W. N. Oloo, A. J. Fielding, L. Que Jr., *J. Am. Chem. Soc.*, **2013**, *135*, 6438-6441. (b) L. Que Jr., *Acc. Chem. Res.*, **2007**, *40*, 493-500. (c) W. Nam, *Acc. Chem. Res.*, **2007**, *40*, 522-531. (d) K. P. Bryliakov, E. P. Talsi, *Coord. Chem. Rev.*, **2014**, *276*, 73-96. (e) A. R. McDonald, L. Que Jr., *Coord. Chem. Rev.*, **2013**, *257*, 414-428. (f) K. Ray, F. F. Pfaff, B. Wang, W. Nam, *J. Am. Chem. Soc.*, **2014**, *136*, 13942-13958.
- (3) M. S. Chen, M. C. White, *Science*, **2007**, *318*, 783-787.
- (4) M. S. Chen, M. C. White, *Science*, **2010**, *327*, 566-571.
- (5) T. Newhouse, P. S. Baran, *Angew. Chem., Int. Ed.*, **2011**, *50*, 3362-3374.
- (6) (a) L. Gómez, M. Canta, D. Font, I. Prat, X. Ribas, M. Costas, *J. Org. Chem.*, **2013**, *78*, 1421-1433. (b) I. Prat, L. Gómez, M. Canta, X. Ribas, M. Costas, *Chem.-Eur. J.*, **2013**, *19*, 1908-1913. (c) P. E. Gormisky, M. C. White, *J. Am. Chem. Soc.*, **2013**, *135*, 14052-14055.
- (7) G. Olivo, G. Arancio, L. Mandolini, O. Lanzalunga, S. Di Stefano, *Catal. Sci. Technol.* **2014**, *4*, 2900-2904.
- (8) D. S. Nesterov, O. V. Nesterova, M. F. C. Guedes da Silva, A. J. L. Pombeiro, *Catal. Sci. Technol.*, **2015**, *5*, 1801-1812.
- (9) (a) J. Tang, P. Gamez, J. Reedijk, *Dalton Trans.*, **2007**, 4644-4646. (b) B. Retcher, J. S. Costa, J. Tang, R. Hage, P. Gamez, J. Reedijk, *J. Mol. Catal. A: Chem.*, **2008**, *286*, 1-5. (c) S. Tanase, J. Reedijk, R. Hage, G. Rothenberg, *Top. Catal.*, **2010**, *53*, 1039-1044.
- (10) (a) M. Lenze, E. T. Martin, N. P. Rath, E. B. Bauer, *ChemPlusChem*, **2013**, *78*, 101-116. (b) P. Shejwalkar, N. P. Rath, E. B. Bauer, *Dalton Trans.*, **2011**, *40*, 7617-7631. (c) G. J. P. Britovsek, J. England, S. K. Spitzmesser, A. J. P. White, D. J. Williams, *Dalton Trans.*, **2005**, 945-955. (d) G. J. P. Britovsek, J. England, A. J. P. White, *Dalton Trans.*, **2006**, 1399-1408. (e) O. Martínez-Ferraté, G. J. P. Britovsek, C. Claver, P. W. N. M. Van Leeuwen, *Inorg. Chim. Acta*, **2015**, *431*, 156-160.
- (11) G. Olivo, M. Nardi, D. Vidal, A. Barbieri, A. Lapi, L. Gómez, O. Lanzalunga, M. Costas, S. Di Stefano, *Inorg. Chem.*, **2015**, *54*, 10141-10152.
- (12) (a) Z. Codolà, J. Lloret-Fillol, M. Costas, *Prog. Inorg. Chem.*, **2014**, *59*, 447-53. (b) M. A. Bigi, S. A. Reed, M. C. White, *J. Am. Chem. Soc.*, **2012**, *134*, 9721-9726. (c) Y. Hitomi, K. Arakawa, T. Funabiki, M. Kodera, *Angew. Chem., Int. Ed.*, **2012**, *51*, 3448-3452. (d) D. Clemente-Tejeda, A. López-Moreno, F. A. Bermejo, *Tetrahedron*, **2013**, *69*, 2977-2986. (e) Y. He, J. D. Gorden, C. R. Goldsmith, *Inorg. Chem.*, **2011**, *50*, 12651-12660. (f) V. A. Yazerski,

- P. Spanning, D. Gatineau, C. H. M. Woerde, S. M. Wieclawska, M. Lutz, H. Kleijn, R.R. J. M. Klein Gebbink, *Org. Biomol. Chem.*, **2014**, *12*, 2062-2017.
- (13) J.-E. Backwall, Ed., *Modern Oxidation Methods*, Wiley-VCH, Weinheim, Germany, **2010**.
- (14) R. A. Sheldon and J. K. Kochi, *Metal-Catalyzed Oxidations of Organic Compounds*, Academic Press, New York, **1981**.
- (15) (a) J. M. Hoover and S. S. Stahl, *J. Am. Chem. Soc.*, **2011**, *133*, 16901-16910. (b) J. M. Hoover, J. E. Steves and S. S. Stahl, *Nat. Protoc.*, **2012**, *7*, 1161-1166.
- (16) R. Noyori, A. Masao and K. Sato, *Chem. Commun.*, **2003**, 1977-1986.
- (17) S. Enthaler, K. Junge and M. Beller, *Angew. Chemie - Int. Ed.*, **2008**, *47*, 3317-3321.
- (18) (a) K. Chen and L. Que Jr., *J. Am. Chem. Soc.*, **2001**, *123*, 6327-37. (b) L. Gómez, I. Garcia-Bosch, A. Company, J. Benet-Buchholz, A. Polo, X. Sala, X. Ribas and M. Costas, *Angew. Chemie - Int. Ed.*, **2009**, *48*, 5720-5723. (c) G. Olivo, O. Lanzalunga, L. Mandolini and S. Di Stefano, *J. Org. Chem.*, **2013**, *78*, 11508-11512. (d) O. Cussó, X. Ribas and M. Costas, *Chem. Commun.*, **2015**, *51*, 14285-14298. (e) C. Zang, Y. Liu, Z.-J. Xu, C.-W. Tse, X. Guan, J. Wei, J.-S. Huang and C.-M. Che, *Angew. Chemie Int. Ed.*, **2016**, *55*, 2-7.
- (19) (a) M. Lenze and E. B. Bauer, *Chem. Commun.*, **2013**, *49*, 5889-91. (b) T. Kikuchi and K. Tanaka, *Eur. J. Inorg. Chem.*, **2014**, *2014*, 607-618. (c) H. Hosseini-Monfared, C. Näther, H. Winkler and C. Janiak, *Inorg. Chim. Acta*, **2012**, *391*, 75-82. (d) J. E. Chàvez, C. Crotti, E. Zangrando and E. Farnetti, *J. Mol. Catal. A Chem.*, **2016**, *421*, 189-195. (e) B. Biswas, A. Al-Hunaiti, M. T. Räisänen, S. Ansalone, M. Leskelä, T. Repo, Y.-T. Chen, H.-L. Tsai, A. D. Naik, A. P. Railliet, Y. Garcia, R. Ghosh and N. Kole, *Eur. J. Inorg. Chem.*, **2012**, *2012*, 4479-4485. (f) S. Tanaka, Y. Kon, T. Nakashima and K. Sato, *RSC Adv.*, **2014**, *4*, 37674. (g) S. Tanaka, Y. Kon, A. Ogawa, Y. Uesaka, M. Tamura and K. Sato, *ChemCatChem*, **2016**, 10.1002/cctc.201600362.
- (20) (a) P. Saisaha, L. Buettner, M. van der Meer, R. Hage, B. L. Feringa, W. R. Browne and J. W. de Boer, *Adv. Synth. Catal.*, **2013**, *355*, 2591-2603. (b) J. J. Dong, D. Unjaroen, F. Mecozzi, E. C. Harvey, P. Saisaha, D. Pijper, J. W. de Boer, P. Alsters, B. L. Feringa and W. R. Browne, *ChemSusChem*, **2013**, *6*, 1774-1778. (c) D. Shen, C. Miao, D. Xu, C. Xia and W. Sun, *Org. Lett.*, **2015**, *17*, 54-57. (d) M. T. Räisänen, A. Al-Hunaiti, E. Atosuo, M. Kemell, M. Leskelä and T. Repo, *Catal. Sci. Technol.*, **2014**, *4*, 2564.
- (21) (a) S. Niwa, M. Eswaramoorthy, J. Nair, A. Raj, N. Itoh, H. Shoji, T. Namba, F. Mizukami, *Science*, **2002**, *295*, 105-107. (b) J. P. Hage, A. Llobet, D. T. Sawyer, *Bioorganic Med. Chem.*

- 1995**, 3, 1383-1388. (c) S. Enthaler, A. Company, *Chem. Soc. Rev.*, **2011**, 40, 4912-4924. (d) P. T. Tanev, M. Chibwe, T. J. Pinnavaia, *Nature*, **1994**, 368, 321-323. (e) B. Lücke, K. V. Narayana, A. Martin, K. Jähnisch, *Adv. Synth. Catal.*, **2004**, 346, 1407-1424. (f) Y. Morimoto, S. Bunno, N. Fujieda, H. Sugimoto, S. Itoh, *J. Am. Chem. Soc.*, **2015**, 137, 5867-5870. (g) K. Kamata, T. Yamaura, N. Mizuno, *Angew. Chem. Int. Ed.*, **2012**, 51, 7275-7278.
- (22) C. Yuan, Y. Liang, T. Hernandez, A. Berriochoa, K. N. Houk, D. Siegel, *Nature.*, **2013**, 499, 192-196.
- (23) (a) A. Conde, M. M. Díaz-Requejo, P. J. Pérez, *Chem. Commun.*, **2011**, 47, 8154-8156. (b) M. Yamada, K. D. Karlin, S. Fukuzumi, *Chem. Sci.*, **2016**, 7, 2856-2863. (c) K. D. Karlin, J. C. Hayes, Y. Gultneh, R. W. Cruse, J. W. McKown, J. P. Hutchinson, J. Zubieta, *J. Am. Chem. Soc.*, **1984**, 106, 2121-2128.
- (24) (a) A. Thibon, V. Jollet, C. Ribal, K. Sénéchal-David, L. Billon, A. B. Sorokin, F. Banse, *Chem. - A Eur. J.*, **2012**, 18, 2715-2724. (b) G. C. Silva, N. M. F. Carvalho, A. Horn Jr., E. R. Lachter, O. A. C. Antunes, *J. Mol. Catal. A Chem.*, **2017**, 426, Part, 564-571. (c) A. Raba, M. Cokoja, W. Herrmann, F. E. Kühn, *Chem. Commun.*, **2014**, 50, 11454-11457. (d) A. C. Lindhorst, S. Haslinger, F. E. Kühn, *Chem. Commun.*, **2015**, 51, 17193-17212. (e) P. Liu, Y. Liu, E. L.-M. Wong, S. Xiang, C.-M. Che, *Chem. Sci.*, **2011**, 2, 2187-2195. (f) E. V. Kudrik, A. B. Sorokin, *J. Mol. Catal. A Chem.*, **2017**, 426, 499-505.
- (25) Carneiro, L.; Silva, A. R. *Catal. Sci. Technol.* **2016**, 6, 8166-8176.
- (26) K. Hirose, K. Ohkubo, S. Fukuzumi, *Chem. Eur. J.*, **2016**, 22, 12904-12909.
- (27) (a) M. P. Jensen, M. P. Mehn, L. Que Jr., *Angew. Chemie - Int. Ed.*, **2003**, 42, 4357-4360. (b) N. Y. Oh, M. S. Seo, M. H. Lim, M. B. Consugar, M. J. Park, J.-U. Rohde, J. Han, K. M. Kim, J. Kim, L. Que Jr., W. Nam, *Chem. Commun.*, **2005**, 3, 5644-5646. (c) O. V Makhlynets, P. Das, S. Taktak, M. Flook, R. Mas-Ballesté, E. V. Rybak-Akimova, L. Que Jr., *Chem. - A Eur. J.*, **2009**, 15, 13171-13180. (d) S. P. de Visser, K. Oh, A.-R. Han, W. Nam, *Inorg. Chem.*, **2007**, 46, 4632-4641. (e) O. V. Makhlynets, E. V. Rybak-Akimova, *Chem. - A Eur. J.*, **2010**, 16, 13995-14006.
- (28) A. M. Adams, J. Du Bois, H. A. Malik, *Org. Lett.*, **2015**, 17, 6066-6069.
- (29) A. C. Lindhorst, J. Schutz, T. Netscher, W. Bonrath, F. E. Kühn, *Catal. Sci. Technol.*, **2017**, 7, 1902-1911.
- (30) E. Baciocchi, S. Belvedere, M. Bietti and O. Lanzalunga, *Eur. J. Org. Chem.*, **1998**, 299-302.

- (31) A. D. N. Vaz and M. J. Coon, *Biochemistry*, **1994**, 33, 6442-6449.
- (32) *Comprehensive Handbook of Chemical Bond Energies*, Y.-R. Luo, CRC Press, Boca Raton, Florida, USA, **2007**.
- (33) F. Minisci, F. Faletti, R. Paganelli, G. F. Pedulli, *European J. Org. Chem.*, **2004**, 109-119.
- (34) C. Annunziatini, M. F. Gerini, O. Lanzalunga, M. Lucarini, *J. Org. Chem.*, **2004**, 69, 3431-3438.
- (35) P. A. MacFaul, K. U. Ingold, D. D. M. Wayner, L. Que Jr., *J. Am. Chem. Soc.*, **1997**, 119, 10594-10598.
- (36) (a) C. Walling, R. A. Johnson, *J. Am. Chem. Soc.*, **1975**, 97, 363-367. (b) D. I. Metelitsa, *Russ. Chem. Rev.*, **1971**, 40, 563-580. (c) A. Kunai, S. Hata, S. Ito, K. Sasaki, *J. Am. Chem. Soc.*, **1986**, 108, 6012-6016.
- (37) A. Kejriwal, P. Bandyopadhyay, A. N. Biswas, *Dalton Trans.*, **2015**, 44, 17261-17267.
- (38) (a) R. R. Fernandes, M. V. Kirillova, J. A. L. da Silva, J. J. R. Fraústo da Silva, A. J. L. Pombeiro, *Appl. Catal. A Gen.*, **2009**, 353, 107-112. (b) B. Xu, W. Zhong, Z. Wei, H. Wang, J. Liu, L. Wu, Y. Feng, X. Liu, *Dalton Trans.*, **2014**, 43, 15337-15345. (c) A. Thibon, J. F. Bartoli, R. Guillot, J. Sainton, M. Martinho, D. Mansuy, F. Banse, *J. Mol. Catal. A Chem.*, **2008**, 287, 115-120. (d) X. Wang, T. Zhang, B. Li, Q. Yang, S. Jiang, *Appl. Organomet. Chem.*, **2014**, 28, 666-672. (e) V. Balland, D. Mathieu, N. Pons-Y-Moll, J. F. Bartoli, F. Banse, P. Battioni, J.-J. Girerd, D. Mansuy, *J. Mol. Catal. A Chem.*, **2004**, 215, 81-87.
- (39) T. Kurata, Y. Watanabe, M. Katoh, Y. Sawaki, *J. Am. Chem. Soc.*, **1988**, 110, 7472-7478.
- (40) A. Mitarai, K. Hikino, M. Hirama, K. Sasaki, *J. Org. Chem.*, **1992**, 57, 6937-6941.
- (41) G. Olivo, O. Lanzalunga, S. Di Stefano, *Adv. Synth. Catal.*, **2016**, 358, 843-863.
- (42) R. P. Hanzlik, K. H. J. Ling *J. Am. Chem. Soc.*, **1993**, 115, 9363-9370.
- (43) K. H. Mitchell, C. E. Rogge, T. Gierahn, B. G. Fox, *Proc. Natl. Acad. Sci.*, **2003**, 100, 3784-3789.
- (44) E. V. Kudrik, A. B. Sorokin, *Chem.-A Eur. J.*, **2008**, 14, 7123-7126.

Chapter 5

Inhibition process of the Mn^{II}/PCA/butanedione catalytic system by catechol and guaiacol substrates

The low efficiency displayed by the Mn^{II}/PCA/butanedione catalytic system in the oxidation of electron rich benzylic alcohols, prompted us to investigate the inhibition process of the Mn^{II} catalyst by catechol and guaiacol substrates.

Differently from most nonheme catalysts, the coordination of manganese with *ortho*-dioxygenated aromatic compounds can deactivate reversibly the system allowing the restart of the oxidative process.

This work was carried out at the Stratingh Institute for Chemistry, University of Groningen (Groningen, The Netherlands) under the supervision of Prof. Dr. Wesley Browne

5.1 Introduction

As described in Chapter 1, a central challenge in modern chemical synthetic methods is the development of cheap and environmentally sustainable methods.¹ In chapters 3 and 4 application of nonheme iron complexes in the oxidations of sulfides, alcohols and aromatic compounds have been described. Besides iron,² heme and nonheme manganese complexes have proven the most promising systems for the development of new catalytic oxidations thanks to the remarkably versatile redox chemistry of manganese metal.³

Recently, an efficient Mn based catalytic system for the oxidation of a broad range of organic compounds (alkanes, olefins, aliphatic and benzylic alcohols) under ambient conditions and low catalyst loadings, has been reported by Browne and his research group.^{3,4-8} This catalytic system, prepared *in situ* by adding a Mn^{II} salt, pyridine-2-carboxylic acid (PCA), a base (*e.g.* NaOH or NaOAc), sub-stoichiometric amounts of ketones such as butanedione and H₂O₂, showed good-to-excellent selectivity and efficiency with a wide solvent and substrate scope. The discovery of this system resulted from mechanistic studies of a series of Mn/polypyridyl ligands catalytic systems (see ligands in Figure 1) that, in mildly basic catalytic conditions, underwent a decomposition to PCA. The latter compound and the Mn ions are the only responsible for the catalytic activity observed.⁵

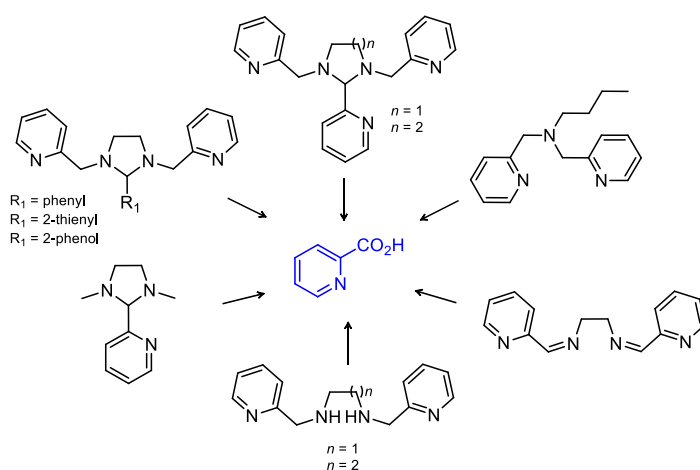


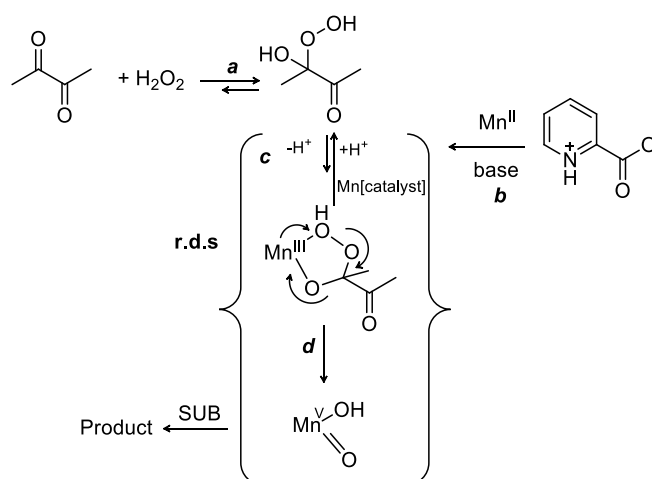
Figure 1. Decomposition of polypyridyl ligands to PCA

The fact that a ligand degradation product could provide such high catalytic activity and selectivity, is unprecedented since ligand decomposition generally causes a release of the metal ion with subsequent catalyst deactivation and trigger of radical reactions.^{9,10} This observation has a significant impact on strategies taken towards simpler ligand design.

The addition of several equivalents of a base, with respect to Mn(II), is necessary for the catalytic activity as well as the use of ketones as solvents (acetone or butanedione).⁶⁻⁸

The proposed activation mechanism is reported in Scheme 1. A prior rapid equilibrium between butanedione and H₂O₂ with formation of 3-hydroxy-3-hydroperoxybutanone (Scheme 1, path a) is followed by reaction, in the rate determining step, of the active hydroperoxy acetal with the reduced form of the catalyst to yield the active oxidizing species (Scheme 1, path c, d).^{7,8}

The insensitivity to the nature of the base used, indicates that its role is the deprotonation of PCA enabling catalyst formation (Scheme 1, path b) rather than a Mn ligand. Despite the apparent simplicity of the system, structural determination of both the reduced and oxidized forms of the Mn/PCA catalyst, is still challenging. The absence of a six-line EPR signal (characteristic of mononuclear Mn^{II}) during the reaction suggests the formation of mononuclear Mn^{III}(PCA)₂ which, by reaction with 3-hydroxy-3-hydroperoxybutanone, yields a highly reactive species: e.g., [(PCA)₂Mn^V(=O)(OH)].^{7,8}



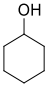
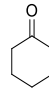
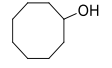
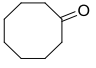
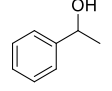
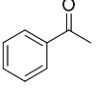
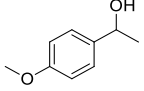
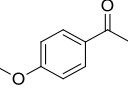
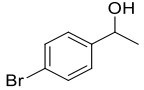
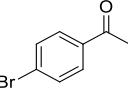
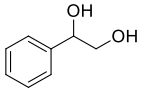
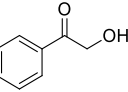
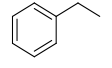
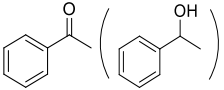
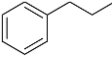
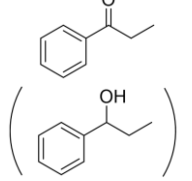
Scheme 1. Proposed activation mechanism for Mn^{II}/PCA/butanedione catalytic system.

The *in situ* preparation of the catalyst, the ambient reaction conditions and fast reaction rates achievable, make this system easily applicable. High turnover numbers (> 1000) have been

achieved in the selective *cis*-dihydroxylation of electron deficient alkenes such as diethyl fumarate⁶ and also in the selective epoxidation of electron-rich alkenes as cyclooctene (up to 300 000).⁷

Good yields of carbonyl products were obtained in the oxidation of alcohols and alkylaromatics with this catalytic system (Table 1).⁴

Table 1. Oxidation of alcohols and alkylaromatics with H₂O₂ catalyzed by Mn/PCA/butanedione in CH₃CN at 25 °C.^a

entry	substrate	conv(%)	product	yield (%)
1		full		91
2		full		78
3		97		90
4 ^{a'}		70		64
5		78		76
6		60		50
7 ^{a''}		80		50 (13)
8 ^{a''}		50		34 (3)

^a0.5-0.25M^a substrate (1-0.5 mmol), Mn(ClO₄)₂·6H₂O (0.01-0.1^a mol%), PCA (0.5-1.0^a mol%), NaOAc (1-2^a mol%), butanedione (0.5-1.5^a equiv.), H₂O₂ (3-4^a equiv.) in CH₃CN for 12-16 h.

Cyclic alcohols were converted cleanly to their corresponding ketones with excellent conversion and good yields (Table 1, entry 1, 2). Oxidation of secondary benzylic alcohols *p*-X-1-phenylethanol (X=H, Br, OCH₃, Table 1, entries 3-5) and the diol 1-phenyl-1,2-ethandiol (entry 6) proceeded in moderate-to-good conversion showing a good selectivity of the Mn/PCA/butanedione system towards the alcoholic moiety instead of the aromatic ring, contrary to what observed for the oxidations catalyzed by the imine iron complex [(L₁)₂Fe(OTf)₂] (see Tables 2, Chapter 4 for a comparison). The preferential side-chain oxidation is evident in the oxidation of ethylbenzene and propylbenzene where the corresponding aryl ketones were obtained with good selectivity (see Table 1, entry 7 and 8 and Table 3 in Chapter 4 for comparison). The high selectivity for the side-chain oxidation in the reactions catalyzed by Mn/PCA/butanedione system, prompted us to investigate the oxidation of electron rich benzylic alcohols in order to test its synthetic application in the oxidative degradation of lignin. Lignin, a three-dimensional phenolic polymer built from phenylpropane units linked together by different bonds, is one of the most abundant biopolymers on earth (Figure 2).^{11,12}

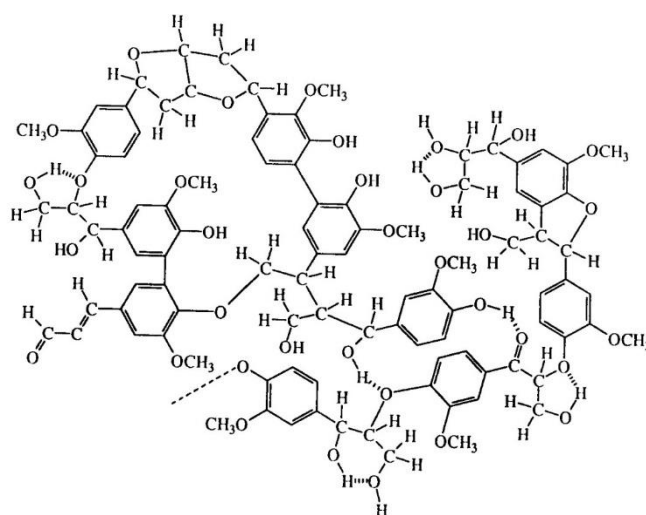


Figure 2. Representation of the lignin structure.

Studies concerning the oxidative degradation of lignin, have been raised continuous interest in the last period not only because they can convert lignin into low molecular weight aromatic compounds, thus making this polymer a renewable source for the industrial preparation of a number of chemicals¹³, but also because the selective degradation of lignin and its removal from the carbohydrate component of wood, is a key step in the pulp and paper industry.¹⁴ Among the most important linkages of the lignin polymers, the most abundant (ca. 55 %) is the β -O-4 linkage shown in Figure 3.^{15,16} Substrates having the possibility to be oxidized in the functional groups present in this linkage, and in particular of the benzylic position, represent a convenient targets for the degradation of the entire polymer.^{11,12,17-19}

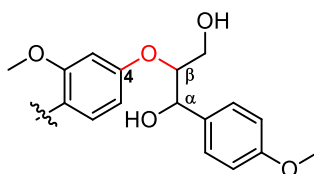


Figure 3. Representation of β -O-4 linkage (pointed out in red).

Considering the complexity of the lignin polymer, model compounds with linkages and functional groups commonly found in the native polymer, are often valuable to find efficient and renewable degradation pathways.^{11,12}

The application of the Mn^{II}/PCA/butanedione catalytic system to the oxidation of a dimeric [2-(2-methoxyphenoxy)-1-phenylethanol (**1**)] and a monomeric lignin model (veratryl alcohol) led unexpectedly to a very low efficiency. Thus, we decided to turn our attention on the substrate structural factors responsible for the deactivation of the catalytic systems.

5.2 Results and Discussion

In order to test the efficiency of the Mn/PCA/butanedione system in the oxidative degradation of lignin, we employed the dimeric lignin model, 2-(2-methoxyphenoxy)-1-phenylethanol (**1**) and the monomeric veratryl alcohol, as benchmark substrates (Figure 4).

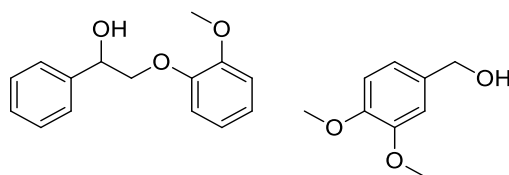


Figure 4. 2-(2-methoxyphenoxy)-1-phenylethanol (**1**) and veratryl alcohol.

The oxidation of **1** and veratryl alcohol have been investigated using experimental conditions previously optimized for the oxidation of secondary aliphatic and benzylic alcohols.⁴ The catalyst, prepared *in situ* by mixing $\text{Mn}(\text{ClO}_4)_2 \cdot 6\text{H}_2\text{O}$ (0.01 mol%) and pyridine-2-carboxylic acid (0.5 mol%), was added to a solution of substrate (0.5 M), sodium acetate (1.0 mol%) as base, butanedione (0.5 equiv.), AcOH (20 mol%) and H_2O_2 (3 equiv.) as terminal oxidant in CH_3CN .

Raman spectroscopy has been used as experimental technique to investigate the evolution of the reaction by following the changes in intensities of reagents and products Raman peaks. Raman spectra are recorded at $\lambda_{\text{exc}} = 785$ nm every min (20 seconds as exposure time \times 3 acquisitions) and the kinetics are obtained monitoring the intensity change of the band at a characteristic Raman shift during the time.

No trace of oxidation products were detected by ^1H NMR analysis in the oxidation of **1** and veratryl alcohol. The absence of reactivity was also supported by the absence of variation in the Raman spectra recorded in one hour (see Experimental section).

In order to understand the origin of the deactivation of the Mn/PCA/butanedione system, some competitive experiments have been carried out between the 1-phenyl-1,2-ethandiol (a good substrate for this catalytic system), and different amounts of **1** (from 0 mol% to 100 mol% w.r.t. 1-phenyl-1,2-ethandiol). Reaction monitoring with Raman spectroscopy focused primarily on the intensity of O-O stretching mode of H_2O_2 at 864 cm^{-1} , C=O or C-O stretching band of 2-hydroxy-1-phenylethanone at 1692 cm^{-1} and 1230 cm^{-1} and C-O stretching band of 1-phenyl-1,2-ethandiol at 828 cm^{-1} by comparison with authentic specimens. In Figure 5 is shown, as example, the time evolution Raman spectra for the 1-phenyl-1,2-ethandiol oxidation.

1-Phenyl-1,2-ethandiol underwent 60% conversion to α -hydroxyketone in the absence of **1**, however when the amount of **1** started to increase, a significant decrease in the catalytic activity was clearly observed.

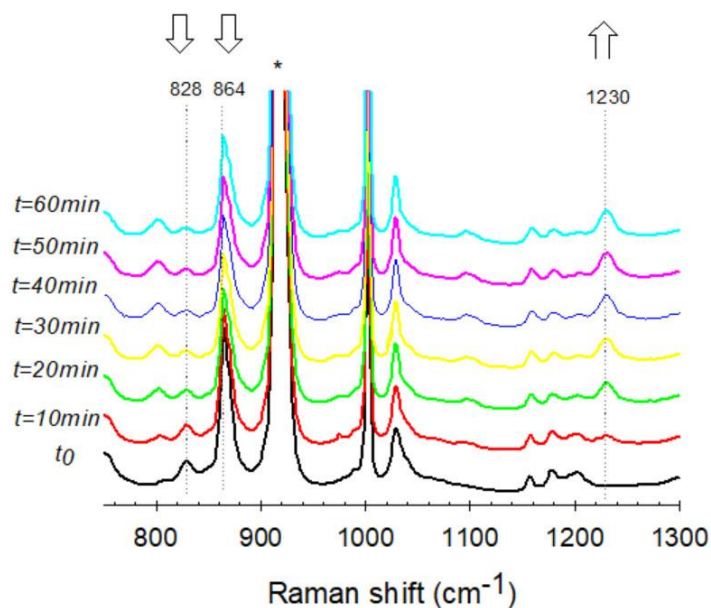


Figure 5. Time evolution Raman spectra for the 1-phenyl 1,2-ethandiol oxidation. * Spectra are normalized to solvent band at 914 cm^{-1} .

The drop in the catalytic efficiency became relevant by passing from 5 mol% to 20 mol% of **1** (Figure 6).

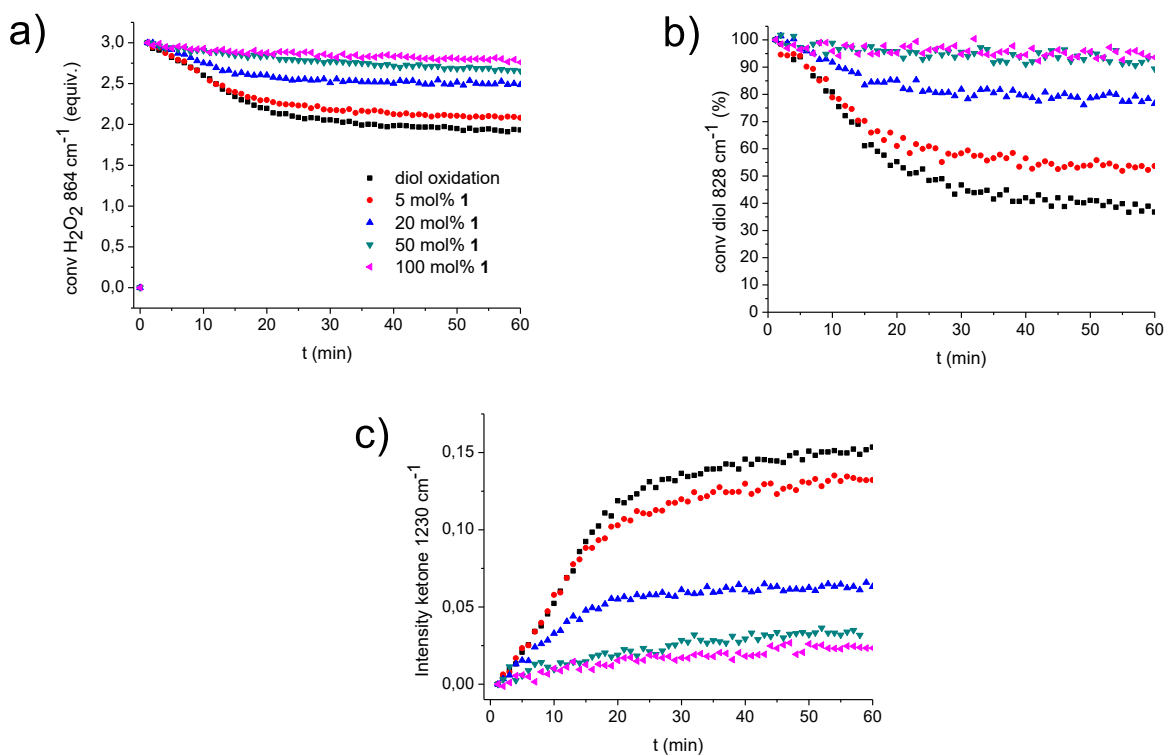


Figure 6. 1-Phenyl 1,2-ethandiol oxidation in absence of **1** (black line), in presence of 5 mol% of **1** (red line), 20 mol% of **1** (blue line), 50 mol% of **1** (green line), 100 mol% of **1** (pink line); (a) conversion of H₂O₂ obtained following the decrease of the Raman band at 864 cm⁻¹. (b) Conversion of 1-phenyl 1,2-ethandiol obtained following the decrease of the Raman band at 828 cm⁻¹. (c) Intensity change of 2-hydroxy-1-phenylethanone obtained following the increase of the Raman band at 1230 cm⁻¹. Plots obtained from Raman analysis ($\lambda_{\text{exc}}=785\text{nm}$).

A competitive experiment using 1-phenyl-1,2-ethandiol and 5 mol% of **1** has been carried out in which the diol was added 5 min after the addition of H₂O₂ (Figure 7, black line). The reaction rate and the catalytic activity of the system were lower with respect to the experiment described before (Figure 6, red line). Since the main structural difference between 1-phenyl-1,2-ethandiol and **1**, lies in the guaiacol moiety, the competitive reaction has been repeated in presence of 5 mol% of guaiacol in the place of **1**, obtaining a complete suppression in the catalytic activity (Figure 7, red line). From this results, it derives that an oxidation product of **1**, as the guaiacol or a product obtained from its further oxidation, is likely involved in the deactivation of the catalytic system.

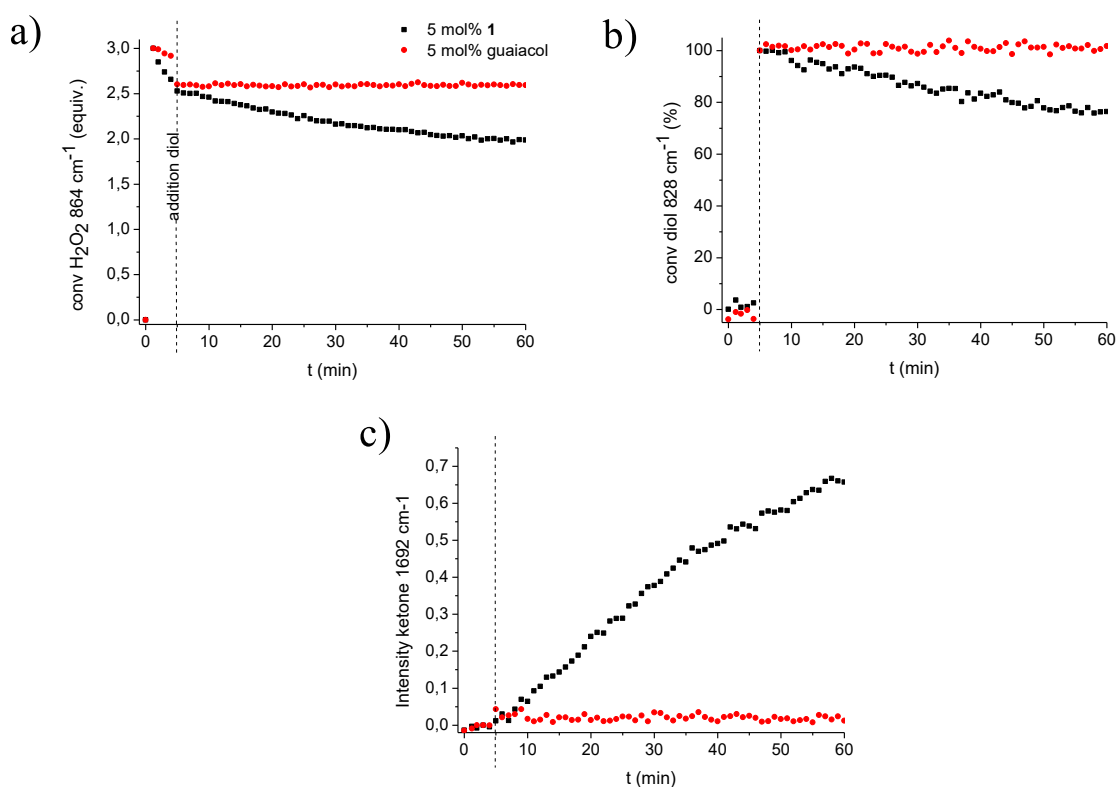


Figure 7. 1-Phenyl-1,2-ethandiol oxidation in presence of 5 mol% of **1** (black line) and in presence of 5 mol% of guaiacol (red line); (a) conversion of H_2O_2 obtained following the decrease of the Raman band at 864 cm^{-1} . (b) Conversion of 1-phenyl 1,2-ethandiol obtained following the decrease of the Raman band at 828 cm^{-1} . (c) Intensity change of 2-hydroxy-1-phenylethanone obtained following the increase of the Raman band at 1692 cm^{-1} . Plots obtained from Raman analysis ($\lambda_{exc}=785\text{nm}$).

The inhibition of the oxidative process observed with the activated phenol guaiacol led us to investigate the possible inhibition effect of the *o*-dihydroxylated benzene (catechol), thus similar competitive experiments have been performed using different amount of catechol (see Experimental Section). In light of preliminary inhibition experiments showing a greater deactivating power of the catechol respect to the guaiacol, the amount of the *o*-dihydroxylated compound used in the competitive experiments, was lower (from 0.05 mol% to 1 mol%). In all the experiments the diol was added 5 min after the beginning of the reactions (Figure 8).

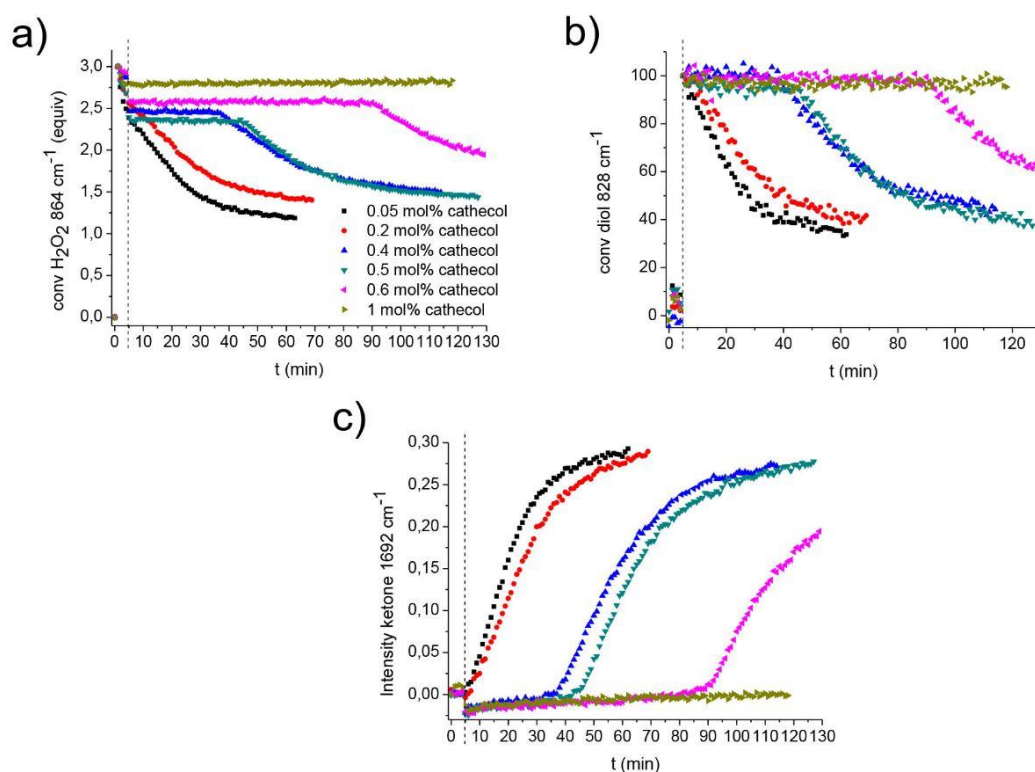


Figure 8. 1-Phenyl 1,2-ethandiol oxidation in presence of 0.05 mol% of catechol (black line), 0.2 mol% of catechol (red line), 0.4 mol% of catechol (blue line), 0.5 mol% of catechol (green

line), 0.6 mol% of catechol (pink line) and 1 mol% of catechol (mustard color line); (a) conversion of H₂O₂ obtained following the decrease of the Raman band at 864 cm⁻¹. (b) Conversion of 1-phenyl 1,2-ethandiol obtained following the decrease of the Raman band at 828 cm⁻¹. (c) Intensity change of 2-hydroxy-1-phenylethanone obtained following the increase of the Raman band at 1692 cm⁻¹. Plots obtained from Raman analysis ($\lambda_{\text{exc}}=785\text{nm}$).

It is interesting to note that when the amount of catechol was kept low (0.05 mol% and 0.2 mol%), the reaction proceeded smoothly, but an increase in the amount of the inhibitor from 0.4 mol% to 0.6 mol%, affected the catalytic system inducing the appearance of a lag phase, the longer the greater was the quantity of catechol. After the lag phase, the reaction restart with a reaction rate similar to that observed in presence of lower amounts of catechol. In the presence of higher amounts of catechol (1 mol%), the catalytic activity of the system was definitely lost. Hence a deactivating interaction of the catechol with the Mn catalyst occurs with 1:40 <Mn:catechol<1:60 until the Mn catalyst is released again in the medium allowing the reaction to start again.

To demonstrate that the Mn:catechol catalyst ratio is a fundamental parameter for the activity/inactivity of the system, a competitive experiment was performed using 10 times larger amounts of Mn(ClO₄)₂ (0.1 mol%) in presence of 1 mol% of catechol (Mn:catechol, 1:10).

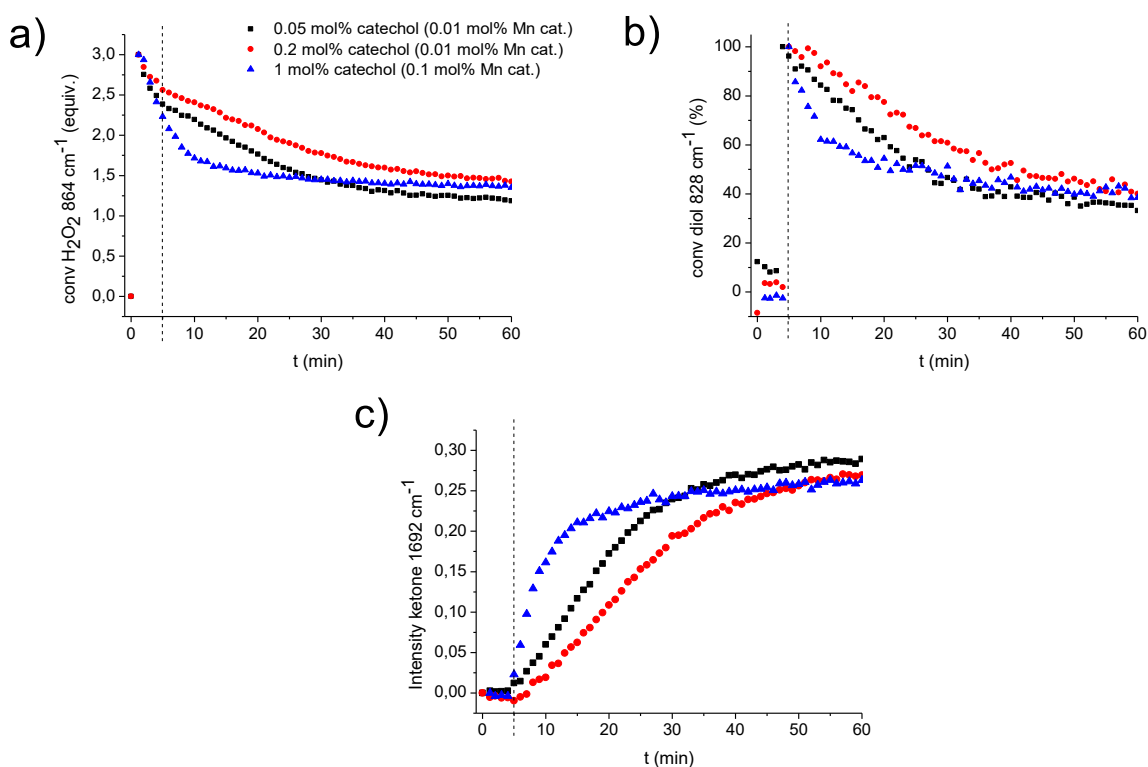


Figure 9. 1-Phenyl-1,2-ethandiol oxidation in presence of Mn(ClO₄)₂ 6H₂O 0.01 mol% and catechol 0.05 mol% (black line), in presence of Mn(ClO₄)₂ 6H₂O 0.01 mol% and catechol 0.2 mol% (red line), and in presence of Mn(ClO₄)₂ 6H₂O 0.1 mol% and catechol 1 mol% (blue line); (a) Conversion of H₂O₂ obtained following the decrease of the Raman band at 864 cm⁻¹. (b) Conversion of 1-phenyl 1,2-ethandiol obtained following the decrease of the Raman band at 828 cm⁻¹. (c) Intensity change of 2-hydroxy-1-phenylethanone obtained following the increase of the Raman band at 1692 cm⁻¹ Plots obtained from Raman analysis ($\lambda_{\text{exc}} = 785\text{nm}$).

Figure 9 shows a comparison between the two competitive experiments carried out with 0.01 mol% Mn(ClO₄)₂ 6H₂O in presence of 0.05 mol% and 0.2 mol% of catechol in which Mn:catechol was 1:5 (black line) and 1:20 (red line) respectively and the competitive experiment carried out with a greater amount of Mn(ClO₄)₂, 0.1 mol% and 1 mol% of catechol (blue line). In all the experiments the reactions reach almost the same conversion with the only difference that the reaction rate is higher in presence of a 10 times greater amount of the catalyst Mn(ClO₄)₂. No reaction was observed in presence of the same amount of catechol (1 mol%) and 10 times lower amount of Mn(ClO₄)₂ 6H₂O (Figure 8, mustard color line) because a too large ratio Mn:catechol was used (1:100). On the basis of these results, it derives that the activity/inactivity of the catalytic system depends on the ratio Mn:catechol. For Mn:catechol

ratios comprised between 1:5 and 1:60, the oxidation of 1-phenyl 1,2-ethandiol to 2-hydroxy-1-phenylethanone proceeds even after an induction period. When the amount of catechol is too high (100 times with respect to Mn catalyst), the system is permanently deactivated.

5.3 Conclusion

Despite the promising results obtained in the oxidation of benzylic alcohols as 1-phenyl ethanol and 4-methoxy-1-phenylethanol, the Mn/PCA/butanedione system has demonstrated to be unsuitable for the oxidative degradation of lignin model compounds. In light of the results obtained from the competitive experiments, we believe that small amounts of *ortho*-dioxxygenated aromatic compounds (e.g. guaiacol and catechol) coordinate the manganese center leading to catalyst deactivation. Such deactivating coordination has been already described for other nonheme iron oxidation catalysts, for which a metal-based oxidation has been firmly established.²⁰

However unlike most catalytic systems, the Mn(ClO₄)₂/catechol ratio controls the activity/inactivity of this system. Accordingly, the right proportion between Mn catalyst and catechol might prevent an irreversible deactivation of the complex. Further studies are needed to understand the mechanism of inhibition and the dependence of the inhibition process on the structure of the aromatic compounds.

5.4 Experimental Section

General procedure for the oxidation reactions by Mn/PCA/butanedione

Stock solutions containing Mn(ClO₄)₂·6H₂O (0.1 μmol, 0.01mol% or 1 μmol, 0.1mol%) and pyridine-2-carboxylic acid (5 μmol, 0.5mol%) were mixed and stirred at room temperature for 20 minutes. Substrate (1 mmol, 0.5 M), stock water solution of NaOAc (10 μmol, 1 mol%), butanedione (0.5 mmol, 0.5 equiv.) and acetic acid (0.2 mmol, 0.2 equiv) were added to generate a final volume of 2 mL in CH₃CN. The solution was stirred for other 5 minutes. Then 3 equivalents of H₂O₂ 50 wt% were added and the reaction has been followed by Raman

spectroscopy ($\lambda_{\text{exc}} = 785 \text{ nm}$). After 1 hour, acetophenone or 1,2-dichloroethane (0.5 mmol, 0.5 equiv.) were added as internal standard and a small aliquot of the reaction mixture, diluted in CD_3CN , has been analyzed by ^1H NMR. The competitive experiments were carried out following the same procedure with the substrates 1-phenyl-1,2-ethandiol, catechol, guaiacol and 2-(2-methoxyphenoxy)-1-phenylethanol added in the sequence described in the main text.

References

- (1) (a) R. Noyori, M. Aoki, K. Sato, *Chem. Commun.*, **2003**, 1977-1986. (b) H. Adolfsson, *In Modern Oxidation Methods*, 2nd ed.; J.-E. Backvall, Ed; Wiley-VCH: Weinheim, **2010**, Chapter 2. (c) R. Hage, J. E. Iburg, J. Kerschner, J. H. Koek, E. L. M. Lempers, R. J. Martens, U. S. Racherla, S. W. Russell, T. Swarthoff, M. R. P. van Vliet, J. B. Warnaar, L. van der Wolf, B. Krijnen, *Nature*, **1994**, *369*, 637-639. (d) P. T. Anastas, M. M. Kirchff, *Acc. Chem. Res.*, **2002**, *35*, 686. (e) I. Hermans, E. S. Spier, U. Neuenschwander, N. Turrà, A. Baiker, *Top. Catal.*, **2009**, *52*, 1162. (f) B. S. Lane, K. Burgess, *Chem. Rev.* **2003**, *103*, 2457.
- (2) (a) P. C. A. Bruijninx, G. van Koten, R. J. M. Klein Gebbnk, *Chem. Soc. Rev.*, **2008**, *37*, 2716-2744. (b) M. Costas, *Coord. Chem. Rev.*, **2011**, *255*, 2912-2932. (c) K. P. Bryliakov, E. P. Talsi, *Coord. Chem. Rev.*, **2014**, *276*, 73-96.
- (3) A. Murphy, T. D. P. Stack, *J. Mol. Catal. A: Chem.*, **2006**, *251*, 78-88. (b) C. B. Woitiski, Y. N. Kozlov, D. Mandelli, G. V. Nizova, U. Schuchardt, G. B. Shul'pin, *J. Mol. Catal. A: Chem.*, **2004**, *222*, 103-119. (c) J. W. De Boer, J. Brinksma, W. R. Browne, A. Meetsma, P. L. Alsters, R. Hage, B. L. Feringa, *J. Am. Chem. Soc.*, **2005**, *127*, 7990-7991. (d) E. M. McGarrigie, D. G. Gilheany, *Chem. Rev.*, **2005**, *105*, 1563-1602. (e) E. P. Talsi, K. P. Bryliakov, *Coord. Chem. Rev.*, **2005**, *105*, 1563-1602. (f) A. Company, L. Gómez, M. Costas, *Nature, RCS Publishing*, **2011**, 148-208. (g) H. Srour, P. Le Maux, S. Chevance, G. Simonneaux, *Coord. Chem. Rev.*, **2013**, *257*, 3030-3050. (h) G. De Faveri, G. Ilyashenko, M. Watkinson, *Chem. Soc. Rev.*, **2011**, *40*, 1722-1760. (i) B. S. Lane, K. Burgess, *Chem. Rev.*, **2003**, *103*, 2457-2473. (l) P. Saisaha, J. W. de Boer, W. R. Browne, *Chem. Soc. Rev.*, **2013**, *42*, 2059. (m) P. Saisaha, L. Buettner, M. van der Meer, R. Hage, B. L. Feringa, W. R. Browne and J. W. de Boer, *Adv. Synth. Catal.*, **2013**, *355*, 2591-2603.

-
- (4) J. J. Dong, D. Unjaroen, F. Mecozzi, E. C. Harvey, P. Saisaha, D. Pijper, J. W. de Boer, P. Alsters, B. L. Feringa and W. R. Browne, *ChemSusChem*, **2013**, *6*, 1774-1778.
- (5) (a) D. Pijper, P. Saisaha, J. W. de Boer, R. Hoen, C. Smit, A. Meetsma, R. Hage, R. P. van Summeren, P. L. Alsters, B. L. Fering, W. R. Browne, *Dalton Trans.*, **2010**, *39*, 10375-10381.
- (6) P. Saisaha, D. Pijper, R. P. van Summeren, R. Hoen, C. Smit, J. W. de Boer, R. Hage, P. L. Alsters, B. L. Feringa, W. R. Browne, *Org. Biomol. Chem.*, **2010**, *8*, 4444-4450.
- (7) J. J. Dong, P. Saisaha, T. G. Meinds, P. L. Alsters, E. G. Ijpeij, R. P. van Summeren, B. Mao, M. Fananàs-Mastral, J. W. de Boer, R. Hage, B. L. Feringa, W. R. Browne, *ACS Catal.*, **2012**, *2*, 1087-1096.
- (8) P. Saisaha, J. J. Dong, T. G. Meinds, J. W. de Boer, R. Hage, F. Mecozzi, J. B. Kasper, W. R. Browne, *ACS Catal.*, **2016**, *6*, 3486-3495.
- (9) J. England, C. R. Davies, M. Banaru, A. J. P. White, G. J. P. Britovsek, *Adv. Synth. Catal.*, **2008**, *350*, 883-897.
- (10) M. Grau, A. Kyriacou, F. Cabedo Martinez, I. M. de Wispelaere, A. J. P. White, G. J. P. Britovsek, *Dalt. Trans.*, **2014**, *43*, 17108-17119.
- (11) J. Zakzeski, P. C. A. Bruijninx, A. L. Jongerius, B. M. Weckhuysen, *Chem. Rev.*, **2010**, *110*, 3552-3599.
- (12) Z. Zhang, J. Song, B. Han, *Chem. Rev.*, **2017**, *117*, 6834-6880.
- (13) H.-R. Børsvik, F. Minisci, *Org. Proc. Res. & Dev.*, **1999**, *3*, 330.
- (14) J. C. Roberts (Ed.); *The Chemical of Paper, The Royal Society of Chemistry, Cambridge, UK, 1996*.
- (15) F. S. Chakar, A. J. Ragauskas, *Ind. Crops Prod.*, **2004**, *20*, 131.
- (16) M. Y. Balakshin, E. A. Capanema, H.-M. Chang, *In Characterization of Lignocellulosic Materials*, T. Q. Hu, Ed.; Blackwell: Oxford, U.K., **2008**, 148.
- (17) C. Fabbri, C. Aurisicchio, O. Lanzalunga, *Eur. J. Chem.*, **2008**, *6*, 145-153.
- (18) C. Zhu, W. Ding, T. Shen, C. Tang, C. Sun, S. Xu, Y. Chen, J. Wu, H. Ying, *ChemSusChem*, **2015**, *8*, 1768-1778.
- (19) S. H. Lim, K. Nahm, C. S. Ra, D. W. Cho, U. C. Yoon, J. A. Latham, D. Dunaway-Mariano, P. S. Mariano, *J. Org. Chem.*, **2013**, *78*, 9431-9443.
- (20) (a) O. V. Markhynets, P. Das, S. Taktak, M. Flook, R. Mas-Ballesté, E. V. Rybak-Akimova, L. Que Jr., *Chem.-A Eur. J.*, **2009**, *15*, 13171-13180. (b) N. Y. Oh, M. S. Seo, M. H. Lim, M. B. Consugar, M. J. Park, J.-U. Rohde, J. Han, K. M. Kim, J. Kim, L. Que Jr., W. Nam,
-

Chem. Commun., **2005**, 3, 5644-5646. (c) M. P. Jensen, S. J. Lange, M. P. Mehn, E. L. Que, L. Que Jr., *J. Am. Chem. Soc.*, **2003**, 125, 2113-2128.

Chapter 6

Selective methylene oxidation of linear alkyl amines with H₂O₂ catalyzed by a Mn-nonheme complex guided by supramolecular recognition.

In this chapter a supramolecular and bioinspired approach to achieve site-selective C-H functionalization of aliphatic alkyl chains, is described. The ditopic catalyst contains a manganese complex as the active site which catalyzes C-H hydroxylation with H₂O₂ and benzo-18-crown-6 ether as a supramolecular receptor that reversibly binds the substrate. Linear protonated primary amines bind the crown ether receptor in a reversible pre-association that dictates the site-selectivity of the oxidation on C8 and C9 methylene positions, overriding the intrinsic reactivity of the other C-H bonds. This supramolecular control provides a suitable strategy to predictably promote selective oxidation of linear amines.

Part of this work was carried out in collaboration with Prof. Miquel Costas and Dr. Giorgio Olivo of the Institut de Química Computacional i Catàlisi (IQCC) and Departament de Química, Universitat de Girona (Girona, Spain).

The work reported in this Chapter has been published:

G. Olivo, G. Farinelli, A. Barbieri, O. Lanzalunga, S. Di Stefano, M. Costas, *Angew. Chem. Int. Ed.*, **2017**, doi: 10.1002/ange.201709280.

6.1 Introduction

As described in Chapters 1 and 4, nonheme metal complexes represent an important class of catalysts able to promote the C-H functionalization with high levels of regio- and chemo-selectivity.¹ Accordingly, these complexes can oxidize non-activated C-H bonds, even in complicate molecular scaffolds, with good predictable selectivity patterns, using inexpensive and environmentally friendly H₂O₂ as terminal oxidant.²

However in many organic molecules, the great similarity in strength and properties of the numerous C-H bonds, makes the control in the oxidation very challenging to achieve.^{2m-o,3} For instance, in the case of linear alkyl chains, the C-H bonds are particularly strong (~96 kcal mol⁻¹) and only the C-H bonds close to a substituent (i.e. α CH-bonds) and the final methyl groups (ω CH-bonds) can be differentiated by electronic and steric factors, respectively (see Figure 1).^{2m-o} By contrast, the internal C-H bonds result practically indistinguishable and their functionalization consequently brings to an almost statistical mixture of products.

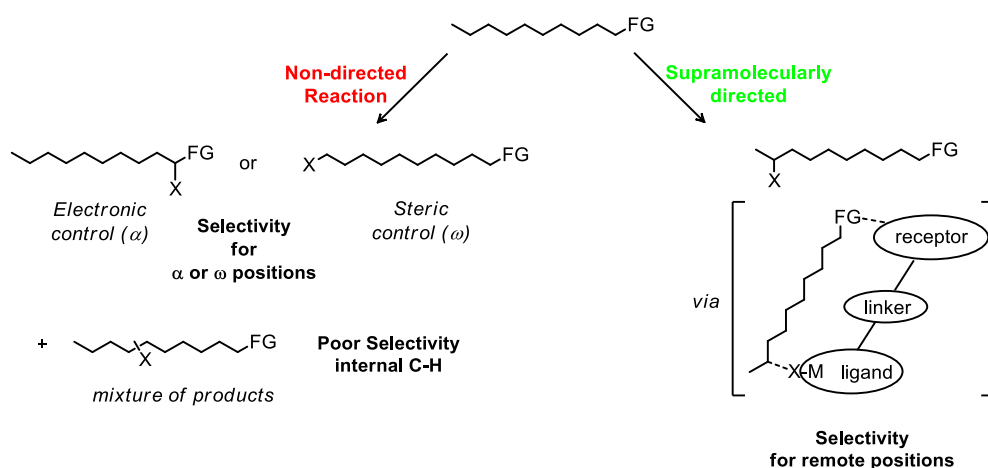


Figure 1. Different approaches for selective C-H functionalization of alkyl substrates.

In nature the excellent selectivity in the functionalization of specific C-H bond in some metal dependent oxygenases such as heme dependent P450 and nonheme iron dependent proline

hydroxylases, is solved by precisely positioning the substrates inside the enzyme active site thanks to multiple and specific weak interactions between the aminoacidic residues and/or cofactors within the cavity.⁴⁻⁷

Nevertheless, reproduction of such elaborated architecture that allows optimal substrate-catalyst interactions, is not so simple in the synthetic systems. (Figure 1).⁸⁻¹¹

Several bioinspired catalysts decorated with recognition motifs able to selective promote C-H oxidations thanks to precise substrate orientation have been studied¹²⁻¹⁶ (Figure 2), however the highly elaborated nature of these catalysts limits the typology of the substrates, moreover precise geometric and shape constraints are required.

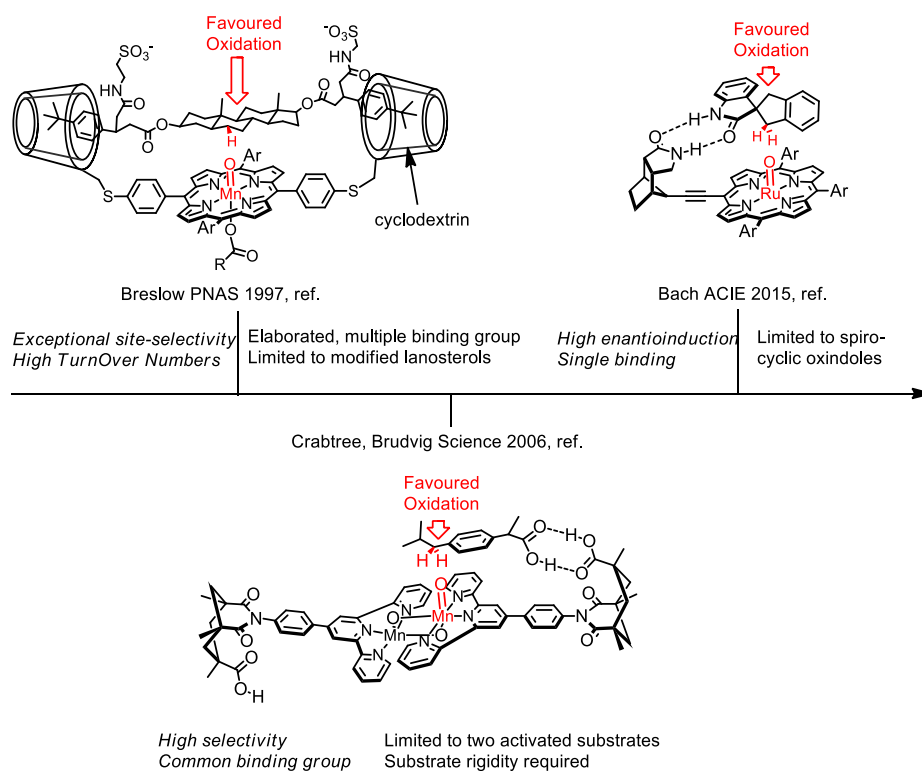


Figure 2. Weak interactions-governed C-H oxidation reactions reported in literature.

In addition, with a single exception,¹² these catalysts oxidize activated and relatively weak C-H bonds in substrates that contain at most two sites susceptible to oxidation.

In this chapter is described the synthesis and the applications of ditopic catalysts **1-Fe** and **1-Mn** made up of a core catalytic center (the active site) and a receptor site able to bind and orient the substrate towards the active site thanks to weak interactions (Figure 3).

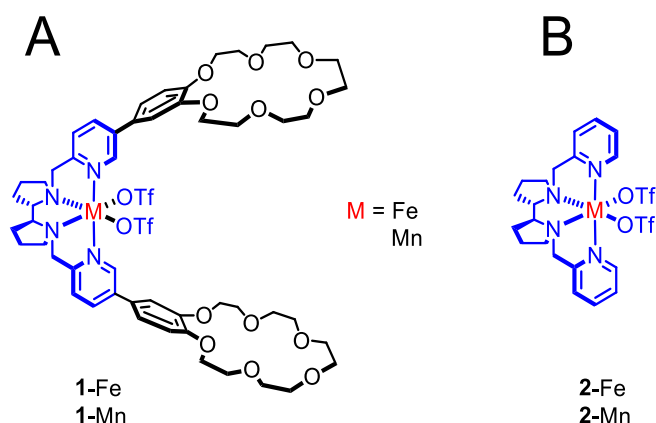


Figure 3. Structures of the catalysts: (A) **1-Fe** and **1-Mn**; (B) **2-Fe** and **2-Mn**. In blue is represented the PDP core.

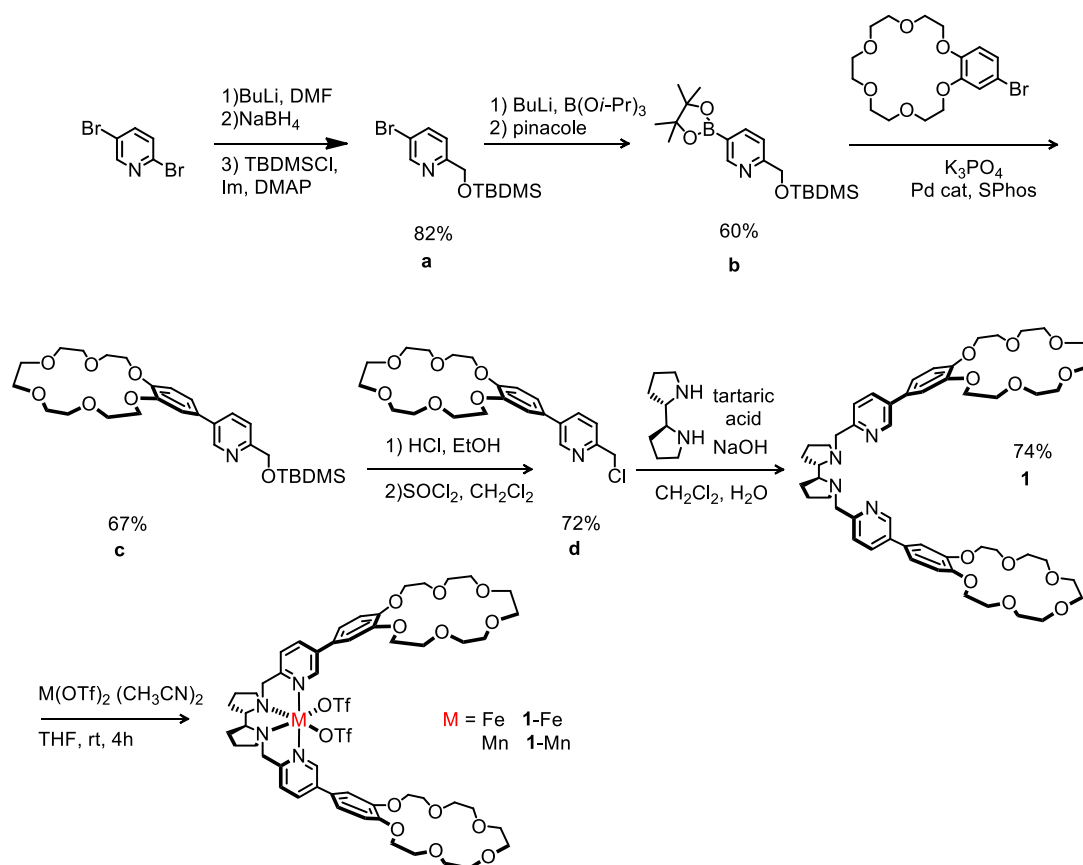
We chose as a core of our catalyst, manganese¹⁷ or iron^{2a} PDP complexes (**2-Mn** and **2-Fe**) because of their well established efficiency in the hydroxylation of aliphatic C-H bonds via a highly reactive oxidizing species formed upon reaction with H₂O₂ and carboxylic acids.¹⁸⁻²¹ The two benzo-18-crown-6 ethers receptors have high affinity for ammonium ions and spherical metal cations²²⁻²⁵ and have been attached on the β position of the two pyridine moieties in order not to interfere with the H₂O₂ activation mechanism.^{18,26}

Ammonium ions, easily obtained by simple and reversible protonation of amine functions, represent ideal substrates to test the efficiency and selectivity of catalysts **1-Fe** and **1-Mn**. Moreover, differently from the amines, the ammonium ions do not coordinate to the metal center, preventing both catalyst poisoning²⁷⁻²⁹ and competition between the receptor and the catalytic center for the substrate.

6.2 Results and Discussion

6.2.1 Synthesis, characterization and features of **1-Fe** and **1-Mn** complexes

The crown ether decorated ligand **1** was prepared starting from 2,5-dibromopyridine which was initially converted, following a reported procedure,^{2h} into the intermediate **a** through formylation, reduction of the aldehyde moiety and alcohol protection. The intermediate **b** was then prepared through boronation followed by pinacol exchange^{2h}. Suzuki coupling allowed the insertion of the crown ether moiety on the pyridine ring. Subsequent deprotection, chlorination and double *N*-alkylation of (*S,S*)-2,2'-bipyrrolidine yielded the desired ligand **1** with a total yield of 20%. The iron and manganese complexes were prepared by reaction of the ligand with Fe(OTf)₂ or Mn(OTf)₂ respectively (Scheme 1, see Experimental Section).



Scheme 1. Synthetic scheme of the complexes **1-Fe** and **1-Mn**.

Solid-state structure of complex **1**-Fe (Figure 4), determined by single-crystal X-ray diffraction, revealed that the receptor site is rather far from the catalytic center, which is an important requirement for the remote selectivity. The crystal structure of **1**-Mn is more disordered but shows the same topological arrangement of the complex. The first coordination sphere of the iron center is essentially coincident with those of the parent **2**-Fe,^{2a} with Fe-N and Fe-O distances characteristic of a high spin ferrous complex, indeed, the ¹H NMR spectra of **1**-Fe in CD₃CN at room temperature, exhibits a wide spectral window (from 60 ppm to -20 ppm), characteristic of a paramagnetic molecule.

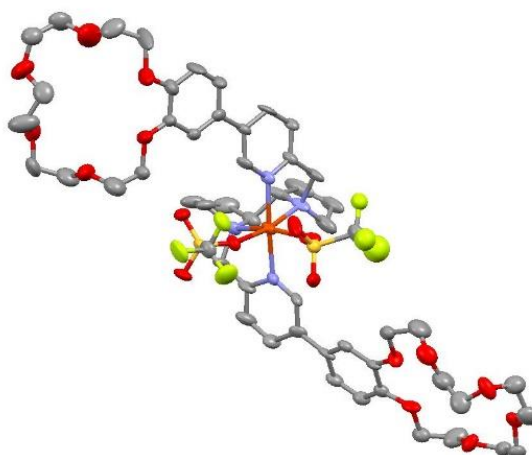


Figure 4. ORTEP Plot (30% probability) of the crystal structure of **1**-Fe (hydrogen atoms omitted for clarity).

A clear ¹H NMR spectrum of **1**-Fe in CD₃CN solution was obtained by the presence of spin crossover temperature dependence. Thus, cooling down to -40 °C, the complex is converted in a diamagnetic one. This gives the opportunity to confirm the strong 1:2 interaction (10⁴ M⁻¹ for each recognition event) between **1**-Fe and primary ammonium substrates such as 1-decylammonium tetrafluoroborate (DecNH₃BF₄) by monitoring the upfield shift of the OCH₂CH₂O protons of the complex during the titration (Figure 5, see Experimental Section).

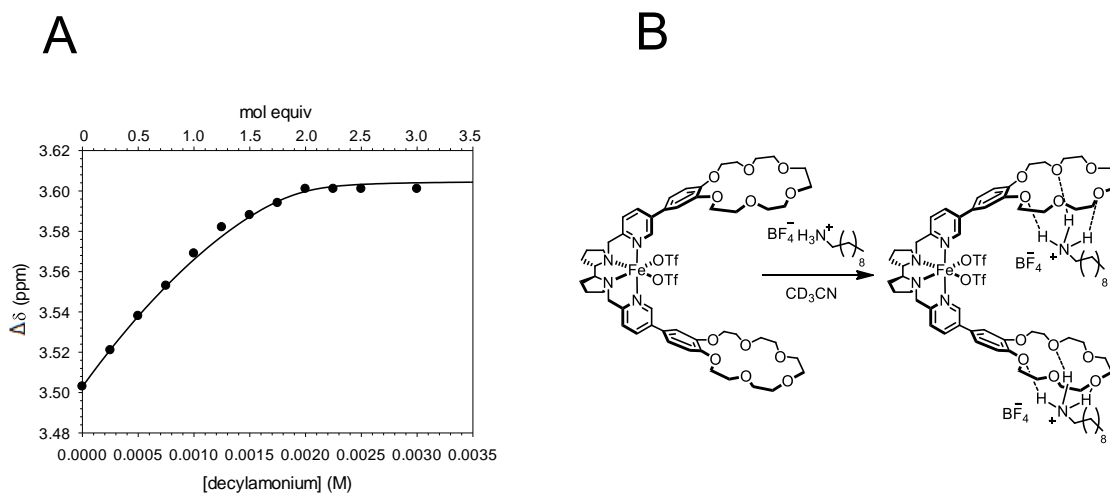


Figure 5. (A) Titration of 1.0 mM **1-Fe** with DecNH₃BF₄ in CD₃CN at -40 °C. The chemical shift of central OCH₂CH₂O of the crown ether is plotted against guest concentration. (B) Binding of DecNH₃BF₄ to **1-Fe**.

The paramagnetism of **1-Mn**, even at -40 °C and the no significant changes in the UV-Vis spectra of **1-Mn** after the addition of the ammonium compound, do not allow to monitor the titration by NMR and by UV-Vis, however the strong ammonium binding was detected by mass spectral analysis. Remarkably, the binding is not affected by addition of AcOH or H₂O, which are required for H₂O₂ activation¹⁸⁻²⁰ and the recognition is highly specific for primary ammonium²²: neither secondary nor tertiary protonated amines interact with the crown ether receptor. Furthermore, the build-up of positive charge close to the metal center does not influence the electronic properties of **1-Fe**, accordingly, there are no significant changes both in the Fe^{III}/Fe^{II} redox potential and in the energy of the MLCT (metal-ligand charge transfer) Vis band of **1-Fe** upon binding with cations as NH₄PF₆, KOTf, Ca(OTf)₂ and Ba(ClO₄)₂ (Figure 6). These results suggest that the core Fe center is not affected by cation coordination in the receptor unit and the only significant changes are related to the benzocrown moiety, which becomes harder to oxidize.

Compound ^a	Bound cation	Fe ^{III} /Fe ^{II} Wave (V)	λ_{\max} ^b
1 -Fe	-	0.75	389
2 -Fe	-	0.73	384
1 -Fe	NH ₄ ⁺	0.77	390
1 -Fe	K ⁺	0.74	390
1 -Fe	Ca ²⁺	0.74	390
1 -Fe	Ba ²⁺	0.76	390

^aRecorded in 1 mM solution in dry CH₃CN with 0.1 M Bu₄NPF₆ electrolyte, against Ag/AgCl electrode at 25 °C under N₂ atmosphere. Error \pm 0.02V. ^bRecorded with 0.025 mM solution of **1**-Fe in presence of 2 eq. of cations.

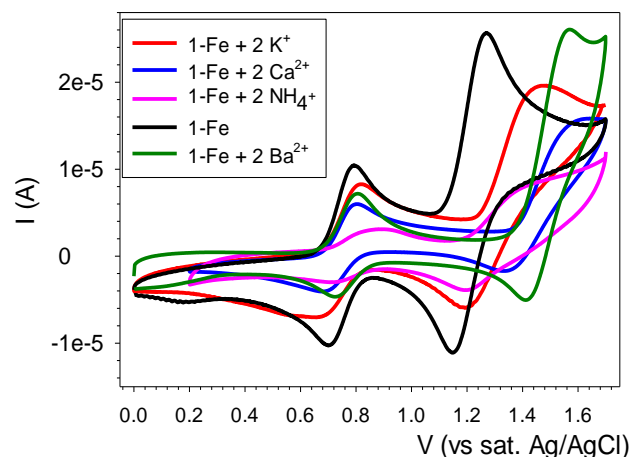
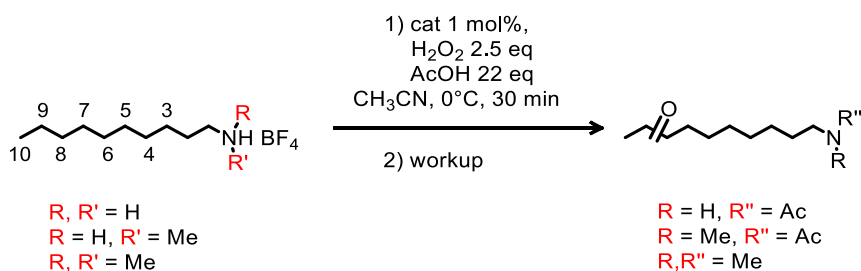


Figure 6. (left side) Effect of cation binding on the Fe^{III}/Fe^{II} redox potential and on the MLCT transition band of **1**-Fe. (right side) Cyclic voltammetry of **1**-Fe in the presence of different cations recorded in 0.1M Bu₄NPF₆ CH₃CN solution under N₂.

6.2.2 Site-selectivity of **1**-Mn guided by Supramolecular recognition

In order to investigate the site-selectivity properties of these supramolecular catalysts in C-H oxidation, we chose DecNH₃BF₄ as a benchmark substrate (Scheme 2, see Experimental Section). The internal C-H bonds of this long chain protonated alkyl amine, have very similar reactivity so mixtures of oxidation products should be consequently obtained with non-directed oxidations. Consequently, several ketone products are obtained with the Mn-PDP complex, **2**-Mn (entry 1, Table 1). The ammonium positive charge protects the nearby positions towards the electrophilic oxidant (from C1 up to C5),²⁷⁻²⁹ as a consequence, ketones K3-K5 are formed in low yields. C6 and C7 positions are oxidized in almost statistical yields while the last positions (C8 and C9), due to the lower steric hindrance, are slightly favored towards the oxidation and the K8 and K9 account for roughly half of the total yield (53%).



Scheme 2. DecNHRR'BF₄ oxidation with H₂O₂ catalyzed by 1-Fe/Mn and 2-Fe/Mn.

Table 1. Site-selectivity in DecNHRR'BF₄ oxidation mediated by different catalysts.^a

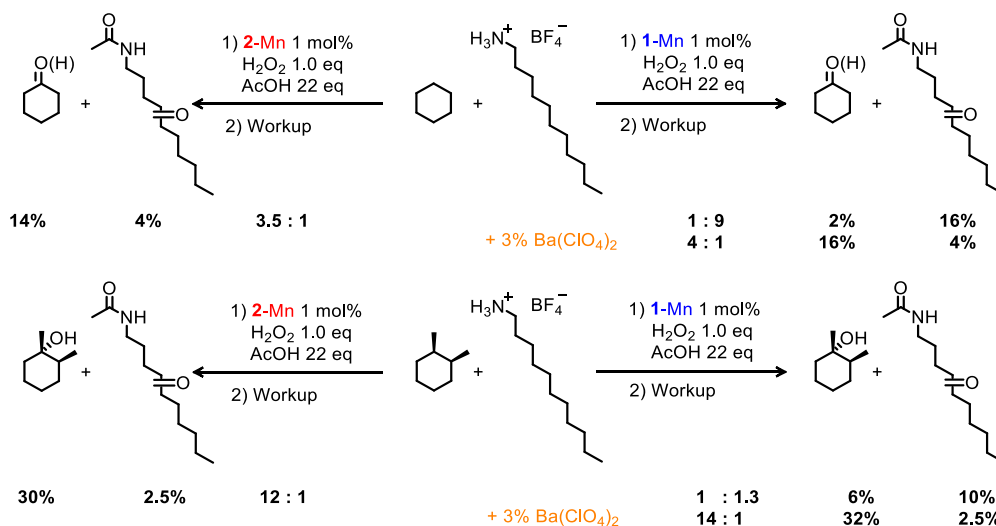
Entry	cat	R, R'	Add. (%)	Conv/ tot yield (%)	AcRN	AcHN	AcHN	AcRN	AcRN	AcRN	AcRN	C8 + C9 Sel. ^b
					K3 (%)	K4 (%)	K5 (%)	K6 (%)	K7 (%)	K8 (%)	K9 (%)	
1	2-Mn	H,H	-	43/34	0.5	2	2.5	5.5	5.5	8	10	53
2	1-Mn	"	-	50/36	-	-	0.5	1.5	5	13	16	81
3	2-Fe	"	-	48/36	-	0.5	4	8	8	7	10	45
4	1-Fe	"	-	36/30	-	-	0.5	5	6	6	12	61
5	2-Mn	"	BC 2 ^c	41/35	0.5	1.5	3	6	6	7.5	10	51
6	2-Mn	"	BC 10 ^c	25/21	0.5	1	1.5	3	3	5	6	54
7	2-Mn	"	BC 100 ^c	8/trace	-	-	-	-	-	-	-	-
8	1-Mn	"	Ba ²⁺ 3 ^d	47/27	trace	2	2	5	5	6	8	58
9	1-Mn	H, Me	-	9/7	trace	0.5	0.5	1.5	1.5	2	2	50
10	2-Mn	H, Me	-	28/26	0.5	1	3	4.5	4.5	5	7.5	49
11	1-Mn	Me,Me	-	11/3	trace	trace	trace	0.5	0.5	0.5	0.5	50
12	2-Mn	Me,Me	-	60/47	-	2.5	5	7.5	7.5	10	14	52

^aFor the reaction condition see the Experimental Section. Yields are calculated with GC and referred to an internal standard. Error \pm 0.5%. Very low amounts of acetylated alcohols (<4% of total yield) have been detected in GC analysis, with a regioselectivity pattern superimposable to the one of the main ketone products. ^bC8+C9 Selectivity defined as ((K8+K9)/tot. yield). ^cBC = 18-benzocrown-6 ether, added as the reported percentage of the substrate (in moles). ^dAdded as Ba(ClO₄)₂.

The use of our catalyst **1-Mn** remarkably modified the selectivity with a significant amplification of the oxidation on C8 and C9 positions, (now K8 and K9 account for 81% of the oxidized products) accompanied by a decrease in C5, C6 and C7 oxidation (entry 2) and a completely suppression of K3 and K4 formation. A similar effect was found also for Fe-based complexes (entries 3 and 4), but the lower selectivity amplification, prompted us to focus our attention on manganese catalysts.

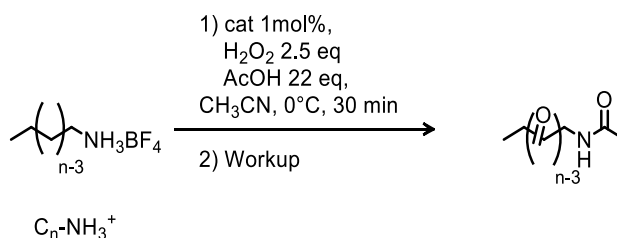
The observed change in selectivity was really due to supramolecular recognition as demonstrated by the following control experiments.

- Addition of free benzo-18-crown-6 ether does not influence the selectivity of the parent **2-Mn** complex, it means that the simple binding of the ammonium to crown ether does not induce any change in the reactivity of C-H bonds (entries 5-7), on the contrary the conversion decreases at increasing unbound crown ether concentrations, probably for the competitive ether oxidation.
- Saturation of the receptor by prior coordination of Ba²⁺ completely suppresses the selectivity amplification of **1-Mn** (entry 8), leading to the same selectivity pattern of **2-Mn**.
- Replacement of DecNH₃BF₄ with protonated *N*-methyldecylamine and *N,N*-dimethyldecylamine, decreases the affinity of the substrate for the crown ether receptor and so the selectivity pattern (entry 9-12, see Experimental Section). Also in this case, the low yield of oxidized products obtained with **1-Mn** derives from catalyst self-oxidation on the electron rich crown ether moiety.
- Competitive oxidations between DecNH₃BF₄ and neutral, more reactive substrate such as cyclohexane and 1,2-*cis*-dimethylcyclohexane (see Experimental Section), bring to the expected preferential oxidation of the more reactive substrate with **2-Mn** (Scheme 3), on the contrary a complete switch of the selectivity is observed in presence of the supramolecular catalyst **1-Mn**. Moreover, the addition of Ba²⁺ completely suppresses the preference for DecNH₃BF₄ oxidation with **1-Mn** also in competitive oxidations and the selectivity pattern is controlled by the reactivity of the substrate, as observed for the **2-Mn** (Scheme 3).



Scheme 3. Competitive oxidation experiments with H_2O_2 catalyzed by **1-Mn** and **2-Mn**.

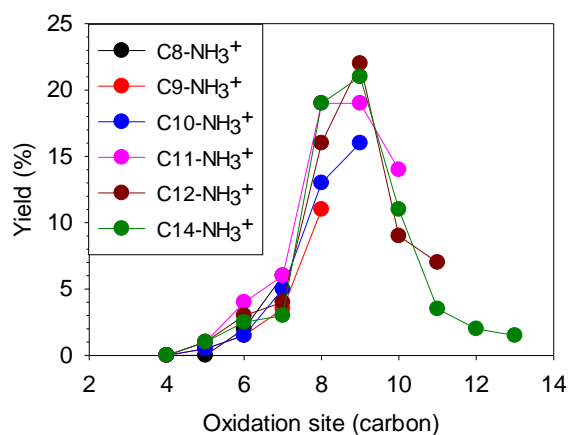
Once verified the origin of the selectivity, in order to understand the precise site of oxidation with **1-Mn**, we investigated the oxidation of a series of protonated linear primary amines, whose chain length spans from C6 to C14 (Scheme 4).



Scheme 4: Oxidation of linear 1-alkylammonium salts with H_2O_2 catalyzed by **1-Mn** and **2-Mn**

With short ammonium chains (hexylammonium), the oxidation does not occur neither with catalysts **1-Mn** nor with **2-Mn**, probably due to the strong deactivation exerted by the proximal positive charge. However, when the chain length increases, in the reactions catalyzed by **2-Mn** the distribution of the products is exactly the same observed for the $\text{DecNH}_3\text{BF}_4$ (Figure 7, B), on the contrary a bell-shaped profile, with the maximum yields on C8 and C9 sites, is obtained, independently of the chain length in the reaction promoted by **1-Mn** (Figure 7, A).

A) Distribution of oxidation products in **1**-Mn catalyzed oxidations



B) Distribution of oxidation products in **2**-Mn catalyzed oxidations

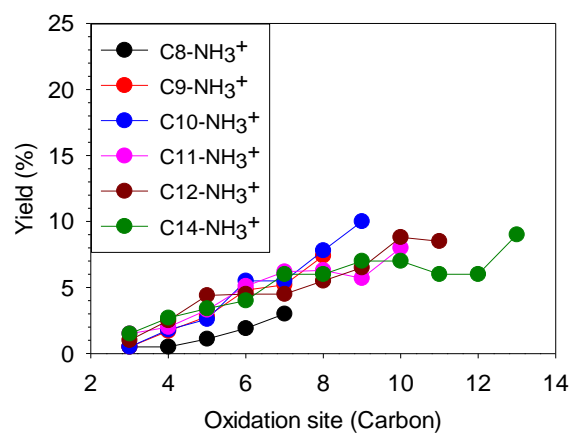


Figure 7: Plot of the ketone yields vs its position (Carbon number, where C1 is the one bearing the amine) on the alkyl chain. A) Reactions catalysed by **1**-Mn. B) Reactions catalysed by **2**-Mn.

The bell-shaped profile is a clear evidence of a site-selectivity guided by a supramolecular control. The interactions between the receptor and the substrates, make the C-H at the positions C8 and C9 in the perfect range for the attack of the oxidizing species.

To the best of our knowledge, this is the first report of a highly selective functionalization of the internal and remote positions of linear alkyl substrates without the aid of enzymes. Furthermore, the preferential oxidation site is dictated only by the distance between the C-H bond and the recognition moiety, allowing a full predictability of the oxidation regioselectivity. Such a predictable control could significantly expand the potential of methylene functionalization in synthesis.

6.3 Conclusion

We have prepared a supramolecular biomimetic catalyst that regioselectively oxidizes remote methylenic sites in linear aliphatic amines thanks to reversible binding between the substrate and the receptor unit of the catalyst. Such recognition does not require elaborated or

specific groups on the substrate and is strong enough to tolerate competitive hydrogen bond partners in the reaction mixtures. Remarkably, the selectivity is maintained in a whole series of linear amine substrates, no matter the chain length or the presence of more (sterically) activated positions, the C-H positions oxidized will be always the same. We believe that the interesting potential of this supramolecular approach, would provide a synthetic attractive way to disclose novel site-selectivities in C-H functionalization reactions.

6.4 Experimental Section

Synthesis 1-Fe and 1-Mn

The crown ether decorated ligand **1** was prepared starting from 2,5-dibromo-pyridine which was converted into intermediate **b** following a reported procedure.^{2h}

5-4'-Benzo-3-[18-crown-6]-2-picoly-tertbutyldimethylsilyl ether (c): 16 mg of Pd(OAc)₂ (71 μmol), 59 mg of *S*-PhOS (142 μmol), 928 mg of 4-bromobenzo[18-crown-6]ether (2.4 mmol) and 1.0 g of K₃PO₄ (4.8 mmol) were added in a Schlenck tube and dried with three vacuum-Argon cycles. Compound **b** (1.25 mg; 3.6 mmol) is dissolved in 4.3 mL of anhydrous toluene and 430 μL of degassed water were cannula-transferred into the reaction mixture. The reaction was heated to 100 °C and left under stirring for 16 hours. The mixture was then cooled to rt, quenched with 1 mL of water and extracted with CH₂Cl₂. The organic phases were collected, dried over Na₂SO₄, filtered and the solvent was removed by rotatory evaporation. Compound **c** was purified by chromatography column (flash SiO₂, 5%÷10% MeOH/CHCl₃), yielding 830 mg (1.6 mmol, 67% yield) of pure product. **¹H-NMR** (300 MHz, CDCl₃) δ: 8.67 (d, *J* = 2.1 Hz, 1H), 7.84 (dd, *J* = 8.2 Hz, *J* = 2.1, 1H), 7.54 (d, *J* = 8.2 Hz, 1H), 7.13 (d, *J* = 2.1 Hz, 1H), 7.10 (s, 1H), 6.96 (d, *J* = 8.2 Hz, 1H), 4.87 (s, 2H), 4.21 (m, 4H), 3.95 (m, 4H), 3.78 (m, 4H), 3.72 (m, 4H), 3.68 (s, 4H), 0.96 (m, 9H), 0.13 (m, 6H). **¹³C-NMR** (75 MHz, CDCl₃) δ: 159.48, 149.33, 149.29, 149.13, 149.09, 146.53, 134.73, 134.53, 131.07, 120.00, 119.85, 114.55, 114.42, 113.35, 113.23, 70.77, 70.68, 69.57, 69.52, 69.38, 69.31, 69.14, 69.10, 65.77, 25.82, 18.27, -5.45. **UV-Vis**: λ=290 nm (ε=8800 M⁻¹ cm⁻¹); λ=268 nm (ε=9400 M⁻¹ cm⁻¹). **HRMS**: C₂₈H₄₃O₇SiN [M+K]⁺: calculated 572.2446, found: 572.2422. **Melting point**: 39 °C ÷ 41 °C.

5-4'-Benzo-3-[18-crown-6]-2-pyridin-hydroxymethyl: 580 mg (1.0 mmol) of compound **c** were dissolved in 6.5 mL of EtOH and 1.3 mL of HCl 3M, and the mixture was left under stirring at rt for 3 hours. NaHCO₃ was added to neutralize the solution, and the mixture was extracted three times with CH₂Cl₂. The organic phases were collected, dried over Na₂SO₄, filtered and the solvent was removed by rotatory evaporation, yielding an orange solid was obtained, which was used without further purifications. ¹H-NMR (400 MHz, CDCl₃) δ: 8.72 (d, *J* = 4 Hz, 1H), 7.81 (dd, *J* = 12 Hz, *J* = 4 Hz, 1H), 7.29 (d, *J* = 12 Hz, 1H), 7.15-7.07 (m, 2H), 7.10 (s, 1H), 6.96 (d, *J* = 12 Hz, 1H), 4.80 (s, 2H), 4.21 (m, 4H), 3.95 (m, 4H), 3.78 (m, 4H), 3.72 (m, 4H), 3.69 (s, 4H). ¹³C-NMR (400 MHz, CDCl₃) δ: 157.2, 149.3, 146.6, 134.8, 130.8, 120.3, 120.1, 114.4, 113.2, 70.85, 70.75, 70.71, 69.63, 69.57, 69.40, 69.12, 64.02. **HRMS:** (C₂₂H₂₉NO₇) found 442.1825, calculated 442.1836 [M+Na]⁺.

5-4'-Benzo-3-[18-crown-6]-2-pyridin-chloromethyl (d): (652 mg, 1.49 mmol) of 5-4'-Benzo-3-[18-crown-6]-2-pyridin-hydroxymethyl was dissolved in 4.6 mL of CH₂Cl₂ and cooled to 0 °C. SOCl₂ (0.74 mL; 10 mmol) was added dropwise over 10 minutes, and the mixture was stirred overnight allowing heating to rt. Then, a saturated aqueous solution of NaHCO₃ was added to neutralize the mixture. Extraction of this mixture with CH₂Cl₂ (three times) and drying of the collected organic phases over Na₂SO₄, followed filtration and rotatory evaporation of the solvent, furnished 340 mg of pure compound **d** (1.1 mmol, overall yield of 74%). ¹H-NMR (300 MHz, CDCl₃) δ: 8.75 (d, *J* = 2.2 Hz, 1H), 7.85 (dd, *J* = 8.2 Hz, *J* = 2.2, 1H), 7.40 (d, *J* = 8.2 Hz, 1H), 7.14 (d, *J* = 2.2 Hz, 1H), 7.10 (dd, *J* = 8.2 Hz, *J* = 2.2 Hz, 1H), 6.98 (d, *J* = 8.2 Hz, 1H), 4.86 (s, 2H), 4.22 (m, 4H), 3.95 (m, 4H), 3.78 (m, 4H), 3.73 (m, 4H), 3.69 (s, 4H). ¹³C-NMR (400 MHz, CDCl₃) δ: 154.7, 149.5, 149.4, 147.6, 135.8, 135.0, 130.4, 127.7, 120.2, 114.3, 113.2, 70.83, 70.82, 70.73, 70.71, 70.70, 69.59, 69.54, 69.36, 69.08, 46.52. **HRMS:** C₂₂H₂₈NO₆Cl [M+Na]⁺: calculated 460.1497, found: 460.1489.

Ligand 1: Compound **d** (450 mg; 1 mmol), (*S,S*)-2,2'-bipyrrrolidine *D*-tartrate trihydrated (148.8 mg; 0.43 mmol) and NaOH (120 mg; 3.0 mmol) were dissolved in CH₂Cl₂/H₂O (1:1, 2.1 mL). The biphasic mixture was left under vigorous stirring at room temperature overnight. Then CH₂Cl₂ (10 mL) and NaOH 1M (10 mL) were added, and the mixture was extracted with CH₂Cl₂ three times. The organic phases were collected, dried over Na₂SO₄, filtered and the solvent was removed under rotatory evaporation. The product was purified over chromatography column (basic Al₂O₃, CH₂Cl₂/1% MeOH/1% Et₃N), yielding 300 mg (0.32 mmol, 74% yield) of pure ligand **1**. ¹H-NMR (300 MHz, CDCl₃) δ: 8.70 (s, 2H), 7.78 (d, *J* =

7.0 Hz, 2H), 7.53 (m, 2H), 7.11 (d, $J = 2.2$ Hz, 2H), 7.08 (m, 2H), 6.94 (d, $J = 8.3$ Hz, 2H), 4.21 (m, 12H), 3.95 (m, 8H), 3.78 (m, 8H), 3.73 (m, 8H), 3.70 (s, 8H), 3.13 (m, 4H), 2.3 (m, 2H), 2.02 (m, 4H), 1.81 (m, 4H). $^{13}\text{C-NMR}$ (75 MHz, CDCl_3) δ : 158.45, 149.12, 148.88, 146.81, 134.34, 131.01, 122.50, 119.84, 114.03, 112.78, 70.69, 70.58, 69.45, 69.04, 68.86, 65.42, 60.67, 55.17, 52.76, 29.58, 26.00, 23.48, 7.92. **UV-Vis**: $\lambda=292$ nm, $\epsilon=32960$ $\text{M}^{-1} \text{cm}^{-1}$; $\lambda=269$ nm, $\epsilon=34320$ $\text{M}^{-1} \text{cm}^{-1}$. **HRMS**: $\text{C}_{52}\text{H}_{70}\text{O}_{12}\text{N}_4$ $[\text{M}+\text{H}]^+$: calculated 943.5068, found 943.5082. Melting point: 121.5 °C \div 123.5 °C. **FT-IR** (ATR) νcm^{-1} : 2871, 1598, 1523, 1486, 1372, 1257, 1209, 1120, 945, 801.

Complex 1-Mn: Ligand **1** and $\text{Mn}(\text{OTf})_2$ were mixed in 0.8 mL of anhydrous THF under nitrogen (in a glove box) and stirred at room temperature for 4 hours. After this time, anhydrous diethyl ether (7 mL) was added, and a pale-yellow solid precipitated out of the solution. The supernatant was removed, the solid was washed with diethyl ether two times and dried at vacuum pump for 3-4 hours. At this point, the solid was suspended in ether (5 mL) and stirred overnight. The supernatant solution was removed and the yellow solid was dried again under vacuum. X-Ray quality crystals have been obtained by layering of hexane on a CH_2Cl_2 solution of the complex overnight. **UV-Vis**: 291 nm ($\epsilon = 21900$ $\text{M}^{-1} \text{cm}^{-1}$), 219 nm ($\epsilon = 35200$ $\text{M}^{-1} \text{cm}^{-1}$). **FT-IR** (ATR) νcm^{-1} : 2924, 2972, 1603, 1493, 1310, 1237, 1216, 1135, 1030, 943, 633.9, 514.5. **Elemental Analysis**: $[\text{Mn}(\text{L1})(\text{OTf})_2] \cdot 0.5\text{CH}_2\text{Cl}_2$, theor. C 50.04%, H 5.44%, N 4.32%. expt. C 48.63%, N 4.46%, H 5.31%. **HRMS**: $[\text{Mn}(\text{C}_{52}\text{H}_{70}\text{N}_4\text{O}_{12})]^{2+}$, calculated 498.7180, found 498.7184.

Complex 1-Fe: Equimolar amounts of ligand **1** (150 mg) and $\text{Fe}(\text{OTf})_2(\text{CH}_3\text{CN})_2$ (69 mg) were mixed in 0.8 mL of anhydrous THF under nitrogen (in a glove box) and stirred at room temperature for 4 hours. After this time, anhydrous diethyl ether (7 mL) was added, and a pale-yellow solid precipitated out of the solution. The supernatant was removed, the solid was washed with diethyl ether two times and dried at vacuum pump for 3-4 hours. At this point, the solid was suspended in ether (5 mL) and stirred overnight. The supernatant solution was removed and the yellow solid was dried again under vacuum. X-Ray quality crystals have been obtained by slow diffusion of ether into a CH_2Cl_2 solution of the complex after two days. **$^1\text{H-NMR}$** (400 MHz, CD_3CN , -40°C): 9.47 (s, 2H, α -Py-CH), 8.08 (d, $J = 8$ Hz, 2H, γ -Py-CH), 7.80 (d, $J = 8$ Hz, 2H, β' -Py-CH), 7.29 (m, 4H, benzocrown C_3H and C_4H), 7.09 (d, $J = 8$ Hz, 2H, benzocrown C_6H), 5.26 (broad s, 2H, py CH_2), 4.29 (d, $J = 32$ Hz, 8H, benzocrown C_7H_2 and C_{16}H_2), 4.13 (d, $J = 16$ Hz, 2H, py CH_2), 3.77 (d, $J = 16$ Hz, 8H, benzocrown C_8H_2 and

C₁₅H₂), 3.58 (m, 8H, benzocrown C₉H₂ and C₁₄H₂), 3.52 (s, 16H, benzocrown C₁₀H₂, C₁₁H₂, C₁₂H₂ and C₁₃H₂), 3.02 (m, 2H,), 2.77 (m, 2H), 2.62 (m, 2H), 2.39 (m, 2H), 2.10 (m, 4H), 1.52 (m, 2H). **UV-Vis**: 393 nm ($\epsilon = 8300 \text{ M}^{-1} \text{ cm}^{-1}$), 302 nm ($\epsilon = 37700 \text{ M}^{-1} \text{ cm}^{-1}$), 274 nm ($\epsilon = 38000 \text{ M}^{-1} \text{ cm}^{-1}$), 228 nm ($\epsilon = 63000 \text{ M}^{-1} \text{ cm}^{-1}$). **FT-IR** (ATR) $\nu \text{ cm}^{-1}$: 2924, 2870, 1603, 1492, 1235, 1125, 1027, 944.3, 633.4, 513.7. **Elemental Analysis**: [Fe(L1)(OTf)₂], theor. C 50.00%, H 5.44%, N 4.32%. expt. C 49.76%, N 4.49%, H 5.33%. **HRMS**: Fe(C₅₂H₇₀N₄O₁₂)(CF₃SO₃)⁺, calculated 1147.3856, found 1147.3849

Binding of cations into the benzo-18-crown-6-receptor of 1-Fe and 1-Mn

The titrations of **1-Fe** with monovalent cations (NH₄⁺, K⁺, RNH₃⁺) have been monitored by ¹H-NMR spectroscopy by following the upfield shift of the crown ether CH₂ signals, while all titrations with divalent ones (Ca²⁺, Ba²⁺) by UV-Vis spectroscopy. Mass spectrometry further confirmed the binding. Titrations with **1-Mn** have been monitored by UV-Vis spectroscopy whenever possible (K⁺, Ca²⁺, Ba²⁺) and again confirmed by mass spectrometry. Binding of ammonium ions to **1-Mn** was observed by mass spectrometry. In each case, the binding was found to occur with the expected 1: 2 stoichiometry between the ditopic host (complex **1-Fe** or **1-Mn**) and the guest (the metal or ammonium cation).

UV-Vis titrations were carried out at 25 °C with CH₃CN under air. The cationic guest was dissolved in a solution of **1-Fe** (or **1-Mn**) of the same concentration of the titrated solution in order to avoid dilution.

General procedure for the oxidation reactions

Mn catalysts (**1-Mn** or **2-Mn**, 0.37 μmol , 0.46 or 0.25 mg respectively, 1 mol%) or Fe catalysts (**1-Fe** or **2-Fe**, 1.11 μmol , 1.38 or 0.75 mg respectively, 3 mol%) and substrate (37 μmol , 1 molar equivalent) were dissolved in AcOH (46 μL , 814 μmol , 22 molar equivalents) and 400 μL CH₃CN (HPLC grade) inside a 8 mL screw-top vial equipped with a magnetic stir bar at 0 °C (ice-bath). A ~0.9 M solution of H₂O₂ in CH₃CN (92 μmol , 2.5 molar equivalents) diluted from commercially available H₂O₂ water solution (70% w/w) was slowly delivered over 16 minutes by syringe pump. The solution homogeneous, transparent turned amber-yellow as soon as the first drop of hydrogen peroxide reached the catalyst solution. At the end of the addition, the reaction was left stirring for additional 15 minutes.

Work up and GC analysis of primary and secondary ammonium ions: after the reaction, 18.5 μmol of internal standard (biphenyl) were added. The mixture was then treated with triethyl amine (200 μL) and acetic anhydride (300 μL) at 0 °C for 50 minutes. After this time, water (2

mL) was added and the mixture was stirred for additional 10 minutes. This solution was extracted with dichloromethane (3 mL) and the organic phase was washed with H₂SO₄ 2 M (4 mL), a saturated NaHCO₃ aqueous solution (4 mL) and water (4 mL), dried over MgSO₄ and analyzed by GC, GC-MS, ¹H NMR and ¹³C NMR.

Workup and GC analysis of tertiary ammonium ions: after the reaction, 18.5 μmol of internal standard (biphenyl) were added. 4 mL of a 2M NaOH solution were added and the mixture was then extracted with CH₂Cl₂ (5 mL) three times. The collected organic layers were dried over MgSO₄ and analyzed by GC, GC-MS, ¹H NMR and ¹³C NMR.

The ketone products were then isolated, purified (whenever possible) and used as standard.

The competitive oxidation between DecNH₃BF₄ and cyclohexane or 1,2-*cis*-dimethylcyclohexane were carried out following the same procedure described above.

References

- (1) (a) L. Que Jr., W. B. Tolman, *Nature*, **2008**, *455*, 333-340. (b) M. C. White, *Science*, **2012**, *335*, 807-809. (c) E. P. Talsi, K. P. Bryliakov, *Coord. Chem. Rev.*, **2012**, *256*, 1418-1434. (d) A. Company, J. Lloret-Fillol, L. Gómez, M. Costas, *In Alkane C-H Activation by Single-Site Metal Catalysis*; P. J. Perez, Ed.; Springer: Dordrecht, The Netherlands, **2013**; Vol. 38.
- (2) (a) M. S. Chen, M. C. White, *Science*, **2007**, *318*, 783-787. (b) L. Gómez, I. Garcia-Bosch, A. Company, J. Benet-Buchholz, A. Polo, X. Sala, X. Ribas, M. Costas, *Angew. Chem., Int. Ed.* **2009**, *48*, 5720-5723. (c) M. S. Chen, M. C. White, *Science*, **2010**, *327*, 566-571. (d) M. A. Bigi, S. A. Reed, M. C. White, *J. Am. Chem. Soc.*, **2012**, *134*, 9721-9726. (e) Y. Hitomi, K. Arakawa, T. Funabiki, M. Kodera, *Angew. Chem., Int. Ed.*, **2012**, *51*, 3448-3452. (f) L. Gómez, M. Canta, D. Font, I. Prat, X. Ribas, M. Costas, *J. Org. Chem.*, **2013**, *78*, 1421-1433. (g) I. Prat, L. Gómez, M. Canta, X. Ribas, M. Costas, *Chem.-Eur. J.*, **2013**, *19*, 1908-1913. (h) P. E. Gormisky, M. C. White, *J. Am. Chem. Soc.*, **2013**, *135*, 14052-14055. (i) D. Clemente-Tejeda, A. López-Moreno, F. A. Bermejo, *Tetrahedron*, **2013**, *69*, 2977-2986. (j) D. S. Nesterov, O. V. Nesterova, M. F. C. Guedes da Silva, A. J. L. Pombeiro, *Catal. Sci. Technol.*, **2015**, *5*, 1801-1812. (k) Y. He, J. D. Gorden, C. R. Goldsmith, *Inorg. Chem.*, **2011**, *50*, 12651-12660. (l) V. A. Yazerski, P. Spanring, D. Gatineau, C. H. M. Woerde, S. M. Wieclawska, M. Lutz, H. Kleijn, R.R. J. M. Klein Gebbink, *Org. Biomol. Chem.*, **2014**, *12*, 2062-2017. (m) W. R.

- Gutekunst, P. S. Baran, *Chem. Soc. Rev.*, **2011**, *40*, 1976-1991. (n) T. Brückl, R. D. Baxter, Y. Ishihara, P. S. Baran, *Accounts of Chemical Research*, **2012**, *45*, 826-839. (o) J. F. Hartwig, M. A. Larsen, *ACS Central Science*, **2016**, *2*, 281-292.
- (3) T. Newhouse, P. S. Baran, *Angew. Chem. Int. Ed.*, **2011**, *50*, 3362-3374.
- (4) D. H. Sherman, et al., *J. Biol. Chem.*, **2006**, *281*, 26289-26297.
- (5) S. Negretti, et al., *J. Am. Chem. Soc.*, **2014**, *136*, 4901-4904.
- (6) R. H. NarayanAlison, et al., *Nat. Chem.*, **2015**, *7*, 653-660.
- (7) J. C. Lewis, P. S. Coelho, Arnold, F. H., *Chem. Soc. Rev.*, **2011**, *40*, 2003-2021.
- (8) P. Dydio, J. N. H. Reek, *Chem. Science*, **2014**, *5*, 2135-2145.
- (9) H. J. Davis, R. J. Phipps, Harnessing, *Chem. Science*, **2017**, *8*, 864-877.
- (10) Y. Kuninobu, H. Ida, M. Nishi, M. Kanai, *Nat. Chem.*, **2015**, *7*, 712-717.
- (11) H. J. Davis, M. T. Mihai, R. J. Phipps, *J. Am. Chem. Soc.*, **2016**, *138*, 12759-12762.
- (12) R. Breslow, Y. Huang, X. Zhang, J. Yang, *PNAS*, **1997**, *94*, 11156-11158.
- (13) R. Breslow, X. Zhang, Y. Huang, *J. Am. Chem. Soc.*, **1997**, *119*, 4535-4536.
- (14) J. Yang, B. Gabriele, S. Belvedere, Y. Huang, R. Breslow, *J. Org. Chem.*, **2002**, *67*, 5057-5067.
- (15) S. Das, C. D. Incarvito, R. H. Crabtree, G. W. Brudvig, *Science*, **2006**, *312*, 1941-1943.
- (16) J. R. Frost, S. M. Huber, S. Breitenlechner, C. Bannwarth, T. Bach, *Angew. Chem. Int. Ed.*, **2015**, *54*, 691-695.
- (17) R. V. Ottenbacher, D. G. Samsonenko, E. P. Talsi, K. P. Bryliakov, *Org. Lett.*, **2012**, *14*, 4310-4313.
- (18) K. Chen, L. Que Jr., *J. Am. Chem. Soc.*, **2001**, *123*, 6327-6337.
- (19) R. Mas-Balleste, L. Que Jr., *J. Am. Chem. Soc.*, **2007**, *129*, 15964-15972.
- (20) W. N. Oloo, L. Que Jr., *Acc. Chem. Res.*, **2015**, *48*, 2612-2621.
- (21) J. Serrano-Plana, et al., *J. Am. Chem. Soc.*, **2015**, *137*, 15833-15842.
- (22) R. M. Izatt, K. Pawlak, J. S. Bradshaw, R. L. Bruening, *Chem. Rev.*, **1991**, *91*, 1721-2085.
- (23) J.-P. Behr, J.-M. Lehn, *J. Chem. Soc., Chem. Commun.*, **1978**, 143-146.
- (24) R. Cacciapaglia, S. Di Stefano, L. Mandolini, *J. Am. Chem. Soc.*, **2003**, *125*, 2224-2227.
- (25) M. R. Kita, A. J. M. Miller, *Angew. Chem. Int. Ed.*, **2017**, *56*, 5498-5502.
- (26) G. Olivo, O. Cussó, M. Costas, *Chemistry – An Asian Journal*, **2016**, *11*, 3148-3158.
- (27) C. T. Mbofana, E. Chong, J. Lawniczak, M. S. Sanford, *Org. Lett.*, **2016**, *18*, 4258-4261.
- (28) M. Lee, M. S. Sanford, *J. Am. Chem. Soc.*, **2015**, *137*, 12796-12799.

(29) J. M. Howell, K. Feng, J. R. Clark, L. J. Trzepakowski, M. C. White, *J. Am. Chem. Soc.*, **2015**, *137*, 14590-14593.

Chapter 7

General Conclusion

Nonheme iron and manganese complexes are versatile and environmentally sustainable catalysts able to promote the oxidation of a broad range of organic compounds with interesting synthetic application. Careful simple modification in the design of this catalytic systems, can contribute to change significantly their selectivity and efficiency.

In this Ph.D. thesis, some aspects related to the mechanistic analysis and catalytic activity of three different nonheme catalytic systems: aminopyridine iron complexes, imine iron complexes and aminopyridine supramolecular iron and manganese complexes, have been investigated in detail.

The occurrence of an electron transfer-oxygen rebound process in the oxidation of aryl sulfides promoted by two tetradentate ($[(PDP)Fe^{II}]$ and $[(BPMCNC)Fe^{II}]$) and two pentadentate ($[(N4Py)Fe^{II}]$ and $[(Bn-TPEN)Fe^{II}]$) aminopyridine iron complexes, has been highlighted through detailed product and kinetic studies of the oxidation of two series of aromatic sulfides (aryl 1-methyl-1-phenylethyl sulfides and aryl diphenylmethyl sulfides) whose corresponding radical cations are characterized by high C-S fragmentation rate constants. Using aryl 1-methyl-1-phenylethyl sulfides as substrates, it has been possible, moreover, to estimate the rate constants of the oxygen rebound process (k_{OT}) from the reduced nonheme iron-oxo complexes to the sulfide radical cations.

A bioinspired supramolecular version of the aminopyridine iron and manganese complexes, $[(PDP)Fe^{II}]$ and $[(PDP)Mn^{II}]$ containing benzo-18-crown-6 ether as receptor that reversibly bind the substrate, has been prepared. The ditopic catalysts have been applied with success to achieve high site-selective C-H functionalization on C8 and C9 methylene positions of a series

of linear protonated primary amines thanks to reversible pre-association between ammonium moiety and the benzo-18-crown-6 ether recognition sites.

Imine based iron complexes represent another interesting class of nonheme catalysts. Iminopyridine iron(II) complex, easily prepared *in situ* by self-assembly of cheap and commercially available 2-picolylaldehyde, 2-picolylamine, and Fe(OTf)₂, in a 2:2:1 ratio, displayed good-to-moderate efficiency in the oxidation of aliphatic alcohols with H₂O₂. Quite surprisingly, benzylic alcohols are oxidized to aromatic ketones with low efficiency due to strong competitive aromatic hydroxylation. The remarkable selectivity for the oxidation of the aromatic ring in benzylic alcohols, has been exploited in the oxidation of alkyl aromatic compounds. In the presence of an aliphatic chain, the catalyst is highly selective for the aromatic nucleus hydroxylation with a selectivity pattern that closely matched that of electrophilic aromatic substitutions with a metal-based S_EAr pathway, without a significant involvement of free diffusing radical pathways.

A low efficiency in the oxidation of electron rich benzylic alcohols has been also observed, moreover, for the Mn^{II}/pyridine carboxylic acid/butanedione catalytic system. The analysis of the inhibition process of this catalytic system by catechol and guaiacol substrates indicated that the Mn/inhibitor ratio is a key parameter for the activity/inactivity of the system. The right proportion between them may prevents an irreversible deactivation of the complex.

Finally, the fundamental importance of the identification of the active intermediates involved in the catalytic cycles, has prompted us to project an innovative approach consisting in the simultaneously use of time-resolved Energy Dispersive X-Ray Absorption (EDXAS) and UV/Vis spectroscopies with millisecond resolution to follow the time evolution of the catalyst activation processes. The excellent results obtained for the evolution of [(TPA)Fe^{II}(CH₃CN)₂]²⁺ with H₂O₂ and CH₃COOOH, could give the opportunity to follow the evolution of less know systems and to detect and quantitatively monitor some elusive species, such as Fe^V intermediates.

Appendix

Instrument

Simultaneous energy dispersive X-ray absorption spectroscopy (EDXAS) and UV/Vis data were collected at ID24 beam-line of the European Synchrotron Radiation Facility (ESRF), Grenoble.¹ The ring energy was 6.0 GeV and the current 150–200 mA. The x-ray source consists of two undulators whose gaps were tuned to place the first harmonic at 7100 eV. The beam was focused horizontally to an 8 μm full width at half maximum (FWHM) spot on the sample by the curved Si(111) polychromator crystal in Bragg geometry. In the vertical direction, the beam was focused using a bent Si mirror at a glancing angle of 3 mrad with respect to the direct beam. To minimize sample radiation damage, the vertical spot size was set at 40 μm FWHM. Spectra were recorded in transmission mode using a FReLoN (fast read out low noise) high frame-rate detector based on charge coupled device (CCD) cameras optically coupled with a scintillator screen. Acquisition time was 40 ms for each spectrum. Sequences of 50-100 individual spectra were acquired, covering a total time span of 2-4 seconds during the reaction. Each sequence was repeated three times, and the data were averaged to obtain a better signal-to-noise ratio. The energy calibration was made by measuring the absorption spectrum of a Fe foil that was set at 7111 eV. All measurements were carried out at 25 °C. The raw EDXAS spectra correspond to measurements of the absorption coefficient A defined as follows:

$$A = \log [(I_0 - I_{0\text{bck}}) / (I_1 - I_{1\text{bck}})]$$

where I_0 is the incident intensity of the beam on the CCD and $I_{0\text{bck}}$ is the dark image of the CCD when there is nothing on the beam pathway, I_1 is the transmitted intensity coming from the sample and $I_{1\text{bck}}$ is the dark of the CCD when the sample is on the beam pathway. Simultaneous EDXAS and UV/Vis spectra were recorded with a Bio-Logic SFM-400 stopped-flow device

equipped with a flow-through quartz capillary cell.² The quartz capillary cell had a diameter of 1.3 mm and wall thickness of about 10 μm . The dead time of the stopped-flow device is about 2.0 ms for the flow rate of 8 mL/s as calibrated using the procedure described elsewhere² and it defines the shortest kinetic time that is accessible for spectroscopy measurements. However, for the measurements reported, the stopped-flow device was triggered by the EDXAS data acquisition system. Therefore, the overhead corresponding to the movement of the syringe motors needs to be considered and the kinetic time starts to evolve 96 ms after the trigger was sent. Therefore, the first UV/Vis spectrum is recorded at the beginning of the reaction ($t=0$ ms) whereas the first EDXAS spectrum is recorded 24 ms after the reaction starts. From this time on EDXAS and UV/Vis data collection is synchronized. The EDXAS spectrum at $t=0$ has been recorded on a 35 mM $[\text{Fe}^{\text{II}}(\text{TPA})(\text{CH}_3\text{CN})_2]^{2+}$ acetonitrile solution.

GC analyses were carried out on a gas chromatograph equipped with a capillary methylsilicone column (30 m x 0.25 mm x 25 μm) Chrompack CP-Sil 5 CB. GC-MS analyses were performed with a mass detector (EI at 70eV) coupled with a gas chromatograph equipped with a melted silica capillary column (30 m x 0.2 mm x 25 μm) covered with a methylsilicone film (5% phenylsilicone, OV5).

NMR spectra were recorded on either a BrukerDPX300 spectrometer and a Varian Mercury Plus. Chemical shift are denoted relative to the residual solvent peak.

HPLC analyses were performed on a chromatograph equipped with a C18 column (core shell 5 μm , 25 x 4.6 mm).

Laser flash photolysis experiments were carried out with an laser kinetic spectrometer providing 8 ns pulses using the third harmonic (355 nm) of a Quantel Brilliant-B Q-switched Nd:YAG laser. The laser energy was adjusted to ≤ 10 mJ/pulse through the use of the appropriate filter. A 3.5 mL Suprasil quartz cell (10 mm \times 10 mm) was used for all experiments.

UV-vis spectra were recorded on a Analytik Jena Specord S600 spectrophotometer using 1 cm or 2 mm quartz path cuvettes.

Raman spectra were recorded at λ_{exc} 785 nm using Perkin Elmer Raman Station at room temperature. It was focused on the sample through a 2.5 cm diameter plano-convex lens ($f=7.5$ cm) with Raman scattering collected in a 180° backscattering arrangement. The collimated

Raman scattering was focused by a second 2.5 cm diameter plan convex lens ($f=7.5$ cm) through a long pass edge filter (Semrock) into a Shamrock500i spectrograph (Andor Technology) with a 2400 l/mm grating blazed at 300 nm and acquired with an DV420A-BU2 CCD camera (Andor Technology). The spectral slit width was set to 12 μm . Data were recorded and processed using Solis (Andor Technology) with spectral calibration performed using the Raman spectra of acetonitrile/toluene 50:50 (v:v). Samples were held in quartz 2 mm path length cuvettes.

Cyclic voltammetric (CV) experiments were performed in an IJ-Cambria IH-660 potentiostat using a three electrode cell and recorded at 100 $\text{mV}\cdot\text{s}^{-1}$ scan rate. Glassy carbon disk electrode (3 mm diameter) from BAS were used as working electrode, platinum wire was used as auxiliary, and SSCE was used as the reference electrode (all the potentials are given with regard to this reference electrode). The complexes were dissolved in previously degassed solvents containing the necessary amount of Bu_4NPF_6 as supporting electrolyte to yield a 0.1 M ionic strength solution. All $E_{1/2}$ values reported in this work were estimated from cyclic voltammetric experiments as the average of the oxidative and reductive peak potentials $(E_{\text{pa}} + E_{\text{pc}})/2$.

References

- (1) Pascarelli, S.; Mathon, O.; Mairs, T.; Kantor, I.; Agostini, G.; Strohm, C.; Pasternak, S.; Perrin, F.; Berruyer, G.; Chappelet, P.; *J. Synch. Rad.* **2016**, *23*, 353-368.
- (2) Narayanan, T.; Gummel, J.; Gradzielski, M. Iglıc, A., Kulkarni, C.V., Eds.; *Academic Press*: Burlington **2014**, *20*, 171.

Full list of Publication

Included in this PhD thesis

- G. Olivo, A. Barbieri, V. Dantignana, F. Sessa, V. Migliorati, M. Monte, S. Pascarelli, T. Narayanan, O. Lanzalunga, S. Di Stefano and P. D'Angelo, *J. Phys. Chem. Lett.*, **2017**, *8* (13), 2958.

- A. Barbieri, R. Chimenti De Carlo, T. Del Giacco, S. Di Stefano, O. Lanzalunga, A. Lapi, M. Mazzonna, G. Olivo, M. Salamone, *J. Org. Chem.*, **2016**, *81*, 2513.
- A. Barbieri, T. Del Giacco, O. Lanzalunga, A. Lapi, M. Mazzonna, G. Olivo, *J. Org. Chem.*, **2016**, *81*, 12382.
- A. Barbieri, S. Di Stefano, O. Lanzalunga, A. Lapi, M. Mazzonna, G. Olivo, *Phosphorus Sulfur Silicon Relat. Elem.*, **2017**, *192*, 241.
- G. Olivo, M. Nardi, D. Vidal-Sanchez, A. Barbieri, A. Lapi, L. Gómez, O. Lanzalunga, M. Costas, S. Di Stefano, *Inorg. Chem.*, **2015**, *54*, 10141.
- G. Olivo, S. Giosia, A. Barbieri, O. Lanzalunga, S. Di Stefano, *Org. Biomol. Chem.*, **2016**, *14*, 10630.
- G. Capocasa, G. Olivo, A. Barbieri, O. Lanzalunga, S. Di Stefano, *Catal. Sci. Technol.*, **2017**, *7*, 5677.
- G. Olivo, G. Farinelli, A. Barbieri, O. Lanzalunga, S. Di Stefano, M. Costas, *Angew. Chem. Int. Ed.*, **2017**, doi: 10.1002/ange.201709280.

Not included in this PhD thesis

- A. Barbieri, M. De Gennaro, O. Lanzalunga, A. Lapi, M. Mazzonna, G. Olivo, S. Di Stefano, B. Ticconi, *Chem. Commun.*, **2015**, *51*, 5032.

